Crystallization of Polymers under Shear Flow(Dissertation_全文)

AUTHOR(S):

Ogino, Yoshiko

Crystallization of Polymers under Shear Flow

Yoshiko OGINO

2006

Crystallization of Polymers under Shear Flow

Yoshiko OGINO

2006

Contents

Chapter 1

General introduction

1-1 Background of this thesis

Extensive studies have been carried out on polymer crystallization under flows such as elongational and shear flows from both industrial and scientific points of view [1-8]. In many polymer processing operations such as fiber spinning, injection molding and extrusion, polymers experience various kinds of flows and the crystallization kinetics and the final morphology are greatly affected by the flows. It is known [9-13] that when polymers in melts and solutions are crystallized under elongational and/or shear flows the so-called shish-kebab structure is often formed, which consist of long central fiber core (shish) surrounded by lamellar crystalline structure (kebab) periodically attached along the shish. It is believed that the shish is formed by crystallization of completely stretched polymer chains and the kebabs are folded chain lamella crystals and grow to the direction normal to the shish. Recent development of advanced characterization techniques such as in situ rheo-small-angel and wide-angle X-ray scattering (SAXS and WAXS) [14-24] and in situ rheo-small-angle light scattering (SALS) [25-27] and rheo-optical measurements [28-30] has shed light on significant features of the formation mechanism of the shish-kebab structure. In situ rheo-SAXS and rheo-WAXS measurements were extensively carried out on the structure development in fiber spinning process [14,15,17-19,31,32] as well as in shear-induced crystallization process [16,20-22,24]. Some of the works have focused on the structural formation in the early stage of the

crystallization under flow using "short term shearing" technique [33] because it often governs or at least affect the final structure deeply. Despite the extensive studies, the formation mechanism of the shish-kebab structure is not fully understood. One of the reasons is that there are many factors which influence the formation of the shish-kebab structure such as molecular weight, molecular weight distribution, branching in chain, shear rate, shear strain, crystallization temperature and so on. It is necessary in such situation to perform systematic studies on the crystallization process as a function of each factor to elucidate the formation mechanism.

1-1-1 Earlier researchers on flow induced crystallization

The studies of polymer crystallization under flow started in 1960s. Pennings and his co-workers found the shish-kebab structure in crystallization of polyethylene from the xylene solution [9]. They prepared 5% xylene solution of polyethylene and stirred the solution for 3 days keeping the temperature at 102 °C to obtain the fibrillar crystals. They observed the structure of the crystals using a TEM, which is shown in Fig. 1. They also examined the structure of the crystals using electron diffraction and found the c-axis of the crystal is parallel to the fiber axis as seen in the inset of Fig. 1. The fibrillar structure depends on the concentration of the solution, the molecular weight and the condition of stirring. They considered that the fibrillar crystal consisted of backborn (shish) and ribbon-like crystal (kebab). They measured the melting temperature of the fibrillar crystal and found that the backborn did not disappear until the unexpectedly high temperature of 151 °C, suggesting that the backborn of

Fig. 1. Transmission electron microscope (TEM) image of fibrillar polyethylene crystals and electron diffraction pattern (inset).

the crystal would be made of extended chains [9]. In another paper [34], they performed ultrasonic treatment on the fibrillar crystal and found that the ribbon-like crystal (kebab) was removed from the backborn (shish) (see Fig. 2). This result suggests that the kebab structure epitaxitially grows from the surface of the shish structure. Wikjord and Manley also showed that the shish and the kebab could be separable when it was treated with nitric acid, but this method corroded and shortened polymer chain [35].

The shish-kebab structure was found not only in the crystals from solutions under stirring, but also in crystals from bulk under injection molding and extrusion. Keller and co-workers [11,12,36] observed the polyethylene fiber crystals obtained in extrusion molding process using transmission electron microscope (TEM) and suggested the interlocking shish-kebab model (Fig. 3(b)) by analyzing the TEM image. The TEM image in Fig. 3(a) showed that thickness of kebab was about 300 Å, diameter of shish was about 250 Å, and length of shish was 500 μm at longest [36]. A shish-kebab structure was seemed to be interlocked with neighboring shish-kebab structure by kebab structures.

1-1-2 Current researchers on flow induced crystallization

After the works of Pennings' group and Keller's group, extensive studies carried out on the shish-kebab structure [3,9,11,12,34,36]. However, we still have many unsolved problems on the shish-structure, especially on the formation mechanism. Recent advance of instrumental technology such as synchrotron radiation X-ray, strong laser source, and neutron source enables us to perform in-situ measurements on the crystallization process under

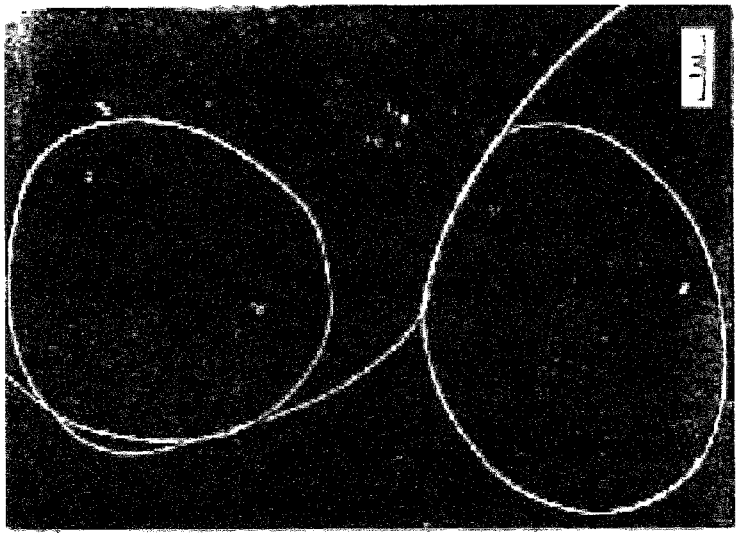

Fig. 2. Shish structure after ultrasonic agitation. Kebab structure was removed by ultrasonic agitation.

(a) (b)

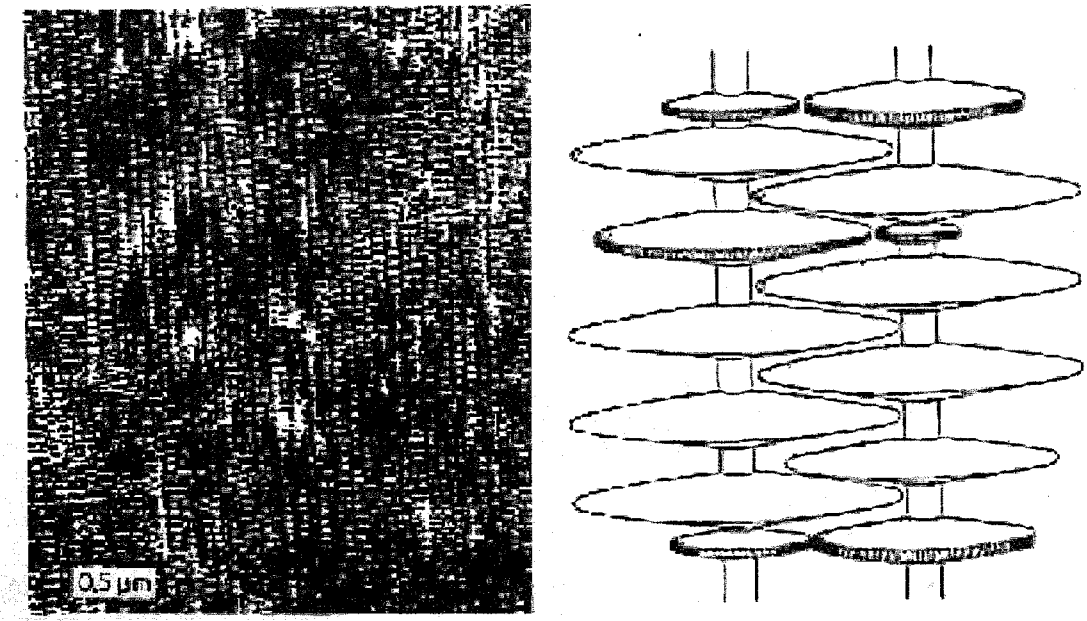

Fig. 3. Extrusion molding polyethylene fiber of TEM image (a) and interlocking shish kebab model for the TEM image (b).

flows. Simultaneous in-situ small-angle X-ray scattering (SAXS) and wide-angle X-ray scattering (WAXS) is one of the most powerful tools to see the structure formation in crystallization process of polymers under flows. For example, in situ rheo-SAXS and rheo-WAXS studies on i-PP and polyethylene (PE) after pulse shear by Hsiao et al. [22-24] have shown that a scaffold or network of oriented structures is formed prior to the full-crystallization. Alfonso et al. performed the spatially resolved measurements by simultaneous small-angle and wide-angle X-ray micro-diffraction using isotactic polystyrene (i-PS). They applied shear flow to the molten state sample by pulling a single glass fiber, quenched to below T_g and scanned the flow position. They proposed the existence of quasi-ordered clusters in the melt whose size and orientation distributions are dictated by characteristics of the flow field [37]. Kornfield et al. [28-30] have preformed in situ birefringence measurements on isotactic polypropylene (i-PP) after short term shearing, and found that the birefringence drops after the shear but shows upturn again, suggesting formation of a precursor of the shish-kebab structure. These studies have indicated that a precursor of the shish is formed in the very early stage during the crystallization process after the shear. A pioneering in situ rheo-SALS study by Katayama et al. [38] also demonstrated that there exists a mesomorphic state during the shear-induced crystallization process about 30 years ago. Recent in situ rheo-SALS measurements on i-PP by Winter et al. [25-27] have revealed that density fluctuations occur before the orientation fluctuations.

As mentioned above, recent researches using advanced experimental

techniques have gradually revealed the formation mechanism of the shish-kebab structure. However we are still far from the final goal. As will be seen in this thesis, in order to understand the shish-kebab formation process we have to examine the formation process in a wide spatial scale from 1 Å to several μm. For this purpose we employed many experimental techniques in this thesis such as wide-angel X-ray scattering, small-angle X-ray scattering, small-angle neutron scattering, depolarized light scattering and optical microscope to cover a wide spatial scale.

1-2 Experimental techniques

1-2-1 Basic theory of scattering

Analysis of the microscopic structure of polymer systems is generally carried out with both real- and inverse- spaces. The former is implemented by various kinds of microscopes [39] such as electron microscopy, atomic force microscopy, and optical microscopy. The latter is implemented by various kinds of scattering experiments such as wide-angle diffraction, small-angle scattering and light scattering. In this section we summarize the basic principles of scattering methods [40-45] in order to give a basis to understand the experimental results presented in this thesis.

Depending on the system under study and the desired resolution, photons in the X-ray and light scattering range, or neutrons are used. The general set up of a scattering experiment is indicated schematically in Fig. 4. There is an incident beam of monochromatic radiation with wavelength λ and intensity I_0. It becomes scattered by a sample and the intensity I of the scattered waves is registered by a detector at a distance A, under variation of

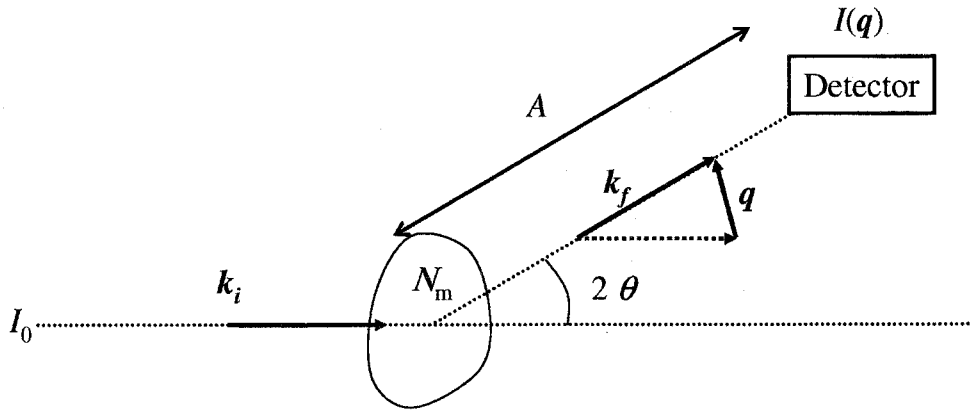

Fig. 4. General scattering experiment setup.

the direction of observation. Employing the scattering vector $\boldsymbol{q}$, defined as

$$\boldsymbol{q} \equiv \boldsymbol{k}_{\mathrm{f}} - \boldsymbol{k}_{\mathrm{i}}, \tag{1.1}$$

where $\boldsymbol{k}_{\mathrm{f}}$ and $\boldsymbol{k}_{\mathrm{i}}$ denote the wave vectors of the incident and the scattered plane waves, respectively. The result of a scattering experiment is usually expressed by giving the intensity distribution in $\boldsymbol{q}$-space, $I(\boldsymbol{q})$. In the majority of scattering experiments on polymers the radiation frequency remains practically unchanged because there is no energy transfer between the incident and scattered beam. These are so called 'elastic scattering' while those in which energy transfer occurs are named 'inelastic scattering'. Then in the case of elastic scattering we have

$$|\boldsymbol{k}_{\mathrm{f}}| \approx |\boldsymbol{k}_{\mathrm{i}}| = \frac{2\pi}{\lambda}, \tag{1.2}$$

and $|\boldsymbol{q}|$ is related to the scattering angle 2λ by

$$|\boldsymbol{q}| = \frac{4\pi}{\lambda}\sin\theta. \tag{1.3}$$

Principles for Static Scattering Experiments Two different functions can be used for representing scattering data in reduced forms. The first one is the differential scattering cross-section per unit volume of the sample described as

$$\Sigma(\boldsymbol{q}) \equiv \frac{1}{V}\frac{\mathrm{d}\sigma}{\mathrm{d}\Omega} = \frac{1}{V}\frac{I(\boldsymbol{q})A^2}{I_0}. \tag{1.4}$$

In light scattering experiments this function is called the Rayleigh-ratio. While the effect of the volume is removed, $\Sigma(\boldsymbol{q})$ remains dependent on the scattering power of the particles in the sample, which varies with the applied

radiation. For X-rays, the scattering power is related to the electron densities, for light scattering to the associated refractive indices and for neutron scattering to the scattering length densities. This dependence is eliminated in the second function which, however, can only be employed if the scattering can be treated as being due to just one class of particles. In polymer systems these can be identified with the monomeric units. For equal particles the scattering properties can be described by the scattering function $S(q)$, which is defined as

$$S(q) \equiv \frac{I(q)}{I_{\mathrm{m}} N_{\mathrm{m}}}, \tag{1.5}$$

where N_m represents the total number of particles or monomers in the sample, and I_m is the scattering intensity produced by one particle, if placed in the same incident beam. The scattering function $S(q)$ is often also addressed as the structure function or structure factor. The interference function expresses the ratio between the actual intensity and measured one, if all particles in the sample were to scatter incoherently. It thus indeed describes the interference effect. The relationship between $\Sigma(q)$ and $S(q)$ is described by the equation as

$$\Sigma(q) = \langle c_{\mathrm{m}} \rangle \left(\frac{\mathrm{d}\sigma}{\mathrm{d}\Omega} \right)_{\mathrm{m}} S(q), \tag{1.6}$$

where $(d\sigma / d\Omega)_m$ represents the scattering cross section per particle or monomer and $<c_m>$ stands for their mean density

$$\langle c_{\mathrm{m}} \rangle = \frac{N_{\mathrm{m}}}{V}. \tag{1.7}$$

Scattering diagrams generally emerge from the superposition and

interference of the scattered waves emanating from all the particles in the sample. If we describe the amplitudes of single scattered waves at the point of registration by the detector in normalized form, by complex numbers of modulus unity and phases φ_i, the total scattering amplitude is obtained as

$$C = \sum_{i=1}^{N_m} \exp(i\varphi_i). \tag{1.8}$$

The phases φ_i are simply determined by the particle positions $\boldsymbol{r}_i$ and the scattering vector $\boldsymbol{q}$ only, being given by

$$\varphi_i = \boldsymbol{q}\boldsymbol{r}_i. \tag{1.9}$$

Thus the scattering amplitude produced by a set of particles at locations $\boldsymbol{r}_i$ is formulated as

$$C(\boldsymbol{q}) = \sum_{i=1}^{N_m} \exp(i\boldsymbol{q}\boldsymbol{r}_i). \tag{1.10}$$

The scattering intensity $I(\boldsymbol{q})$ is proportional to the squared modulus of C

$$I(\boldsymbol{q}) \sim \left\langle |C(\boldsymbol{q})|^2 \right\rangle. \tag{1.11}$$

As the normalization of the amplitudes of the single scattered waves is already implied in the definition of the interference function eq. (1.5), eq. (1.11) can be completed to

$$S(\boldsymbol{q}) = \frac{1}{N_m} \left\langle |C(\boldsymbol{q})|^2 \right\rangle. \tag{1.12}$$

This is a basic equation of general validity and it may serve as starting point for the derivation of other forms of scattering equations. The calculation of the squared scattering amplitude is following.

The first formula is given directly by insertion of eq. (1.10) to eq. (1.12),

leading to

$$S(\boldsymbol{q}) = \frac{1}{N_{\mathrm{m}}} \sum_{i,j=1}^{N_{\mathrm{m}}} \left\langle \exp[\mathrm{i}\boldsymbol{q}(\boldsymbol{r}_i - \boldsymbol{r}_j)] \right\rangle . \tag{1.13}$$

One can also use a continuum description and introduce the particle density distribution $c_m(\boldsymbol{r})$ instead of specifying the discrete positions $\boldsymbol{r}_i$ of all particles. First, the scattering amplitude for a single microstate, as represented by the associated density distribution

$$C(\boldsymbol{q}) = \int_V \exp(\mathrm{i}\boldsymbol{q}\boldsymbol{r}) \cdot [c_{\mathrm{m}}(\boldsymbol{r}) - \langle c_{\mathrm{m}} \rangle] \mathrm{d}^3\boldsymbol{r} . \tag{1.14}$$

Scattering occurs only when c_m varies within the sample that we subtract the mean value $<c_m>$. Thus it is obviously revealed that the scattering is directly relating to the fluctuations. We can also see that $C(\boldsymbol{q})$ equals the Fourier-transition of the fluctuations in the particle density. Insertion of eq. (1.14) into eq. (1.12) and carrying out the ensemble average yields

$$S = \frac{1}{N_{\mathrm{m}}} \int_V \int_V \exp[\mathrm{i}\boldsymbol{q}(\boldsymbol{r}' - \boldsymbol{r}'')] \left\langle [c_{\mathrm{m}}(\boldsymbol{r}') - \langle c_{\mathrm{m}} \rangle] \cdot [c_{\mathrm{m}}(\boldsymbol{r}'') - \langle c_{\mathrm{m}} \rangle] \right\rangle \mathrm{d}^3\boldsymbol{r}' \mathrm{d}^3\boldsymbol{r}'' . \tag{1.15}$$

For all macroscopically homogeneous systems, where the equation of

$$\langle c_{\mathrm{m}}(\boldsymbol{r}') c_{\mathrm{m}}(\boldsymbol{r}'') \rangle = \langle c_{\mathrm{m}}(\boldsymbol{r}' - \boldsymbol{r}'') c_{\mathrm{m}}(0) \rangle \tag{1.16}$$

is approved. This equation can be reduced to a single integral. Substitution of $\boldsymbol{r}'$-$\boldsymbol{r}''$ by $\boldsymbol{r}$ yields

$$S(\boldsymbol{q}) = \frac{1}{\langle c_{\mathrm{m}} \rangle} \int_V \exp(\mathrm{i}\boldsymbol{q}\boldsymbol{r}) \cdot [\langle c_{\mathrm{m}}(\boldsymbol{r}) c_{\mathrm{m}}(0) \rangle - \langle c_{\mathrm{m}} \rangle^2] \mathrm{d}^3\boldsymbol{r} \tag{1.17}$$

This equation expresses $S(\boldsymbol{q})$ as the Fourier-transform of the space dependent correlation function of the particle density.

A third form of the basic scattering equation is obtained if structures are characterized with the aid of the pair distribution function $g(\boldsymbol{r})$. From the definition, the product $g(\boldsymbol{r})\mathrm{d}^3\boldsymbol{r}$ gives the probability that starting from a given particle, the particle itself or some other particle is found in the volume element $\mathrm{d}^3\boldsymbol{r}$ at a distance $\boldsymbol{r}$. The pair distribution function $g(\boldsymbol{r})$ is composed of a sum of two contributions which are self-contributions and the contributions of the other particles. For fluid systems with short-range order, the limiting value of the pair distribution function $g(\boldsymbol{r})$ at large distances ($\boldsymbol{r} \rightarrow \infty$) equals the mean density $<c_m>$. As follows directly from the definitions, density distribution function and pair distribution function are related by

$$\langle c_{\mathrm{m}}(\boldsymbol{r}) c_{\mathrm{m}}(0)\rangle = \langle c_{\mathrm{m}}\rangle \cdot g(\boldsymbol{r}). \tag{1.18}$$

Insertion of the equation in eq. (1.17) gives

$$S(\boldsymbol{q}) = \int_V \exp(\mathrm{i}\boldsymbol{q}\boldsymbol{r}) \cdot [g(\boldsymbol{r}) - \langle c_{\mathrm{m}}\rangle]\mathrm{d}^3\boldsymbol{r}\,. \tag{1.19}$$

It is once again revealed that the scattering function equals a Fourier-transform, now of the pair distribution function. At the same time, we follow the asymptotic values of S for large values of $\boldsymbol{q}$ from this equation. In the limit $\boldsymbol{q} \rightarrow \infty$ only the contribution of the self-correlation part is left, and we find $S(\boldsymbol{q} \rightarrow \infty) \rightarrow 1$. It can be concluded that there are neither constructive nor destructive interferences between the particles for large $\boldsymbol{q}$ so that they behave like incoherent scatters.

In the case of isotropic system, both vector parameters $\boldsymbol{q}$ and $\boldsymbol{r}$ can be treated as length parameters $q\,(= |\boldsymbol{q}|)$ and $r\,(= |\boldsymbol{r}|)$, respectively. Then the Fourier-relation between $g(r)$ and $S(q)$ has the form as

$$S(q)=\int_{r=0}^{\infty}\frac{\sin qr}{qr}4\pi r^2[g(r)-\langle c_{\mathrm{m}}\rangle]\mathrm{d}r. \qquad (1.20)$$

In this chapter, it was formulated three equivalent relations, eqs. (1.13), (1.17) and (1.19), which may be employed in the evaluation of scattering data. All three equations express a Fourier-relation between $S(q)$ and functions which describe properties of the microscopic structure in statistical terms.

Scattering of two layer systems Isotropic samples of partially crystalline polymer essentially correspond to an ensemble of density packed, isotropically distributed stacks of parallel and normal to the lamellar crystallities. If the extensions of the stacks parallel and normal to the lamellar surfaces are large compared to the interlamellar distance, the scattering behavior can be related to the electron density distribution $\rho_e(z)$ measured along a trajectory normal to the surfaces. This trajectory will pass through amorphous regions with density $\rho_{e,a}$ and crystallities with a core density $\rho_{e,c}$. The average density $\langle\rho_e\rangle$ lies between these two limits.

We calculate the scattering cross-section per unit volume by application of eq. (1.21)

$$\sum(q)=r_e^2\int_V\exp iqr\cdot\left(\langle\rho_e(r)\rho_e(0)\rangle-\langle\rho_e\rangle^2\right)\mathrm{d}^3r, \qquad (1.21)$$

and consider at first an ensemble of equally oriented stacks. If we choose the orientation of the surface normal to the z-axis, the electron density distribution depends on z only and we can write

$$\sum(q)=r_e^2\int_{x,y,z}\exp(i(q_xx+q_yy+q_zz))(\langle\rho(z)_e\rho(0)_e\rangle-\langle\rho_e\rangle^2)dxdydz. \qquad (1.22)$$

Carrying out the integrations for x and y we obtain

$$\sum(q) = r_e^2 (2\pi)^2 \delta(q_x)\delta(q_y) \int_{-\infty}^{\infty} \exp(iq_z) \cdot K(z)dz . \tag{1.23}$$

Where $K(z)$ designates the one-dimensional electron density correlation function

$$K(z) \equiv \left\langle (\rho_e(z) - \langle \rho_e \rangle)(\rho_e(0) - \langle \rho_e \rangle) \right\rangle$$

$$= \langle \rho_e(z)\rho_e(0) \rangle - \langle \rho_e \rangle^2 . \tag{1.24}$$

The scattering of an isotropic ensemble of stacks of lamellae, as it is found in melt crystallized samples, follows from eq. (1.23) by calculation of the isotropic average, i.e. by distributing the intensity at $\pm q_z$ equally over the surface of a sphere with the same radius. The resulting isotropic intensity distribution, $\Sigma(q:=|q|)$, is given by

$$\sum(q) = \frac{2}{4\pi q^2} r_e^2 (2\pi)^2 \int_{-\infty}^{\infty} \exp(iqz) \cdot K(z)dz . \tag{1.25}$$

The reverse Fourier-relation is

$$K(z) = \frac{1}{2r_e^2} \frac{1}{(2\pi)^3} \int_{-\infty}^{\infty} \exp(iqz) \cdot 4\pi q^2 \sum(q)dq$$

$$= \frac{1}{r_e^2} \frac{1}{(2\pi)^3} \int_{0}^{\infty} \cos qz \cdot 4\pi q^2 \sum(q)dq , \tag{1.26}$$

eq. (1.26) enable $K(z)$ to be determined if $\Sigma(q)$ is known.

$K(z)$ has a characteristic shape, allowing an evaluation which leads directly to the main parameters of the stack structure. In order to explain the procedure, we first establish the shape of $K(z)$ for a strictly periodic two-phase system and then proceed by a consideration of the modifications

introduced by a stepwise perturbation of the system. Fig. 5 provides an illustration and sketches all the steps.

The periodic structure shows an electron density distribution $\rho_e(z)$ as indicated on the left part (a). It can be described by specifying the 'long period' d_{ac}, the crystallite thickness d_c and the electron density difference $\rho_{e,c} - \rho_{e,a}$. The crystallinity $\phi_c = d_c/d_{ac}$ in this example lies below 50%. We first calculate a special correlation function, denoted $K_a(z)$, defines as

$$K_a(z) \equiv \left\langle \left(\rho_e(z) - \rho_{e,a}\right)\left(\rho_e(0) - \rho_{e,a}\right)\right\rangle . \tag{1.27}$$

When using K_a, all electron densities refer to the electron density of the amorphous regions. Since the ensemble average is identical with an average over all points z' in a stack, $K_a(z)$ may be obtained by an evaluation of the integral

$$K_a(z) = \frac{1}{\Delta}\int_{-\Delta/2}^{\Delta/2}\left[\rho_e(z') - \rho_{e,a}\right]\left[\rho_e(z+z') - \rho_{e,a}\right]dz' . \tag{1.28}$$

The integration range Δ has to be sufficiently large. The functions $\rho_e(z)$ and $\rho_e(z+z')$ are square distributions, and contributions to the integral arise only, if two crystalline regions overlap. Consequently, $K_a(z)$ is proportional to the length of the overlap region, and given by

$$K_a(z) = \begin{cases} (\rho_{e,c} - \rho_{e,a})^2 (d_{c-z})/d_{ac} : & |z| < d_c \\ 0 \qquad\qquad\qquad\quad : & d_c < |z| < d_{ac} - d_c \end{cases} . \tag{1.29}$$

and being periodic, by

$$K_a(z + d_{ac}) = K_a(z) . \tag{1.30}$$

Having determined K_a, one obtains $K(z)$ by

$$K(z) = K_a(z) - \left(\langle \rho_e \rangle - \rho_{e,a}\right)^2 . \tag{1.31}$$

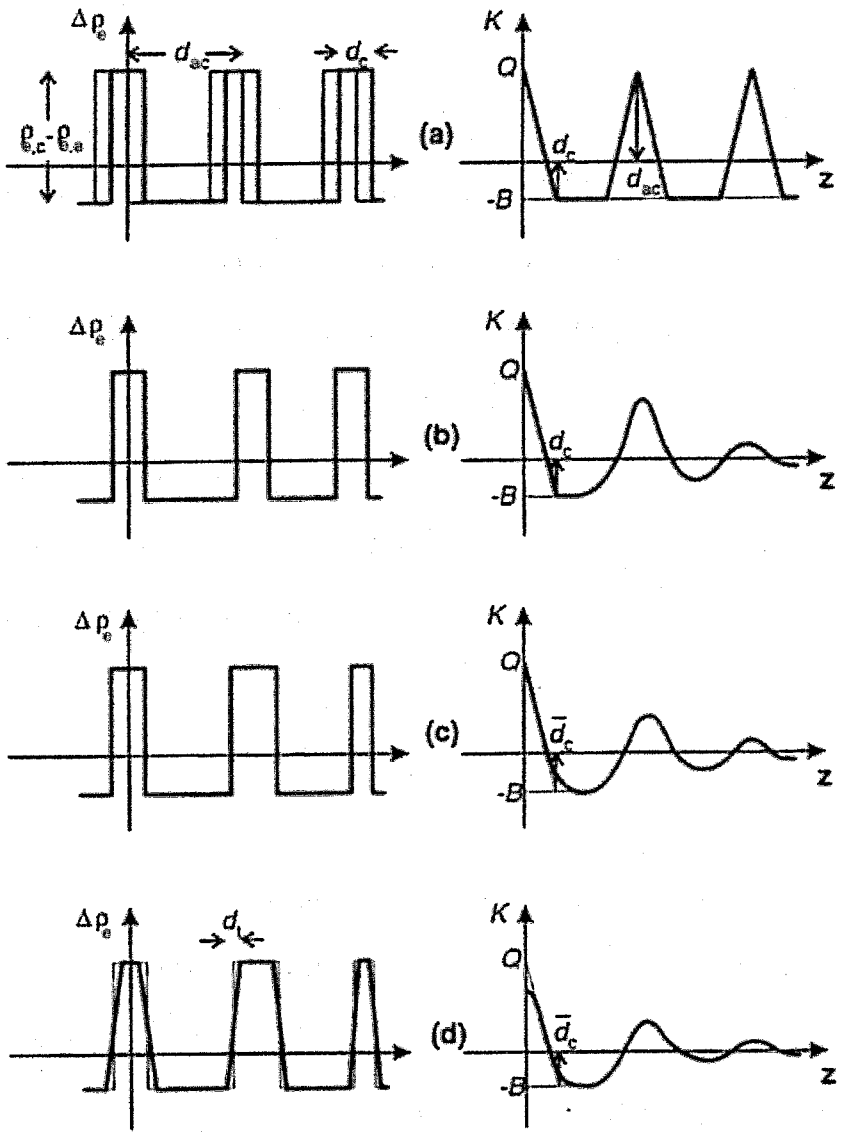

Fig. 5. Two-phase layer system representative for a partially crystalline polymer. Electron density distribution $\Delta\rho_e(z) \equiv \rho_e(z) - \langle \rho_e \rangle$ and the associated one dimensional correlation function $K(z)$ for a perfectly ordered system (a). Effects of varying intercrystalline spacings (b), varying crystallite thickness (c) and diffuse interface (d).

The result is shown on the right of part (a). There is a regular sequence of triangles, centered at $z = 0$, d_{ac}, $2d_{ac}$ etc., which reflect the correlations within one crystallite, between next neighbors, second neighbors etc. The 'self-correlation triangle' centered at the origin exhibits some characteristic properties. The value at $z = 0$, denoted Q, is

$$K(z=0) \equiv Q = \phi_c(1-\phi_c)(\rho_{e,c} - \rho_{e,a})^2 . \tag{1.32}$$

The slope dK/dz is

$$\frac{dK}{dz} = \frac{dK_a}{dz} = -\frac{O_{ac}}{2}(\rho_{e,c} - \rho_{e,a})^2 . \tag{1.33}$$

Here, O_{ac} denotes the 'specific internal surface' given by the area per unit volume of the interface separating crystalline and amorphous regions. For the periodic stack it is related to the long period by

$$O_{ac} = \frac{2}{d_{ac}} . \tag{1.34}$$

The horizontal 'baseline' between the triangles is located at

$$K = -B = -\left(\langle \rho_e \rangle - \rho_{e,a}\right)^2 \tag{1.35}$$

$$= -\phi_c^2(\rho_{e,c} - \rho_{e,a})^2 . \tag{1.36}$$

K(z) reaches the base-line at

$$z_1 = d_c . \tag{1.37}$$

It is now interesting to recognize that application of these relations is not restricted to the ordered periodic system but can be extended, with slight modifications, to real systems which may show variations in the thicknesses of the crystalline and amorphous regions, and may also possess diffuse phase boundaries. The changes in $K(z)$ resulting from a successive perturbation of the initial system are schematically indicated in Fig. 5(b)-(d). All structures

in this sequence are understood as having equal crystallinities and equal specific internal surfaces.

First, as indicated in part(b), fluctuations in intercrystalline spacings are introduced. Since the self-correlation part remains uncharged, the only consequence is a broadening of the peak attributed to next-neighbor correlations. There is a maximum at the position of the most probable distance between neighboring crystallities, and it determines the 'long spacing'.

Secondly, as shown in part(c), we superpose variations in the crystallite thickness. Since ϕ_c and O_{ac} are assumed to be constant, the value of the correlation function at the origin, Q, the initial slope $\mathrm{d}K/\mathrm{d}z$ $(z = 0)$ and the base-line coordinate B are not affected. A modification occurs near to the base of the triangle, where $K(z)$ becomes curved. If we extrapolate the straight part of $K(z)$, it intercepts the base-line at

$$z_1 = -\frac{Q+B}{dK/dz} = \frac{\phi_c}{O_{ac}/2}. \tag{1.38}$$

The number average of the crystallite thickness, $\overline{d_c}$, is given by

$$\frac{O_{ac}}{2}\overline{d_c} = \phi_c. \tag{1.39}$$

Therefore, we have

$$z_1 = \overline{d_c}. \tag{1.40}$$

Finally, in the last step, we associate the crystallite surfaces with transition zone (part(d)). We do it under the condition that for each crystallite i the total number of electrons remains unchanged, i.e.

$$\int[\rho_e(z') - \rho_{e,a}]dz'] = (\rho_{e,c} - \rho_{e,a})d_c^i. \tag{1.41}$$

Using this equation in the other direction, one may attribute to each crystallite with a diffuse surface a corresponding lamella with sharp boundaries and thickness d_c^i. If this replacement is carried out for all crystallites, one retunes to a two-phase structure which we address as the 'corresponding two-phase system'. For a transition zone with an extension d_t there results a change in shape of the correlation function around the origin, within the range $z < d_t$. If d_t is small compared to the thicknesses of all crystallites, there still remains a liner portion in the center of the right-hand side of the self-correlation triangle. This allows us to derive directly the parameters of the 'corresponding two-phase system': Extrapolation of the linear section to $z = 0$ gives Q, and a continuation down to the base-line at $K = -B$ yields $\overline{d_c}$. The crystallinity ϕ_c, the specific internal surface O_{ac} and the electron density difference then follow by

$$\phi_c = \frac{B}{B+Q} \tag{1.42}$$

$$O_{ac} = \frac{2\phi_c}{\overline{d_c}} \tag{1.43}$$

$$(\rho_{e,c} - \rho_{e,a})^2 = \frac{Q}{\phi_c(1-\phi_c)}. \tag{1.44}$$

So far, we have discussed the case $\phi_c < 0.5$. If we wish to investigate samples with $\phi_c > 0.5$, we have to substitute ϕ_c against the volume fraction of the amorphous phase

$$\phi_a = 1 - \phi_c. \tag{1.45}$$

and $\overline{d_c}$ against the number average of the thickness of the amorphous layers, $\overline{d_a}$. The substitution rule follows from Babinet's reciprocity

theorem which declares that an exchange of the analysis lies in the knowledge required of the base-line coordinate B. For samples of low or high crystallinity ($\phi_c < 0.3$ or $\phi_c > 0.7$), the base-line usually shows up. The intermediate region is problematic, as here the base-line may not be observed. Then X-ray scattering experiments have to be complemented by other data such as, for example, the density.

In this discussion of the scattering properties of a polymeric layer system, we have dealt with a specific but generally valid for all two-phase systems, independent of their structure. We give here three equations of particular importance.

First, we come back to eq. (1.32). Use of eq.(1.26) yields

$$Q = (\rho_{e,c} - \rho_{e,a})^2 \phi_c (1-\phi_c) = \frac{1}{r_e^2 (2\pi)^3} \int_{q=0}^{\infty} 4\pi q^2 \sum(q) dq \,. \tag{1.46}$$

Q is often called the 'invariant', for obvious reasons: The total integral, as obtained by an integration over all the reciprocal space, depends only on the volume fractions of the two phases and the electron density difference and is invariant with regard to the detailed structure. Eq.(1.46) is not a specific property of layered systems, but generally valid. The proof is simple. One has to formulate the Fourier-transformation reverse to eq.(1.21), expressing the three dimensional electron density correlation function as a function of $\Sigma(q)$

$$\langle \rho_e(\boldsymbol{r}) \rho_e(0) \rangle - \langle \rho_e \rangle^2 = \frac{1}{r_e^2 (2\pi)^3} \int \exp(-i\boldsymbol{q}\boldsymbol{r}) \cdot \sum(\boldsymbol{q}) d^3\boldsymbol{q} \,, \tag{1.47}$$

and consider the limit $r \rightarrow 0$

$$\left\langle \rho_e^2 \right\rangle - \left\langle \rho_e \right\rangle^2 = \frac{1}{r_e^2 (2\pi)^3} \int \sum (\boldsymbol{q}) d\boldsymbol{q}^3 . \qquad (1.48)$$

Direct calculation shows that for a two-phase system the left-hand sides of eqs. (1.46) and (1.48) agree.

Secondly, we consider the asymptotic behavior $\Sigma(q \to \infty)$, looking first at the layer system. Due to the reciprocity property of Fourier-transforms, $\Sigma(q \to \infty)$ relates to the limiting behavior $K(z \to 0)$. Therefore, using eqs. (1.25), (1.32) and (1.33) in a series expansion, we can write

$$\sum (q \to \infty) = \frac{1}{2\pi q^2} r_e^2 (2\pi)^2 \lim_{q \to 0} \int_{-\infty}^{\infty} \cos qz \cdot \left(Q - \frac{O_{ac}}{2} (\rho_{e,c} - \rho_{e,a})^2 |z| \right) dz . \qquad (1.49)$$

For the purpose of a derivation of the asymptotic properties we may employ the following special representation of K valid for small values of z:

$$Q - \frac{O_{ac}}{2} (\rho_{e,c} - \rho_{e,a})^2 z \approx Q \exp\left(- \frac{O_{ac} (\rho_{e,c} - \rho_{e,a})^2}{2Q} |z| \right) . \qquad (1.50)$$

With this, the integral can be evaluated

$$\sum (q \to \infty) = \frac{2\pi r_e^2}{q^2} \lim_{q \to \infty} \int_{-\infty}^{\infty} \cos qz \cdot Q \exp\left(- \frac{O_{ac} (\rho_{e,c} - \rho_{e,a})^2 |z|}{2Q} \right) dz , \qquad (1.51)$$

which yields

$$\sum (q \to \infty) = \frac{2\pi r_e^2}{q^4} O_{ac} (\rho_{e,c} - \rho_{e,a})^2 , \qquad (1.52)$$

eq. (1.52), known as 'Porod's law', is generally valid for arbitrary two-phase systems. Indeed, an asymptotic law $\Sigma(q) \sim 1/q^4$ is the characteristic signature of two-phase systems with sharp boundaries. According to eq. (1.52), the asymptotic behavior depends only on the interface area per unit volume, multiplied by the square of the density difference.

A third interesting parameter, l_c, is obtained by a combination of Q and O_{ac} in the form of the exponent in eq. (1.50).

$$l_c \equiv \frac{2Q}{O_{ac}(\rho_{e,c}-\rho_{e,a})^2} = \frac{2\phi_c(1-\phi_c)}{O_{ac}}, \tag{1.53}$$

l_c characterizes the length scale of the two-phase structure. Eq(1.53) is generalization of eq. (1.39) which concerns $\overline{d_c}$ and thus also a characteristic length of the layer system. There is one technical advantage in the determination of l_c. As the electron density difference becomes eliminated, there is no need for intensity measurements in absolute units.

1-2-2 Scattering apparatus

Depolarized light scattering We used the home-made light scattering apparatus to measure in-situ depolarized light scattering. The light scattering apparatus has a He-Ne laser as light source and a CCD camera with paraffin paper as detector. The wavelength of the He-Ne laser is 632.8nm. The CCD camera is a model CS8300 of Tokyo Electronic Industry Co. Ltd. We set a paraffin paper, which is a detector plane between the CCD camera and the polarizer and detect the scattering pattern on the paraffin paper using CCD camera in this thesis. Time evolution of scattering pattern was recorded by CCD camera in a time interval of 1/30 s. Fig. 6 shows layout of the light scattering apparatus. This apparatus has two slits; the laser side slit and the sample side slit. Fig. 7 shows a photo of the light scattering apparatus with a shear cell.

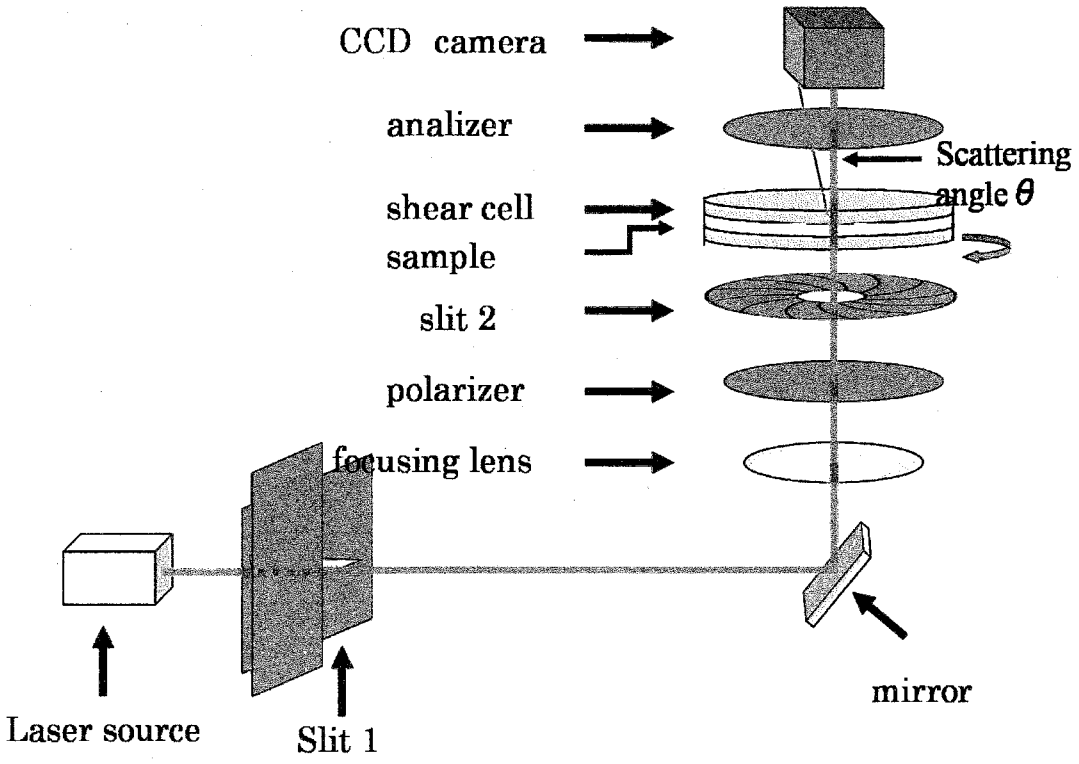

Fig. 6. Layout of the light scattering apparatus composed of laser source, two slits, mirror, lens, sample cell with sample, a set of polarizes and CCD camera.

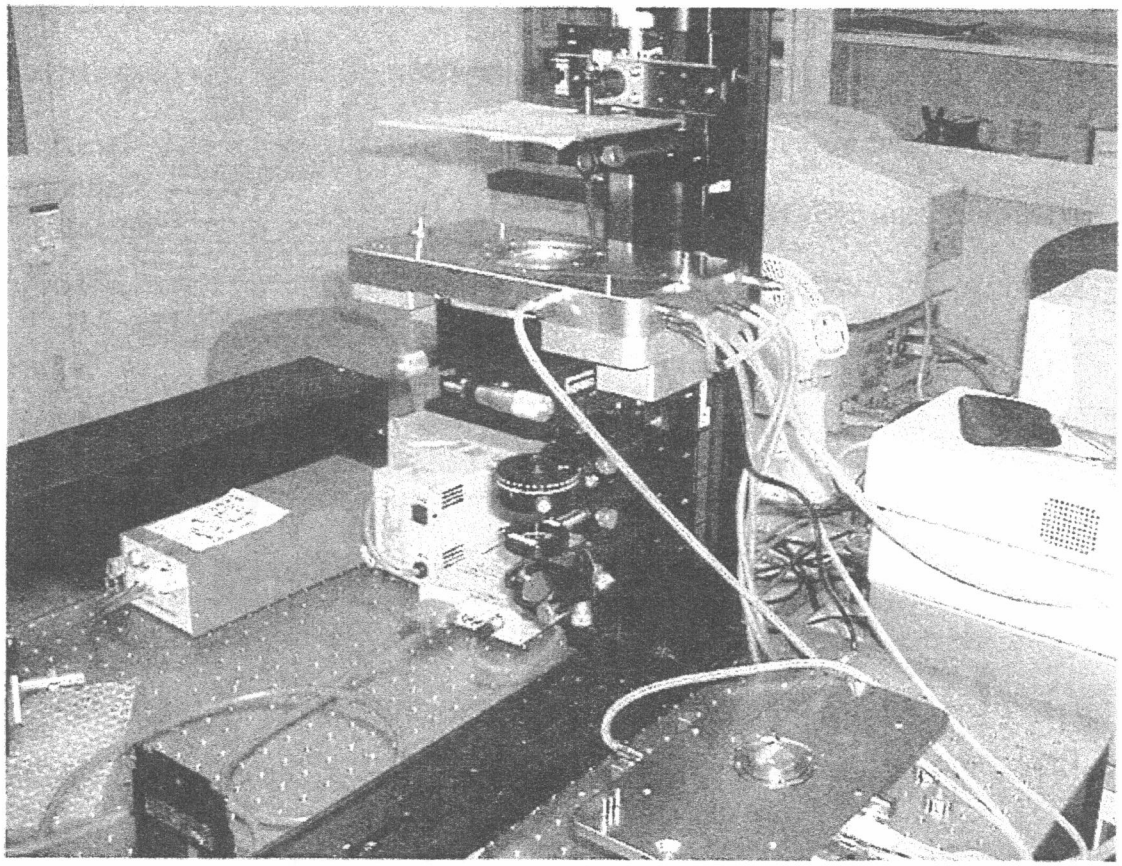

Fig. 7. A photograph of light scattering apparatus with a shear cell.

Small-angle X-ray scattering We used a small-angle X-ray scattering apparatus at the beam line BL45XU in the SR facility, SPring-8, Nishiharima, for in-situ SAXS measurements [46,47]. BL45XU is an undulator beamline with two branches. The branch we used is for small-angle X-ray scattering (SAXS) and the other is for protein crystallography (PX). The beam is split into the two branches by a diamond monochromator so that two experiments can be done simultaneously [48]. The SAXS branch was designed for studying the weak interaction of proteins or subunits of fibrous or protein solutions. The optics makes use of the good parallelism of the undulator beam in order to reduce parasitic scattering. The beamline consists of a double crystal monochromator and a K-B type focusing mirror system. In order to cope with the high flux of the beam, an X-ray image intensifier (Hamamatsu Photonics, V5445P) with a cooled CCD camera (C4880-82) was used. As a result, decreases in both collection time and sample amount were realized in standard static experiments. These improvements will greatly facilitate SAXS experiments under high pressure. Fig. 8(a) [46] shows the layout of BL45XU. When the slits hit the edge of the beam, it usually gives strong parasitic scattering. Slit 1 is used to reduce parasitic scattering on the mirrors and slit 2 is used to eliminate the tail of the beam, which is produced by imperfections in the mirror bend. Slit 3, the so-called guard slit, is used to define the beam size of the sample, and slit 4 is to eliminating parasitic scattering from slit 3. Fig. 8(b) shows a schematic of parasitic scattering in optimization of flux. La and Lb represent the extent of parasitic scattering from slit 2 and 3, respectively. S0, S1, S2, S3, S4, S5 are the beam sizes at the source, mirror, focus, slit2, slit3,

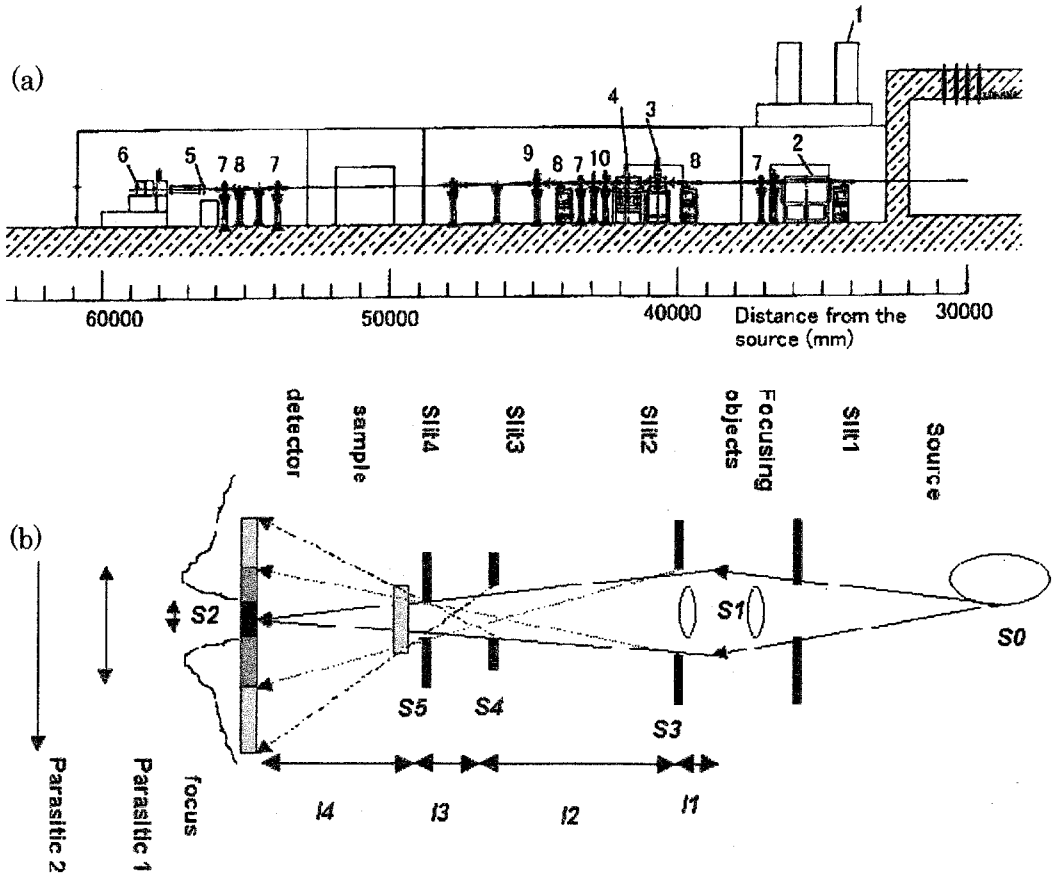

Fig. 8. Layout of optics of SPring-8 BL45XU (a). Schematic of parasitic scattering in optimization of flux (b).

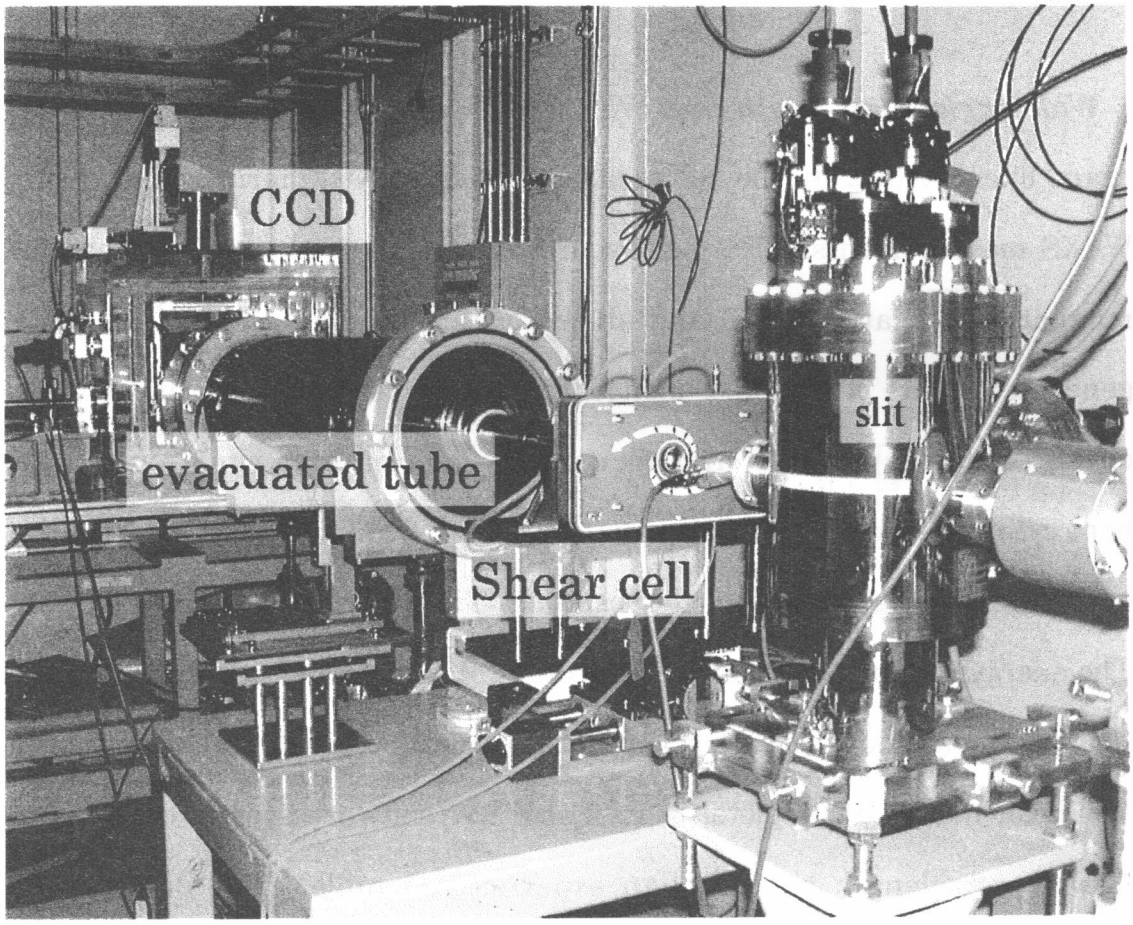

Fig. 9. Shear cell location in the SAXS apparatus at SPring-8 BL45XU.

slit4, respectively. l1, l2, l3, l4 are the distances between slit4-detector, slit3-slit4, slit2-slit3, and slit2-mirror, respectively. In principle the larger in l3 is the smaller in La [46]. Fig.9 shows our setting of shear flow measurement around sample cell. X-ray beam comes from slit side tube.

Wide-angle X-ray scattering We used a wide-angle apparatus at the beam line BL40B2 at the SR facility, SPring-8, Nishiharima, for in-situ WAXS measurements. The light source is a bending magnet that has its magnetic field at 0.679 T and shows critical energy of 28.9 keV. The generated white X-rays are monochromatized using a fixed-exit double crystal monochromator and focused by a 1-m-long rhodium-coated bent-cylinder mirror. The glancing angle of 3.2 mrad is adjusted for the optimum focusing at the detector position. The photon flux is 10^{11} at 12 keV. The energy resolution ($\Delta E/E$) is in the order of 10^{-4} [49]. The total system of monochromatic data collection for routine macromolecular crystallography has been installed completely. Its LabVIEW software system contains to change wavelength and to align experimental table. The detector for protein crystallography is set on camera stage, which camera length of 80 mm - 470 mm is available. A detector choice between CCD and Imaging Plate is easily available using off-line exchange system (Fig. 10). BL40B2 is the beam line for SAXS, but we shortened the camera length to measure wide-angle Q range. There are many beam lines for measurements of crystal diffraction in SPring-8. In the experiments of this thesis we used a Linkam CSS-450 high temperature shear cell, which has two flat quartz plate for applying shear cell. Hence we needed a WAXS apparatus in which

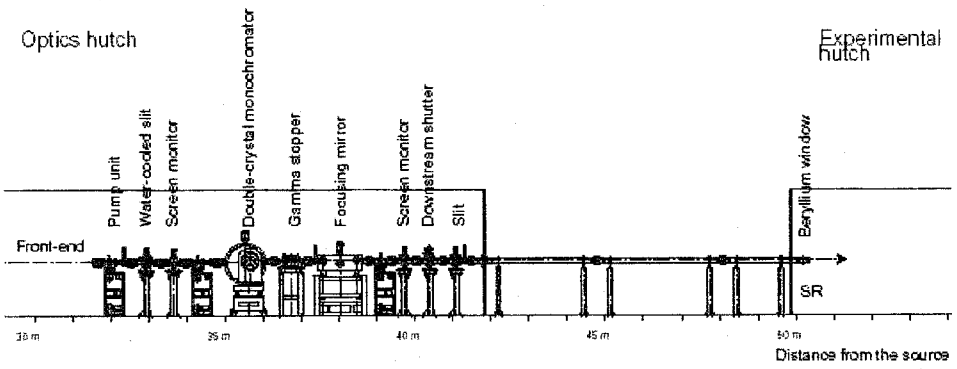

Fig. 10. Layout of optics of SPring-8 BL40B2.

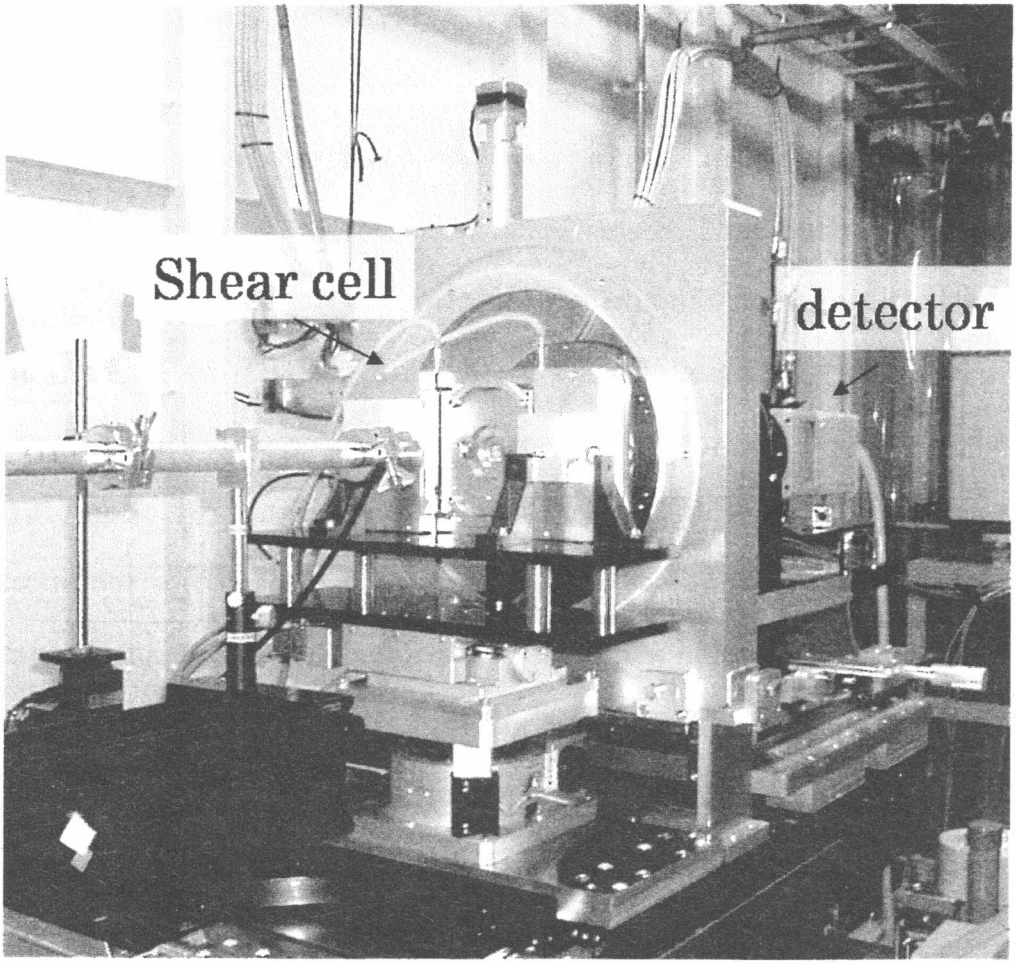

Fig. 11. Shear cell location in the WAXS measurement at SPring-8 BL40B2.

flat sample can be used. For this reason we employed SAXS machine at the beam line BL40B2 for the WAXS measurements. Fig. 11 shows our setting of shear flow measurement around sample cell. X-ray comes from left side tube.

Small-angle neutron scattering We used SANS-U apparatus for small-angle neutron scattering measurements. The SANS-U, owned by the Institute for Solid State Physics, The University of Tokyo, was constructed in the guide hall of the 20 MW research reactor, JRR-3M, of the Japan Atomic Energy Research Institute (JAERI) in 1991 [50]. Fig. 12 shows the layout of SANS-U. This instrument is composed of (a) a mechanical neutron velocity selector (NVS), (b) a pre-sample flight path, (c) a multi purpose sample stage, (d) an evacuated post-sample flight path, (e) an area detector, (f) a point detector for transmission measurements, (g) a beam stop made of B4C, and (h) a data acquisition system. The incident neutron beam from the cold source (white beam flux » 2 × 108 $cm^{-2}s^{-1}$ with the peak wavelength of 0.4 nm) is monochromatized by a NVS with helical slits (ASTRIUM, Germany) (Friedrich, 1989). Cold neutron beam from the reactor was guided to the NVS. If necessary, the beam can be attenuated by (i) polyacrylate slabs with different thicknesses (3, 5, and 7 mm). Just behind the NVS is located the pre-sample flight path, which consists of (j) pinhole tubes coated with B4C inside and (k) alternate neutron guide tubes coated with Ni inside. By replacing the pinholes and the guide tubes in or out of the beam, users can change the effective source-to-sample distance (= collimation length, CL) to 1, 2, 4, 8, 12, or 16 m in order to vary the divergence and flux of the incident

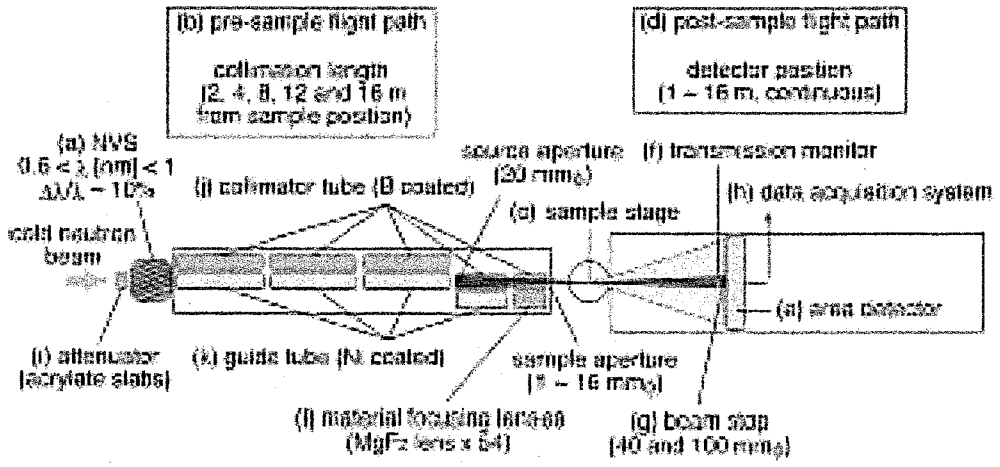

Fig. 12. The layout of optics of SANS-U.

beam at the sample position. Normally, a symmetric optical arrangement, i.e., CL = SDD (sample-to-detector distance), is recommended to optimize the flux and divergence of the beam. The collimator apertures are 20 mmφ each and the sample aperture can be chosen from 1, 3, 5, 7, 8, 10 to 16 mmφ. (1) A set of material focusing lenses (Eskildsen, 1998; Choi, 2000), made of 54 pieces of MgF_2 biconcave lenses, can be inserted at the lower-most collimator tube position for converging optics. The focal length is 8.0 m for λ = 0.70 nm.

Scattered neutrons are fed by an evacuated flight path, in which an area detector of 64.5 cm × 64.5 cm is installed on a truck running on rails to vary the SDD continuously from 1m to 16 m. A slide-in type direct beam stop and beam monitor for measurements of transmission are mounted on the truck just in front of the detector.

1-2-3 Sample preparation and shear flow apparatus

Sample preparation We investigated crystallization processes of some homo polymers and blends of high and low molecular weight components. Here we describe the sample preparation in this thesis.

In chapter 2, we used homo polyethylene (PE). We hot-pressed the PE sample sandwiched with two aluminum plates at 165 °C using a pressing machine manufactured by GONNO Inc. After pressing, we quenched the PE sample into iced water. In this procedure we obtained the sample sheet hundreds μm in thickness. We cut the sheet in a circle with scissors.

In chapters 3 and 4, we used homo isotactic polypropylene (i-PP). i-PP was hot pressed at 230 °C in the same way as PE.

In chapter 5, we used a blend of low molecular weight PE and high molecular weight PE. At first, we added low molecular weight PE and high molecular weight PE to excess xylene. The concentration of total PE was about 1 wt%. We further added 2,6-di-*tert*-buthyl-*p*-cresol to the solution as antioxidant for PE polymer chains. After keeping the solution at 135 °C for about 1 hour with stirring, the solution was quenched into iced water to get the gel. We confirmed that the phase separation did not occur in the blend. We removed the solvent from the gel by filtering and washed with methanol several times. The gel was dried at 70 °C in a vacuum for 2 days. We hot-pressed the PE blend to get a film in the same manner as in the case of homo PE.

In chapter 6, we used homo polyhydroxybutyrate (PHB). Homo PHB films were prepared in hot-pressing at 180 °C in the same way as in the case of homo PE. PHB is weak for heating and we pressed PHB at 180 °C for 1 min to avoid the thermal degradation.

In chapter 7, we used a blend of medium molecular weight PHB and high molecular weight PHB. Both PHBs were added to hot chloroform with stirring to dissolve completely. The solution was then left for a week, guaranteeing complete dryness, and then pressed at 180 °C. Process after pressing is the same as the homo PHB.

Shear flow apparatus We used a Linkam CSS-450 shear apparatus shown in Fig. 13 to control the temperature and shear conditions of the samples. Fig. 14 shows the lower part of the shear cell. The sample films were sandwiched between two quartz plates for light scattering and optical

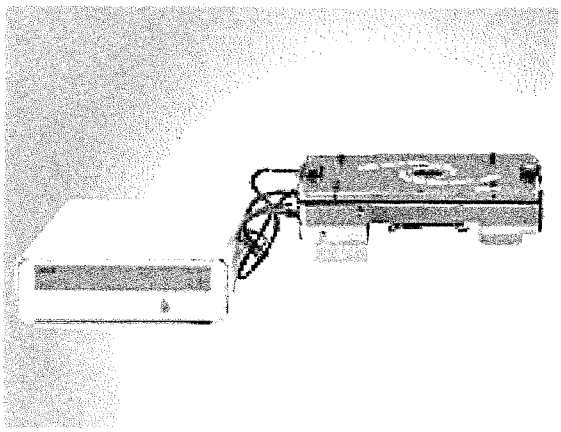

Fig.13. Linkam CSS-450 shear cell and temperature controller.

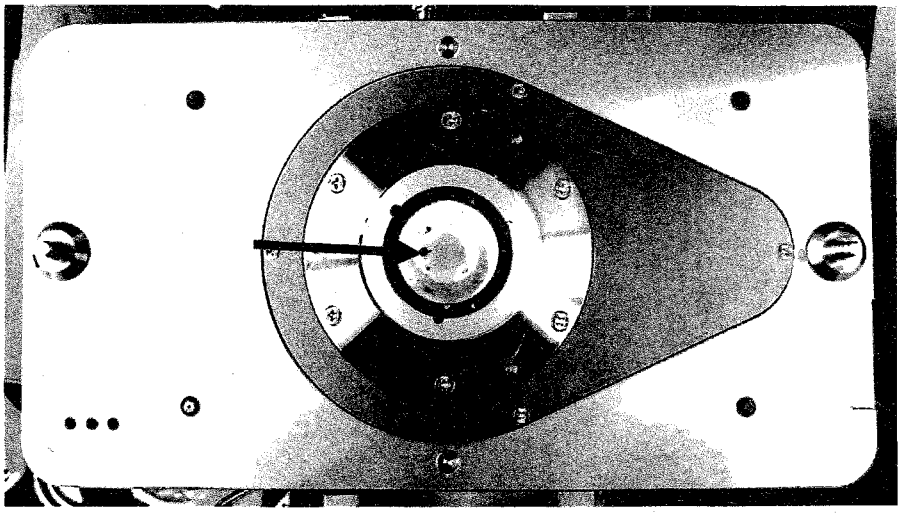

Fig. 14. The lower part of the shear cell. The arrow shows a hole for incident beam for scattering experiments.

microscope measurements and between two stainless plats with Kapton windows for SAXS and WAXS measurements, respectively. We controlled the temperature and the shear conditions of the sample.

References

[1] Ward, I.M. *Structure and properties of oriented polymers*, Wiley, New York **1975**.

[2] Ziabicki, A. *Fundamentals of fiber formation*, Wiley, New York **1976**.

[3] Keller A. and Kolnaar J.W.H.; Meijer, H.E.H. Editor, *Processing of polymers*, VCH, New York **1997**, 189.

[4] Walczak, Z.K. *Processses of fiber formation*, Amsterdam, Elsevier **2002**.

[5] Ohta, Y.; Murase, H.; Hashimoto, T. *Journal of Polymer Science Part B-Polymer Physics* **2005**, *43*, 2639.

[6] Tosaka,M.; Murakami, S.; Poompradub, S.; Kohjiya, S.; Ikeda, Y.; Toki, S.; Sics, I.; Hsiao, B. S. *Macromolecules* **2004**, *37*, 3299.

[7] Yoshioka, T.; Tsuji, M.; Kawahara, Y.; Kohjiya, S.; Manabe, N.; Yokota, Y. *Polymer* **2005**, *46*, 4987.

[8] Yoshioka, T.; Tsuji, M.; Kawahara, Y.; Kikutani, T.; Kohjiya, S *Polymer* **2005**, *46*, 1886.

[9] Pennings, A. J.; Kiel, A. M. Kolloid-Zeitschrift and Zeitschrift Fur Polymere **1965**, *205*, 160.

[10] Pennings, A. J. *Journal of Polymer Science Part C-Polymer Symposium* **1977**, 55.

[11] Odell, J. A.; Grubb, D. T.; Keller, A. *Polymer* **1978**, *19*, 617.

[12] Bashir, Z.; Odell, J. A.; Keller, A. *Journal of Materials Science* **1984**, *19*, 3713.

[13] Bashir, Z.; Odell, J. A.; Keller, A. *Journal of Materials Science* **1986**, *21*, 3993.

[14] Samon, J. M.; Schultz, J. M.; Hsiao, B. S.; Seifert, S.; Stribeck, N.; Gurke, I.; Collins, G.; Saw, C. *Macromolecules* **1999**, *32*, 8121.

[15] Samon, J. M.; Schultz, J. M.; Wu, J.; Hsiao, B.; Yeh, F.; Kolb, R. *Journal of Polymer Science Part B-Polymer Physics* **1999**, *37*, 1277.

[16] Somani, R. H.; Hsiao, B. S.; Nogales, A.; Srinivas, S.; Tsou, A. H.; Sics, I.; Balta-Calleja, F. J.; Ezquerra, T. A. *Macromolecules* **2000**, *33*, 9385-9394.

[17] Schultz, J. M.; Hsiao, B. S.; Samon, J. M. *Polymer* **2000**, *41*, 8887-8895.

[18] Samon, J. M.; Schultz, J. M.; Hsiao, B. S.; Wu, J.; Khot, S. *Journal of Polymer Science Part B-Polymer Physics* **2000**, *38*, 1872.

[19] Samon, J. M.; Schultz, J. M.; Hsiao, B. S.; Khot, S.; Johnson, H. R. *Polymer* **2001**, *42*, 1547.

[20] Nogales, A.; Hsiao, B. S.; Somani, R. H.; Srinivas, S.; Tsou, A. H.; Balta-Calleja, F. J.; Ezquerra, T. A. *Polymer* **2001**, *42*, 5247.

[21] Somani, R. H.; Hsiao, B. S.; Nogales, A.; Fruitwala, H.; Srinivas, S.; Tsou, A. H. *Macromolecules* **2001**, *34*, 5902-5909.

[22] Somani, R. H.; Yang, L.; Hsiao, B. S.; Agarwal, P. K.; Fruitwala, H. A.; Tsou, A. H. *Macromolecules* **2002**, *35*, 9096.

[23] Somani, R. H.; Yang, L.; Hsiao, B. S. *Physica a-Statistical Mechanics and Its Applications* **2002**, *304*, 145.

[24] Yang, L.; Somani, R. H.; Sics, I.; Hsiao, B. S.; Kolb, R.; Fruitwala, H.; Ong, C. *Macromolecules* **2004**, *37*, 4845.

[25] Pogodina, N. V.; Siddiquee, S. K.; van Egmond, J. W.; Winter, H. H. *Macromolecules* **1999**, *32*, 1167.

[26] Pogodina, N. V.; Lavrenko, V. P.; Srinivas, S.; Winter, H. H. *Polymer* **2001**, *42*, 9031.

[27] Elmoumni, A.; Winter, H. H.; Waddon, A. J.; Fruitwala, H. *Macromolecules* **2003**, *36*, 6453.

[28] Kumaraswamy, G.; Issaian, A. M.; Kornfield, J. A. *Macromolecules* **1999**, *32*, 7537.

[29] Kumaraswamy, G.; Verma, R. K.; Issaian, A. M.; Wang, P.; Kornfield, J. A.; Yeh, F.; Hsiao, B. S.; Olley, R. H. *Polymer* **2000**, *41*, 8931.

[30] Kumaraswamy, G.; Kornfield, J. A.; Yeh, F. J.; Hsiao, B. S. *Macromolecules* **2002**, *35*, 1762.

[31] Kolb, R.; Seifert, S.; Stribeck, N.; Zachmann, H. G. *Polymer* **2000**, *41*, 2931.

[32] Kolb, R.; Seifert, S.; Stribeck, N.; Zachmann, H. G. *Polymer* **2000**, *41*, 1497.

[33] Jerschow, P.; JaneschitzKriegl, H. *International Polymer Processing* **1997**, *12*, 72.

[34] Pennings, A. J.; Vanderma.Jm; Kiel, A. M. *Kolloid-Zeitschrift and Zeitschrift Fur Polymere* **1970**, *237*, 336.

[35] Wikjord; Manley, R. St. J, *J. Macromol. Sci.(phys.)* **1968**, *B2*,501.

[36] Bashir, Z.; Hill, M. J.; Keller, A. *Journal of Materials Science Letters* **1986**, *5*, 876.

[37] Gutierrez, M. C. G.; Alfonso, G. C.; Riekel, C.; Azzurri, F. *Macromolecules* **2004**, *37*, 478.

[38] Nogami, K; Murakami, S; Katayama, K; Kobayashi, K. *Bull Inst Chem Res, Kyoto Univ* **1977**, *55*, 227.

[39] Corle . T. R; Kino, G. S, *Confocal scanning optical microscopy and related imaging systems*, Academic Press, San Diego **1996.**

[40] *Modern aspects of small-angle scattering*, edited by H. Brumberger, Kluwer Academic Publishers, Dordrecht, **1995.**

[41] Feigin, L. A; Svergun, D. I, *Structure analysis by small-angle X-Ray and neutron scattering*, edited by G. W. Taylor , Plenum Press, New York, **1987.**

[42] *Small angle X-ray scattering*, edited by Glatter, O; Kratky, O. Academic Press, London ; Tokyo, **1982.**

[43] *Neutron scattering at a pulsed source*, edited by Newport, R. J; Rainford, B. D; Cywinski, R. A. Hilger, Bristol, England ; Philadelphia, PA, USA, **1988.**

[44] G. R. Strobl, *The physics of polymers : concepts for understanding their structures and behavior*, Springer, New York ; Tokyo, **1996.**

[45] C. G. Windsor, *Pulsed neutron scattering*, Taylor & Francis, London, **1981.**

[46] Fujisawa, T.; Inoue, K.; Oka, T.; Iwamoto, H.; Uruga, T.; Kumasaka, T.; Inoko, Y.; Yagi, N.; Yamamoto, M.; Ueki, T. *Journal of Applied Crystallography* **2000**, *33*, 797.

[47] Fujisawa, T *SPring-8 Beamline Handbook* **2003**, 132.

[48] Yamamoto, M.; Fujisawa, T.; Nakasako, M.; Tanaka, T.; Uruga, T.; Kimura, H.; Yamaoka, H.; Inoue, Y.; Iwasaki, H.; Ishikawa, T.; Kitamura, H.; Ueki, T. *Review of Scientific Instruments* **1995**, *66*, 1833.

[49] Shimizu, N.; Inoue, K. *SPring-8 Beamline Handbook* **2003**, 90.

[50] Ito, Y.; Imai, M.; Takahashi, S. *Physica B* **1995**, *213*, 889.

Chapter 2

Crystallization of polyethylene under shear flow

-Effects of shear rate and shear strain-

2-1 Introduction

Crystalline polymers comprise more than two-thirds of the global polymer production and have a wide range of applications from packing, textile, automotive components, to biomedical implants. Polyethylene is one of the most popular polymer materials, and the crystallization process has been researched under various conditions for decades [1-7]. Polyethylene is exposed to various kinds of industrial processes, such as extrusion, injection molding, fiber spinning, film blowing, shear flow and so on. These processes can significantly affect the crystallization kinetics and final morphology [3-15]. There are many factors to affect the kinetics and morphology such as crystallization temperature, molecular weight, molecular weight distribution, shear rate and shear strain. In this chapter, focusing on the effects of shear rate as well as shear strain, we investigated the structural formation of PE in the early stage of crystallization under shear flow using time resolved depolarized light scattering (DPLS) technique. The main purpose of this experiment is to see the formation process of the shish-kebab structure, especially the shish structure. For this purpose we have employed short term shearing technique or pulse shear technique [16]. The PE used in the study has rather low molecular weight and rather wide molecular weight distribution as will be mentioned in the experimental part. The low molecular weight allows us to perform the experiment in wide

ranges of shear rate and shear strain. In addition, we empirically know that the shish-kebab formation is enhanced in samples with wide molecular weight distribution compared with narrow one. This is one of the reasons why we chose this PE with rather wide molecular distribution.

2-2 Experimental

2-2-1 Sample

We used polyethylene with molecular weight M_w = 58,600 and the polydispersity M_w/M_n = 8.01, where M_w and M_n are the weight- and number-average molecular weight, respectively. The PE was kindly supplied by Showa Denko Ltd. The nominal melting temperature of the PE determined by DSC measurements was 134 °C at the heating rate of 20 °C /min.

DSC measurements were carried out to characterize the thermal properties of the sample using Perkin–Elmer DSC-7. All the DSC scans were performed under nitrogen environment.

2-2-2 Measurements

Two-dimensional (2D) depolarized light scattering (DPLS) measurements were carried out using a home-made apparatus with He–Ne laser (80 mW, wavelength λ = 632.8 nm) as a light source and 2D screen and CCD camera as a detector system. The range of length of scattering vector Q in this experiment is 4×10^{-5} to 2.6×10^{-4} Å^{-1}, where Q is given by $Q = 4\pi\sin\theta/n\lambda$ (2θ and n being scattering angle and the refractive index, respectively).

A Linkam CSS-450 high temperature shear cell with quartz windows was

used to control the temperature and the shear conditions. The sample thickness in the cell was 300 μm for all the DPLS measurements. The temperature protocol for the shear experiments is shown in Fig. 1: (a) the polymer sample was heated up to 165 °C from room temperature at a rate of 30 °C/min, (b) held at 165 °C for 5 min, (c) cooled down to the crystallization temperature T_c= 129 °C at a rate of 30 °C/min, and then (d) held at 129 °C for the DPLS measurements. The polymer melt was subjected to pulse shear just after reaching the crystallization temperature T_c of 129 °C. The ranges of the shear rate and the shear strain were 0 to 32 s^{-1} and 800 to 19,200 %, respectively.

2-3 Results and discussion

Fig. 2 shows the time evolutions of the 2D DPLS patterns under quiescent crystallization condition $(\dot{\gamma} = 0s^{-1})$ and after pulse shear with shear rate $\dot{\gamma} = 16s^{-1}$ and shear strain ε = 3200 %. Under the quiescent condition, no scattering intensity is observed in the first 110 s after reaching T_c, corresponding to the so-called induction period, and then isotropic 2D DPLS pattern appears and increases in intensity with annealing time as seen in the upper row in Fig. 2. On the other hand, under the shear condition with $\dot{\gamma} = 16s^{-1}$ and ε = 3200 %, very weak anisotropic scattering pattern begins to appear at about 30 s after applying the pulse shear. This indicates that there are long scattering objects aligned along the flow direction, which must be the shish-like structure. The length of shish-like structure is in μm order judging from the scattering vector range in the DPLS measurements. It is no doubt that the shish-like structure is formed by the effect of the pulse

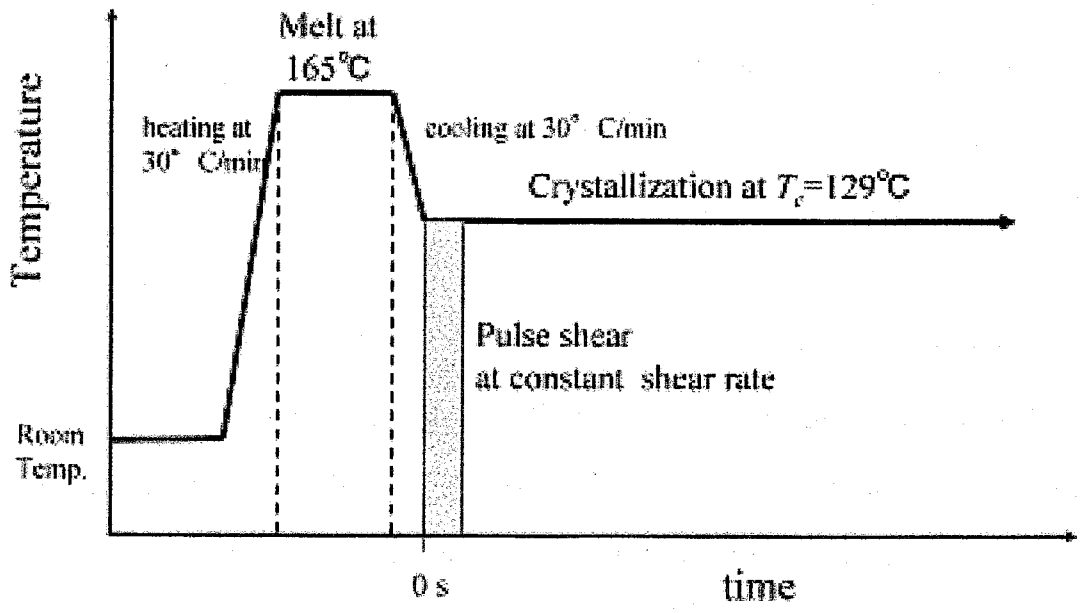

Fig. 1. Temperature protocol for the shear experiments on polyethylene.

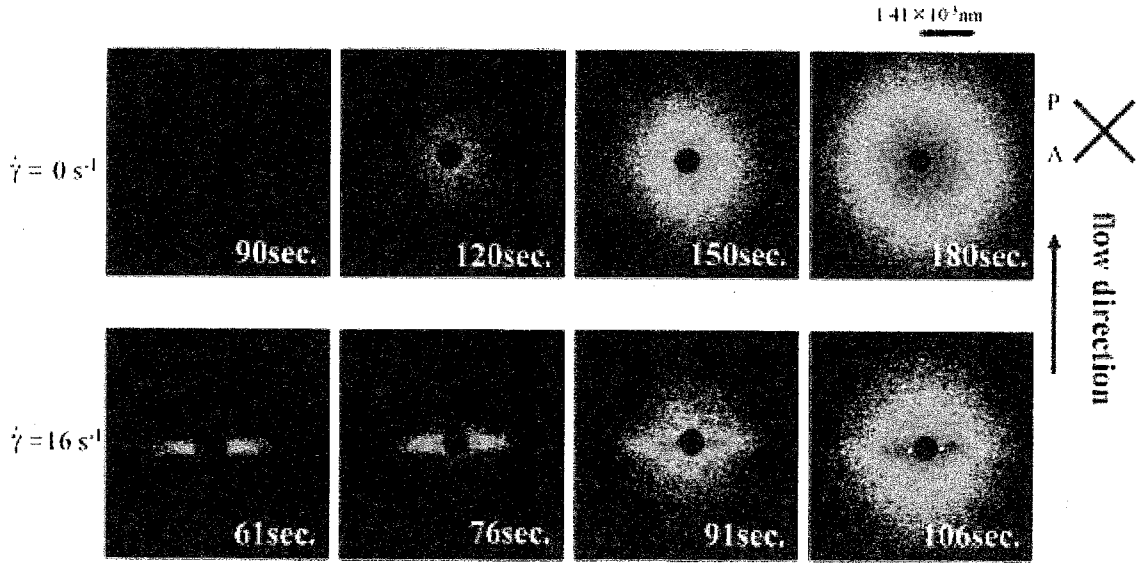

Fig. 2. Time evolution of 2D depolarized light scattering (DPLS) pattern from PE during the crystallization process at 129 °C. Upper: under quiescent condition, lower: after pulse shear with shear rate $\dot{\gamma} = 16s^{-1}$ and shear strain $\varepsilon = 3200$ %.

shear because the 2D pattern under the quiescent condition does not show any anisotropic scattering. The anisotropic streak-like scattering pattern gradually increases in intensity with annealing time while isotropic component also appears at about 80 s as seen in the lower row in Fig. 2. The isotropic scattering component suggests that some parts of PE are not affected by the shear to produce isotropic structure like spherulite.

We would like to briefly discuss if the shish-like structure is crystal or not (a precursor of the shish) in the early stage during the crystallization process because DPLS measurements can detect any oriented structure whether it is crystal or not. We have performed DSC measurements on the crystallization process of the same PE under the quiescent condition at 129 °C. The result is shown in Fig. 3. After the induction time of about 300 s, exotherm due to the crystallization is observed. On the other hand, DPLS intensity is already observed at 110 s (see Fig.2). These results imply that the DPLS measurement is so sensitive as to detect a precursor of the shish before the nucleation or a small amount of the (crystallized) shish compared with the DSC measurement. At the moment, it is hard to say which is correct. Hsiao et al. [17] has performed time resolved small-angle X-ray scattering measurements on structural development of isotactic polypropylene (i-PP) after applying pulse shear above the nominal melting temperature to find a streak-like scattering normal to the flow direction, corresponding to the shish-like structure. It should be emphasized here that this observation was above the nominal melting temperature, suggesting that the shish-like structure is not crystal. So, it is impossible to deny that the observed streak-like scattering pattern is due to the precursor.

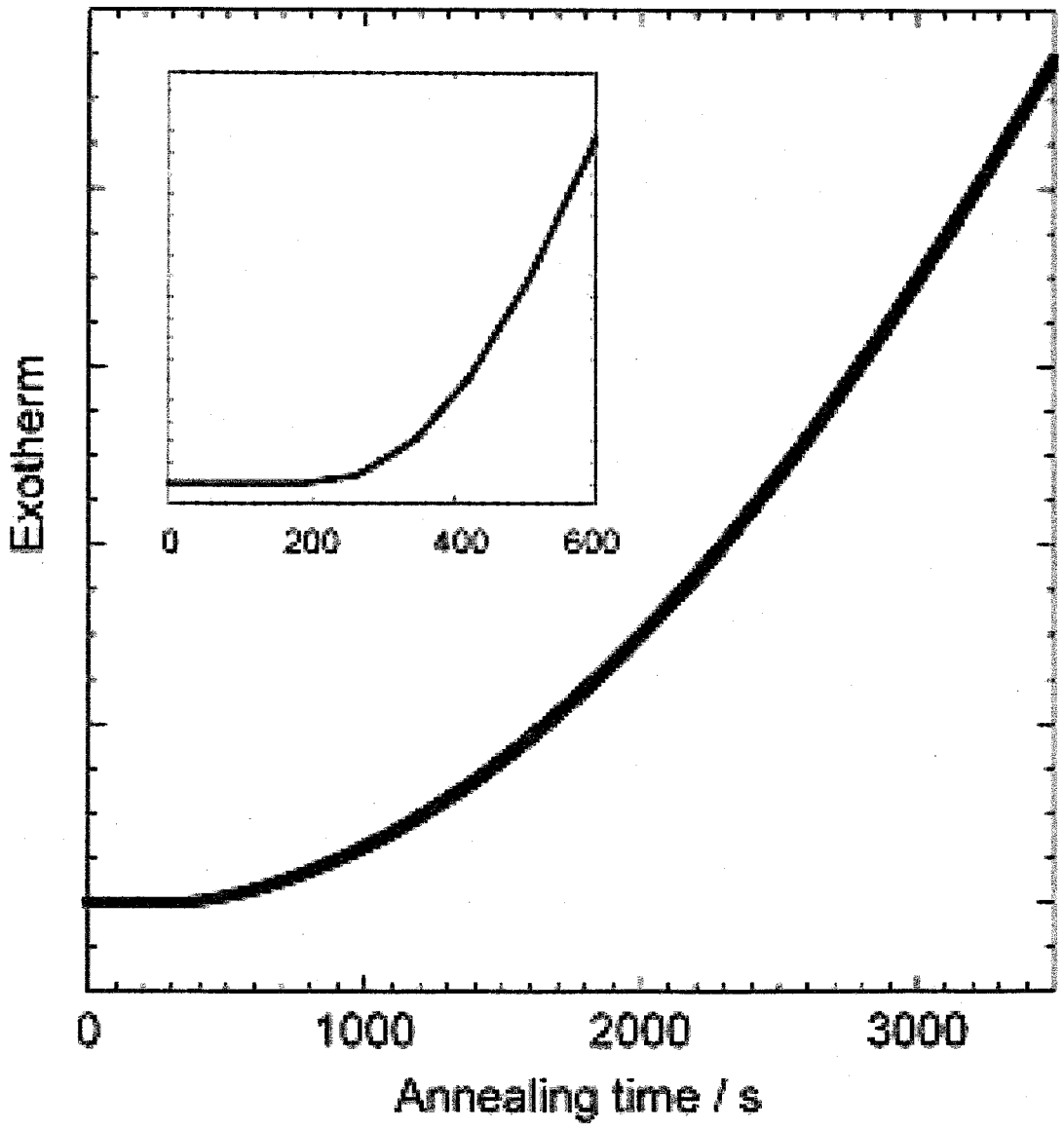

Fig. 3. DSC isotherm of PE at 129 °C after temperature.

Hence, we do not use the shish structure, but the shish-like structure here.

We have examined effects of the shear rate $\dot{\gamma}$ and the shear strain ε on the structure formation during the crystallization after pulse shear. Fig. 4 shows time evolutions of 2D DPLS patterns for shear rates $\dot{\gamma}$ of 1, 4 and 16 s^{-1} at a given shear strain ε of 3200 %. The scattering patterns are isotropic at both the shear rates of 1 and 4 s^{-1}, while the scattering pattern at $\dot{\gamma} = 4s^{-1}$ appears earlier than that at 1 s^{-1}, showing acceleration of the crystallization rate with increasing the shear rate. On the other hand, comparing the scattering patterns between $\dot{\gamma}$ = 4 and 16 s^{-1}, the 2D pattern at 16 s^{-1} is anisotropic and shows the streak-like scattering in addition to the acceleration of the crystallization rate. It is clear that the shear rate affects the crystallization rate as well as the anisotropic structure formation. The acceleration is observed at the relatively low shear rates while the anisotropic structure formation is at the relatively high shear rates.

In Fig. 5, the time evolutions of 2D DPLS patterns are shown for various shear strains ε = 1600, 3200 and 6400 % at a given shear rate $\dot{\gamma} = 4s^{-1}$. Similar to the shear rate effects, the acceleration of the crystallization rate and the appearance of anisotropic scattering patterns are observed as the shear strain increases.

In order to evaluate quantitatively the effects of shear rate on the structure formation, the following two measures are defined in this chapter. In Fig. 6 the integrated DPLS intensity normal to the flow direction is plotted as a function of the annealing time for various shear rates $\dot{\gamma}$ at a given shear strain ε = 3200 %. The scattering intensity is very weak in the induction period and abruptly begins to increase. This induction time t_{ind}

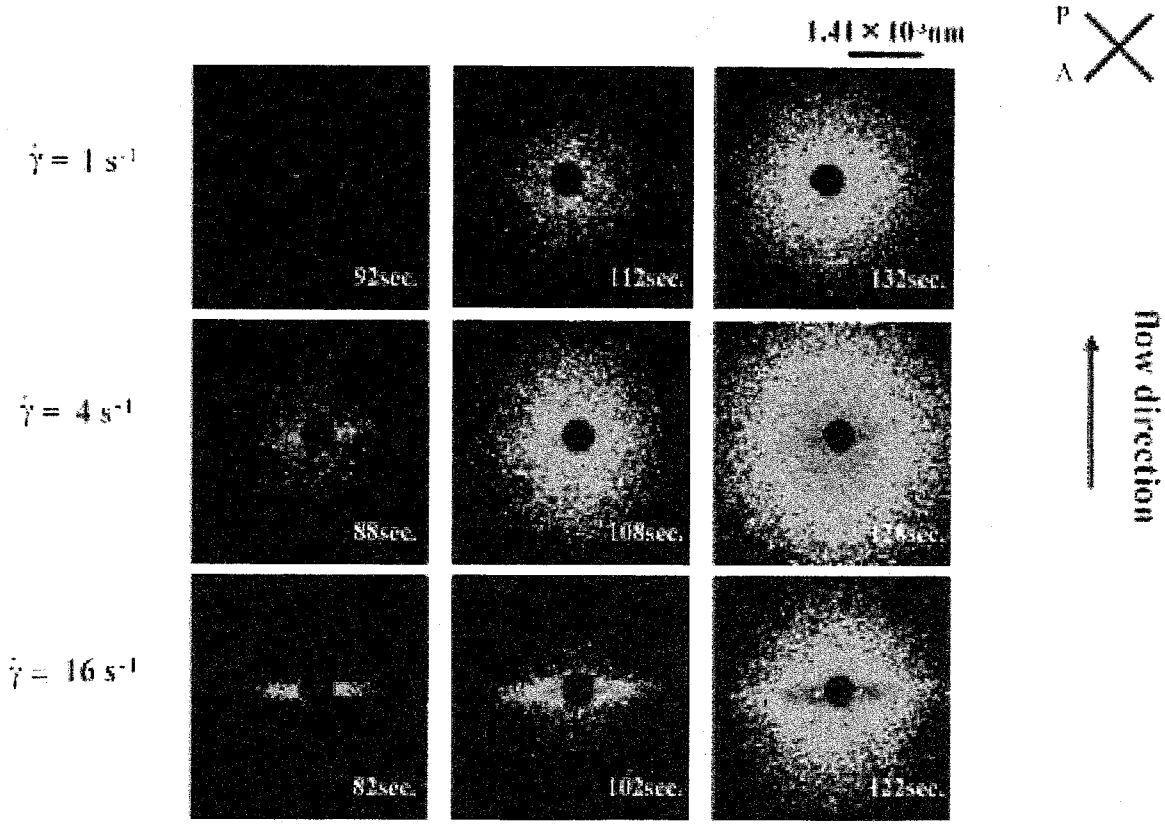

Fig. 4. Time evolution of DPLS pattern form PE during the crystallization process at 129 °C after pulse shear.

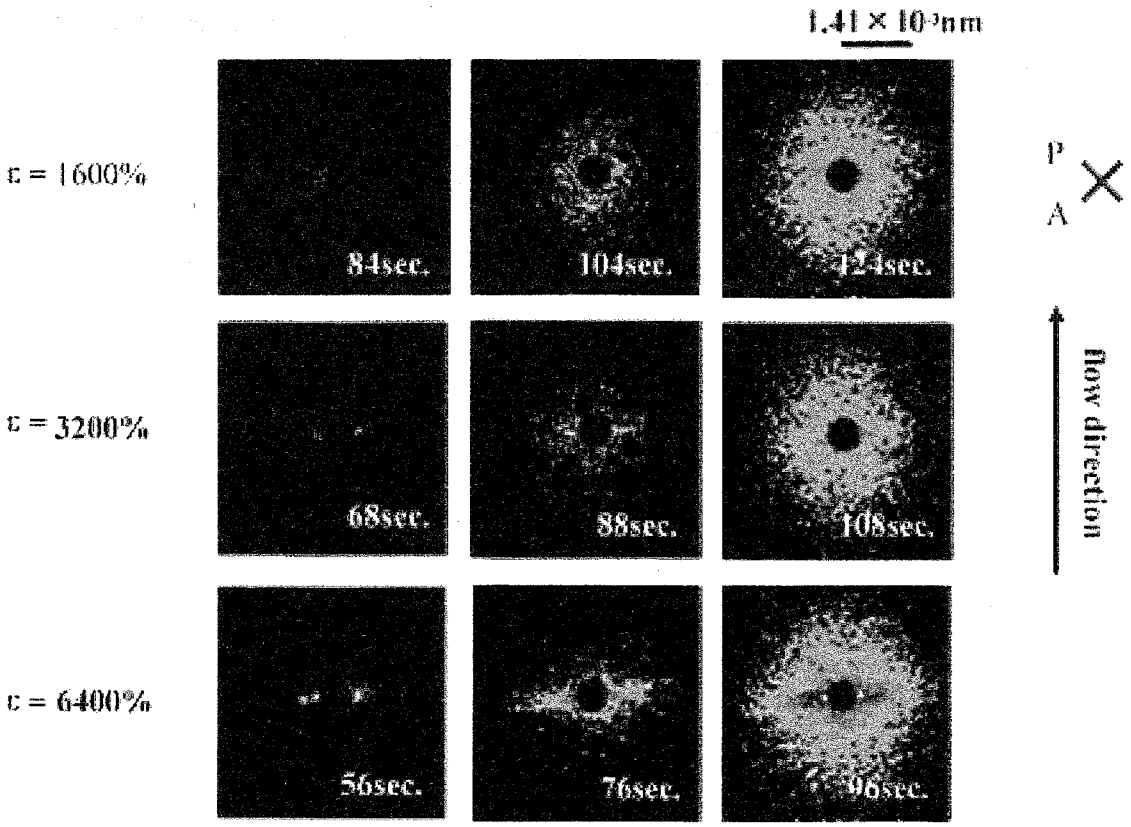

Fig. 5. Time evolution of 2D DPLS pattern form PE during the crystallization process at 129 °C after pulse shear.

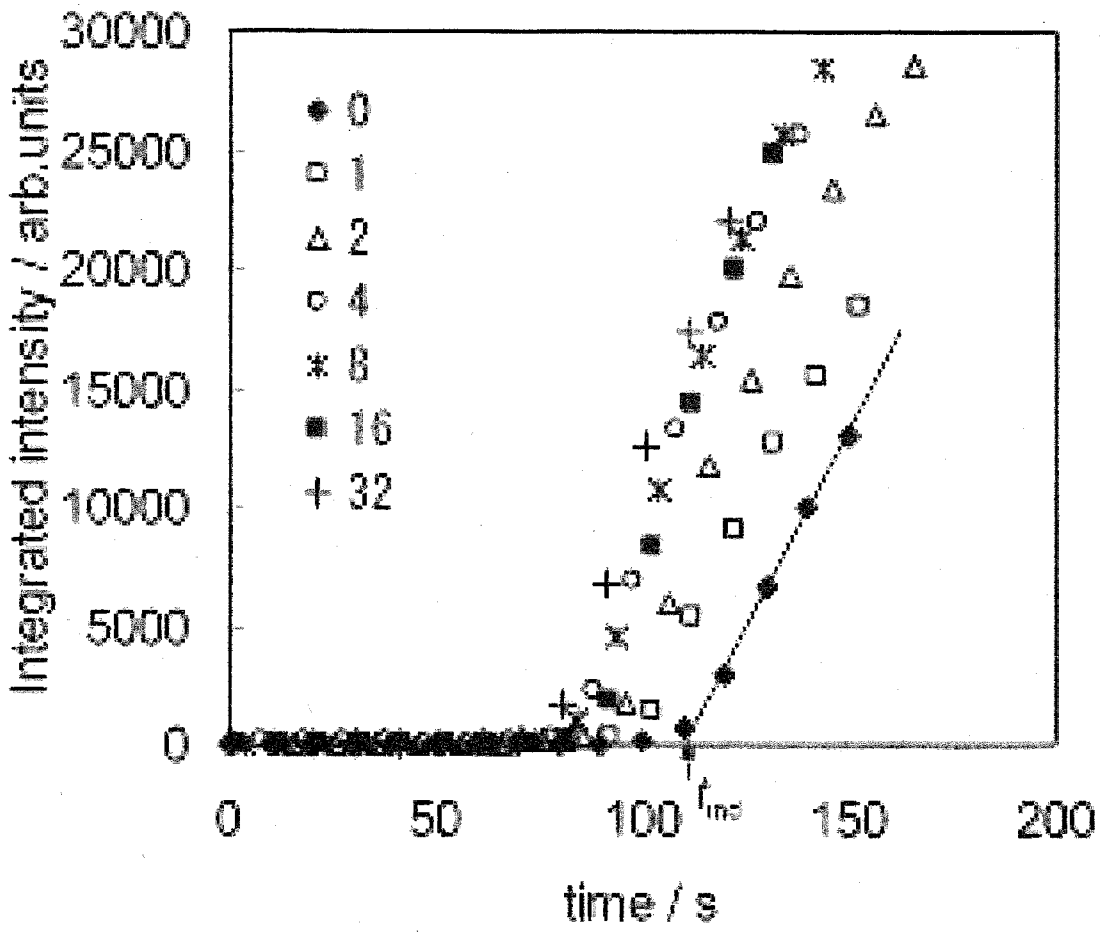

Fig. 6. Time evolution of integrated DPLS intensity of PE at 129 °C normal to the flow direction for various shear rates $\dot{\gamma}$ from 0 to 32 s^{-1}, showing the definition of induction time t_{ind}. The shear strain ε is 3200 % for all the measurements.

decreases with increasing the shear rate, showing the acceleration of the crystallization rate. We then employed the induction time t_{ind} as a measure of the acceleration of crystallization rate. Generally speaking, the crystallization rate is dominated by the nucleation rate and the growth rate, and the induction time t_{ind} is mainly governed by the nucleation rate. Therefore, we discuss the acceleration of the nucleation rate due to the shear flow here. The slope of the scattering intensity vs. time after the induction time would be used as a measure of the crystallization rate, especially the growth rate. However, this measure was not employed here because the sample thickness is rather thick so that the scattering intensity is not proportional to the degree of crystallinity in the late stage. Second measure is for the anisotropy. A typical anisotropic 2D scattering pattern is shown in Fig. 7(a) and the corresponding scattering intensities normal and parallel to the flow direction are plotted against Q in Fig. 7(b). In the high Q range the scattering intensities are very weak and begin to increase at certain onset Q values with decreasing Q, depending on the scattering direction. Here we employed a ratio of the onset Q value normal to the flow direction to the parallel one R_{ani} (= $Q_{\perp}/Q_{//}$) as a measure of anisotropy. The onset $Q_{//}$ parallel to the flow direction was sometimes inside in the beam stopper as shown in Fig. 7(c). In this case we cannot follow the above procedure to determine $Q_{//}$, and hence employed another procedure. We draw the contour curve at a height of d_Q which was used to determine $Q_{\perp}$ (see Fig. 7(d)) and interpolated the contour curve inside the beam stopper. Then, we define the $Q_{//}$ as shown in Fig. 7(c). This definition is slightly different from the first one, but the degree of anisotropy is almost the same within the

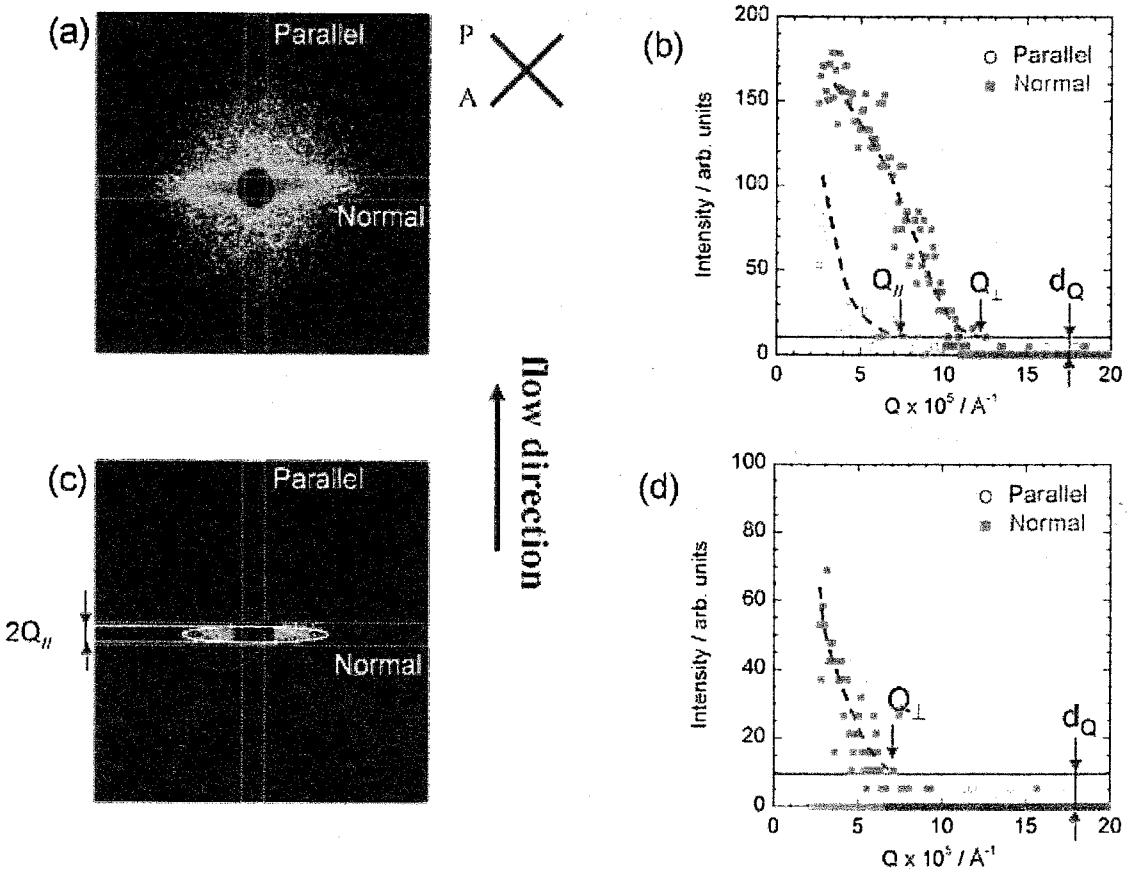

Fig. 7. (a) and (c) Typical 2D DPLS patterns; (b) and (d) the definitions of the degree of anisotropy R_{ani} ($=Q_{\perp}/Q_{//}$) corresponding to (a) and (c), respectively.

experimental error. The measure is a sort of aspect ratio of the 2D scattering pattern and called the degree of anisotropy here.

2-3-1 Evaluation of critical shear rate for anisotropy

We first examined the shear rate effects on the induction time t_{ind} and the degree of anisotropy R_{ani}. The induction time t_{ind} and the degree of anisotropy R_{ani} are plotted against the logarithm of the shear rate $\dot{\gamma}$ in Fig. 8(a) and (b), where the shear strain ε is kept constant at 3200 %. The induction time t_{ind} under the quiescent condition $(\dot{\gamma} = 0)$ is about 110 s and decreases with increasing the shear rate. As seen in Fig. 8(a), the linear relationship between the induction time t_{ind} and the logarithm of the shear rate $\dot{\gamma}$ holds, at least in the shear rate range examined although we do not have any theoretical basis for this relation. The relation is given by:

$$\dot{\gamma}_{ind,c} = \dot{\gamma}\exp\left[\frac{t_{ind} - t_{ind,0}}{\tau_{ind}}\right] \tag{2.1}$$

where $\dot{\gamma}_{ind,c}$, $t_{ind,0}$ and τ_{ind} are the critical shear rate for the induction time, the induction time under quiescent condition and a constant with unit of time. According to the relation, we have extrapolated the induction time to 110 s to find the critical shear rate for the acceleration of the crystallization rate at around $\dot{\gamma}_{ind,c}$ = 0.4s^{-1} (Fig. 8(a)). As for the relation between the degree of anisotropy R_{ani} and the logarithm of the shear rate $\dot{\gamma}$, similar linear relation holds experimentally. That is given by

$$\dot{\gamma}_{ani,c} = \dot{\gamma}\exp\left[-\frac{R_{ani} - R_{ani,0}}{r_{ani}}\right] \tag{2.2}$$

where $\dot{\gamma}_{ani,c}$, $R_{ani,0}$ and r_{ani} are the critical shear rate for the anisotropy, the

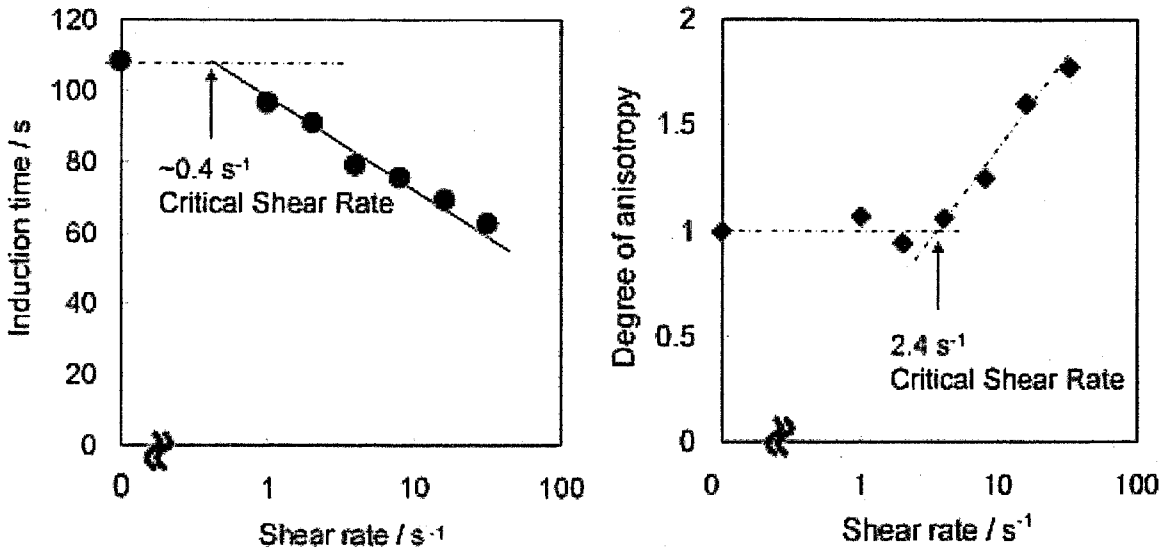

Fig. 8. Shear rate dependence of (a) the induction time t_{ind} and (b) the degree of anisotropy R_{ani}. The shear strain ε is 3200 %.

degree of anisotropy under quiescent condition (= 1), and a dimensionless constant. We also extrapolated the degree of anisotropy to unity and found the critical shear rate for the anisotropy at around $\dot{\gamma}_{ani,c}$ = 2.4s^{-1}. This value is much larger than the critical shear rate for the acceleration of crystallization rate $\dot{\gamma}_{ind,c}$ (= 0.4s^{-1}). In other words, the acceleration effect is observed in a low shear rate region while relatively large shear rate is necessary for the anisotropic structure formation. This problem is briefly discussed in terms of chain relaxation in what follows. Applying pulse shear polymer chains are somewhat extended, and after the cessation of the shear they tend to relax to recover the original non-oriented conformations. This process must be governed by the longest relaxation time. On the other hand, the chains want to crystallize because they are in the supercooled state below the melting temperature although the crystallization rate is not fast at the present T_c (= 129 °C) under quiescent condition, meaning that there must be a competition between the crystallization and the relaxation. In the present DPLS experiments, we observed that the detector screen was completely dark at 2 or 3 s after the cessation of the shear, suggesting the polymer chains completely relax to the original non-oriented conformation, at least in a length scale of light scattering. However, we observed the acceleration of the crystallization rate or the reduction in the induction time. This may mean that the local orientation remains in the chains, which induces the crystallization (orientation-induced crystallization). At the shear rates below the critical value for the anisotropy $\dot{\gamma}_{ani,c}$, the orientation must be too local to result in the anisotropic structure (the shish-like structure) in the light scattering scale. As the shear rate increases above

the critical value $\dot{\gamma}_{ani,c}$, the chains are more extended and crystallize earlier before the relaxation in the extended conformation, resulting in the anisotropic structure in the light scattering scale.

2-3-2 Estimation of the critical shear rate of infinite shear strain

We have determined the critical shear rates as a function of shear strain. The critical shear rate for the induction time $\dot{\gamma}_{ind,c}$ was almost zero at the shear strains above 3200 %, and hence it was hard to estimate the shear strain dependence of the critical shear rate $\dot{\gamma}_{ind,c}$ in the experimental accuracy. Therefore, we focus on the shear strain dependence of the critical shear rate for the degree of anisotropy $\dot{\gamma}_{ani,c}$. In Fig. 9, the degree of anisotropy R_{ani} is plotted against the logarithm of the shear rate $\dot{\gamma}$ for various shear strains, where the data in Fig. 8(b) is also included. As seen in figure, the critical shear rate for the degree of anisotropy $\dot{\gamma}_{ani,c}$ decreases with increasing the shear strain. The linear relation between the degree of anisotropy R_{ani} and the logarithm of the shear rate $\dot{\gamma}$ holds for all the shear strains examined in this study. Extrapolating the degree of anisotropy to unity we have evaluated the critical shear rate as a function of the shear strain, and plotted against the inverse of the shear strain in Fig. 10. The plot shows a good linear relationship. Extrapolating this linear relationship to the inverse of the shear strain = 0, we found that the critical shear rate at the infinite shear strain is about 1.5 s^{-1}. This corresponds to the critical shear rate under continuous shear flow.

The same analysis has been done on the shear strain dependence of the degree of anisotropy R_{ani}. The degree of anisotropy R_{ani} is plotted against

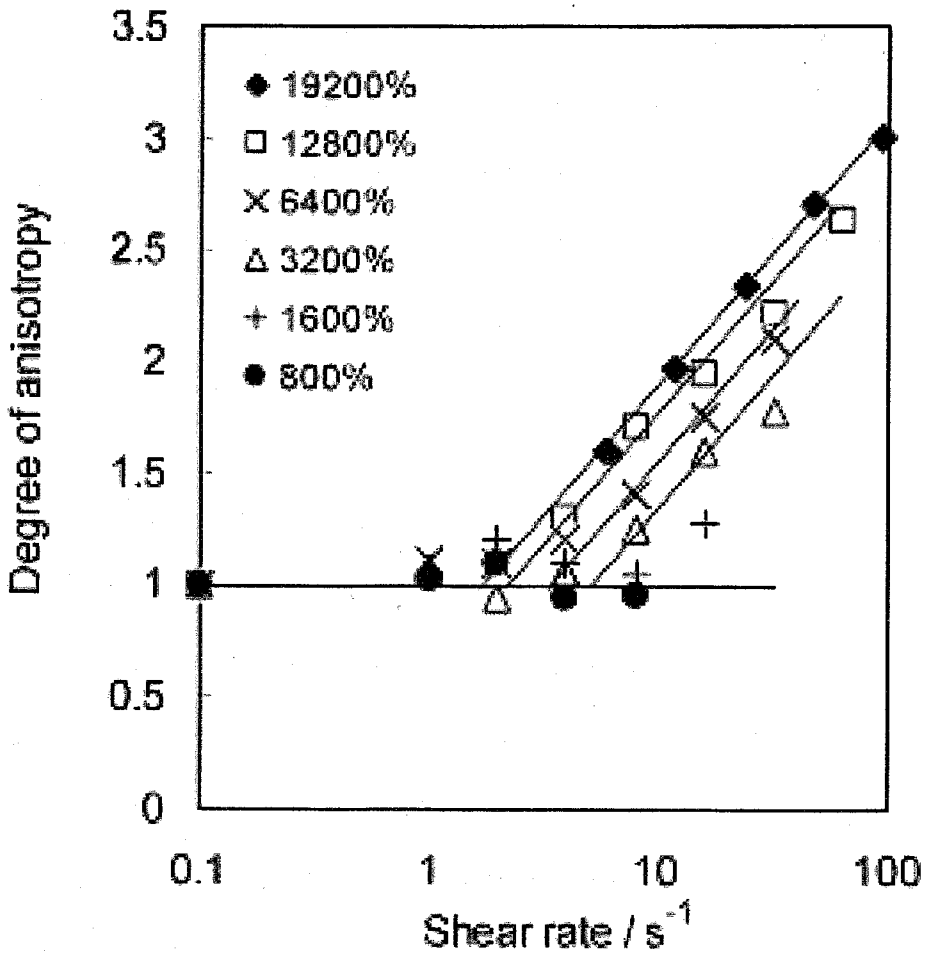

Fig. 9. Shear rate dependence of the degree of anisotropy R_{ani} for various shear strains ε from 800 % to 19,200 %.

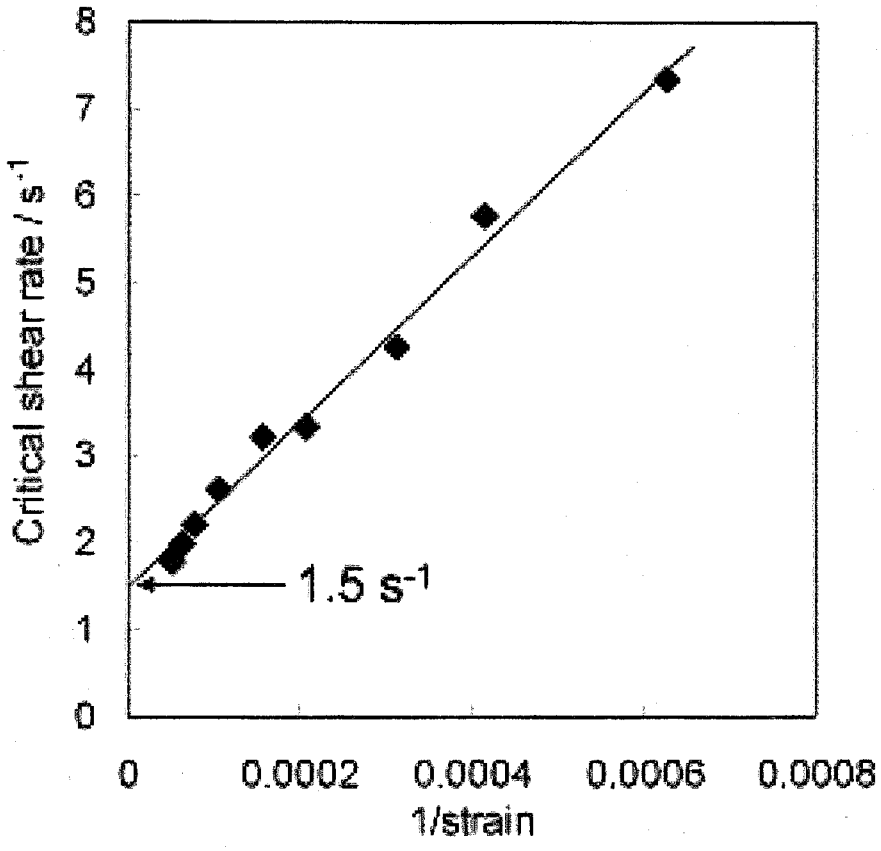

Fig. 10. Critical shear rate for the anisotropy $\dot{\gamma}_{ani,c}$ against inverse of shear strain ε.

the shear strain for various shear rates of 1-32 s^{-1} in Fig. 11. In this plot, we also assumed that the linear relationship holds between the degree of anisotropy R_{ani} and the logarithm of shear strain ε. Note that the anisotropy at the low shear rates below 4 s^{-1} is very low and not reliable. Extrapolating the linear relation to the degree of anisotropy = 1, we have evaluated the critical shear strain at each shear rate, and the inverse of the critical shear stain is plotted against the shear rate in Fig. 12, giving a straight line. Again, extrapolating this relation to inverse of the critical shear strain = 0, we have evaluated the critical shear rate at the infinite shear strain to be 1.5 s^{-1}. This value agrees very well with the critical shear rate at the infinite shear strain evaluated from the relation between the critical shear rate and the inverse of shear strain (see Fig. 10). This suggests the validity of the analysis. Here we would like to consider a possible physical meaning of the critical shear rate at the infinite shear strain, which must correspond to the continuous shear flow. In this situation, the extension of polymer chain is almost dominated by the relation between the shear rate $\dot{\gamma}$ and the longest relaxation time τ. If the shear rate is larger than the relaxation rate (or inverse of the relaxation time) τ^{-1}, the polymer chains are somewhat extended and oriented under the flow. The polymer chains are in the supercooled state below the melting temperature, and hence tend to crystallize. The orientation must accelerate the crystallization rate (orientation-induced crystallization). Thus, the critical shear rate is related to the relaxation rate: $\dot{\gamma}_{ani,c} \sim \tau^{-1}$, if we neglect a numerical factor in order of unity. This is one of tentative scenarios for the shish formation in the early stage of crystallization. In order to confirm this

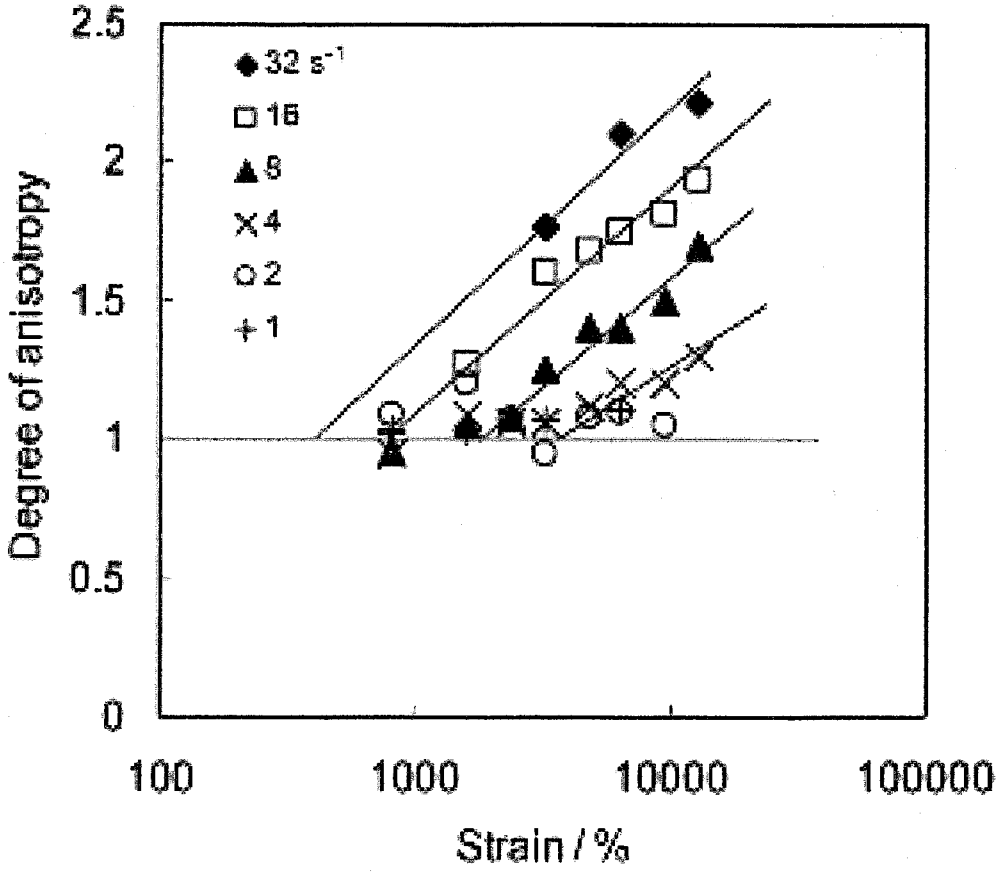

Fig. 11. Shear strain dependence of the degree of anisotropy R_{ani} for various shear rates $\dot{\gamma}$ from 1 to 32 s^{-1}.

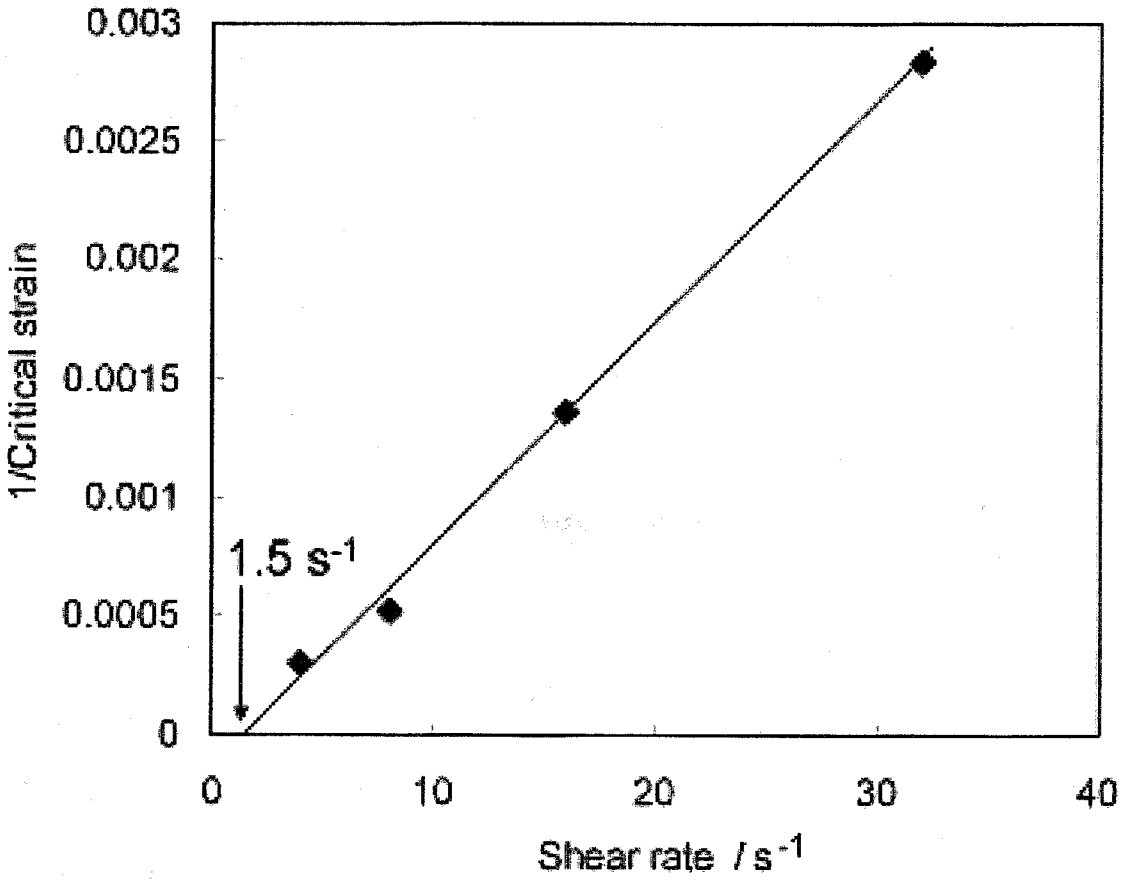

Fig. 12. Inverse of critical shear strain $1/\varepsilon_{ani,c}$ against shear rate $\dot{\gamma}$.

scenario it must be essential to examine effects of the molecular weight distribution and the rheological properties on the crystallization.

2-4 Conclusion

We have investigated the structure formation of PE in the early stage during the crystallization after pulse shear using depolarized light scattering (DPLS), focusing on the effects of the shear rate and the shear strain. The objective of this study is to elucidate the formation mechanism of the so-called shish-kebab structure. In the early stage during the crystallization after pulse shear 2D DPLS pattern clearly shows the streak-like scattering normal to the flow direction, suggesting the formation of shish-like structure in μm scale along the flow. Defining measures for the acceleration of the crystallization rate and the degree of anisotropy, we have determined the critical shear rate for both of the measures at a given shear strain, and found that the critical shear rate for the former is much smaller than the latter. Analyzing the shear strain dependence of the critical shear rate for the anisotropy we have estimated the critical shear rate at the infinite shear strain, which must correspond to the continuous flow. This critical shear rate was discussed in relation to the competition between the chain relaxation and the orientation-induced crystallization rate.

References

[1] Keller, A. *Polymer* **1962**, *3*, 393.

[2] Pennings, A. J.; Kiel, A. M. *Kolloid-Zeitschrift and Zeitschrift Fur Polymere* **1965**, *205*, 160.

[3] Odell, J. A.; Grubb, D. T.; Keller, A. *Polymer* **1978**, *19*, 617.

[4] Bashir, Z.; Odell, J. A.; Keller, A. *Journal of Materials Science* **1984**, *19*, 3713.

[5] Bashir, Z.; Odell, J. A.; Keller, A. *Journal of Materials Science* **1986**, *21*, 3993.

[6] Samon, J. M.; Schultz, J. M.; Hsiao, B. S.; Seifert, S.; Stribeck, N.; Gurke, I.; Collins, G.; Saw, C. *Macromolecules* **1999**, *32*, 8121.

[7] Yang, L.; Somani, R. H.; Sics, I.; Hsiao, B. S.; Kolb, R.; Fruitwala, H.; Ong, C. *Macromolecules* **2004**, *37*, 4845.

[8] Flory, P. J. *Journal of Chemical Physics* **1947**, *15*, 397.

[9] Ward, I. M. *Structure and Properties of Oriented Polymers*, Willy, New York **1975**.

[10] Ziabicki, A. *Fundamentals of Fiber Formation*, Wiley, New York **1976**.

[11] Ziabicki, A., Kawai, H., Eds.; *High-Speed Fiber Spinning*, Interscience, New York **1985**.

[12] Keller, A.; Kolnaar, J. W. H.; Meijer, H. E. H., *Processing of polymers,* VCH, New York **1997**, *18*, 189.

[13] Eder, G.; Janeschitz-Kriegl, H. *Mater. Sci. Technol.,* **1997** *18*, 268.

[14] Wilkinson, A. N.; Ryan, A. J. *Polymer Processing and Structure Development;* Kluwer: Dordrecht **1998**.

[15] Lee, O.; Kamal, M. R. *Polymer Engineering and Science* **1999**, *39*, 236.

[16] Jerschow, P.; JaneschitzKriegl, H. *International Polymer Processing* **1997**, *12*, 72.

[17] Samon, J. M.; Schultz, J. M.; Hsiao, B. S.; Seifert, S.; Stribeck, N.; Gurke, I.; Collins, G.; Saw, C. *Macromolecules* **1999**, *32*, 8121.

Chapter 3

Crystallization of isotactic polypropylene under shear flow

- Effects of shear rate and shear strain -

3-1 Introduction

Isotactic polypropylene (i-PP) is one of the most popular polymer materials and used in various industrial fields. The structure and the property depend on crystallization process, and hence extensive studies have been performed on the crystallization process of i-PP to control the structure and the properties [1-10]. i-PP is usually utilized after various processing processes such as spinning and moulding processes. In the processing processes, i-PP are exposed to various kinds of flows; shear flow, elongation flow and mixed flow. It is well known that when polymers are crystallized under flows, the so-called shish-kebab structure is often formed, which is molecular origin of ultra-high modulus and ultra-high strength polymers [11-16]. In order to elucidate the formation process of the shish-kebab structure many researches were carried out on the crystallization process of i-PP under flows using various experimental methods. In this chapter, we studied the crystallization process of i-PP under shear flow using depolarized light scattering, especially focusing on the shish structure, and discussed the effects of shear rate and shear strain on the formation of shish-kebab structure as done in Chapter 2 for polyethylene (PE).

3-2 Experimental

3-2-1 Sample

In the experiment we used isotactic polypropylene (i-PP) with the molecular weight M_w = 238,000 and the polydispersity M_n/M_w = 5.1, where M_w and M_n are the weight-average and number-average molecular weights, respectively. The i-PP was synthesized using metallocene catalysis. Tetrad tacticity determined by NMR measurements was *mmmm* = 0.974. The melting temperature T_m determined by DSC measurement is 149.3 °C and the glass transition temperature T_g from the literature is -3.2 °C [17].

3-2-2 Measurements

Two-dimensional (2D) depolarized light scattering (DPLS) measurements were carried out using a home-made apparatus. The apparatus has a He-Ne laser (80 mW, wavelength λ = 632.8nm) as a light source and a CCD camera with 2D screen as a detector system. The range of length of scattering vector Q in this experiment is 3.5 x 10^{-5} to 3 x 10^{-4} Å^{-1}, where Q is given by $Q = 4\pi\sin\theta/n\lambda$ (2θ and n being scattering angle and the refractive index, respectively). Linkam CSS-450 high temperature shear cell with quartz windows was used to control the temperature and the shear conditions. The sample thickness in the cell was 300μm for all the DPLS measurements. We performed experiments in a shear rate range of 0 to 35 s^{-1} and a shear strain range of 0 to 14000 %. Fig. 1 shows the temperature protocol in the experiments in this chapter: (a) the polymer sample was heated up to 210 °C from room temperature at a rate of 30 °C/min, (b) held at 210 °C for 5min, (c) cooled down to the crystallization temperature T_c = 132 °C at a rate of 30 °C/min, and then (d) held at 132 °C for the DPLS measurements. When the temperature reached the crystallization

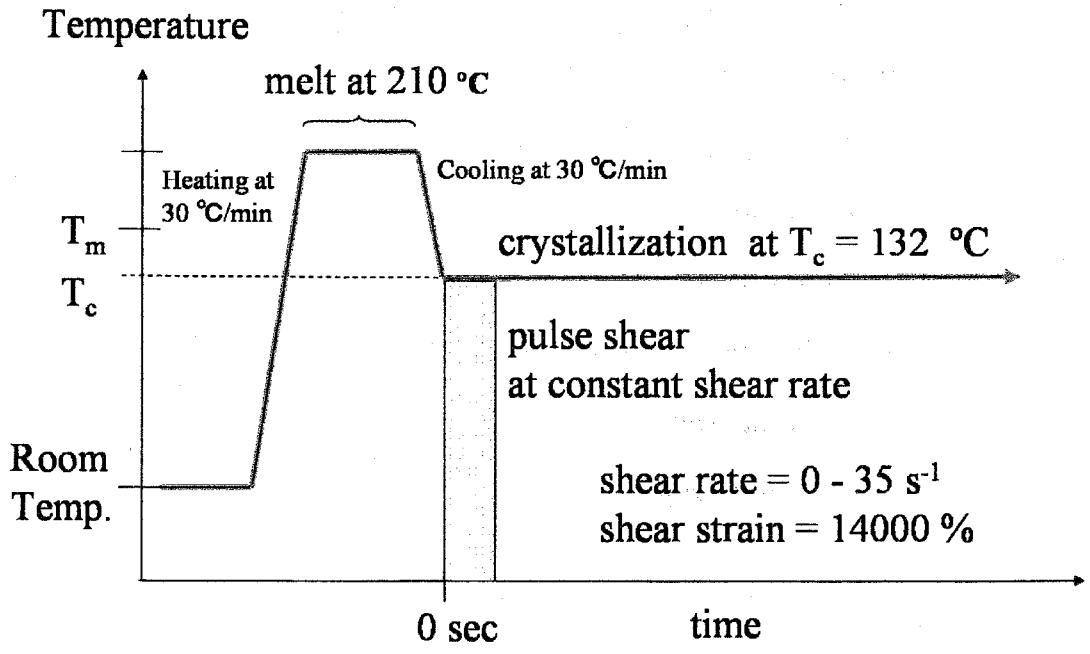

Fig. 1. Temperature protocol for the shear experiments for isotactic polypropylene.

temperature T_c, we applied a pulse shear flow to the sample and observed the time evolution of scattering pattern under the isothermal condition.

3-3 Results and discussion

Fig. 2 shows the time evolution of 2D DPLS scattering patterns during the crystallization process under the quiescent and shear conditions with shear strain ε = 5600 % and shear rate $\dot{\gamma}$ = 1, 28 s^{-1}. Under the quiescent condition, we can not see any scattering at 1min after applying shear flow, which is the so-called induction period. The scattering intensity appears at 5 min after the pulse shear. Onset time of the scattering intensity becomes earlier with increasing the shear rate although the scattering pattern is isotropic in the low shear rates region below about 5 s^{-1} for the shear strain ε = 5600 %. On the other hand, at the shear rate $\dot{\gamma}$ = 28 s^{-1}, streak-like scattering appears at around 3 min in the direction normal to the flow. As the annealing time increases isotropic scattering also appears and the whole scattering pattern becomes isotropic. These results indicate that crystallization rate was accelerated even in the rather low shear rate region, but the anisotropic structure is formed only at higher shear rate above about 5 s^{-1} for the shear strain ε = 5600 %. Isotropic and anisotropic scatterings may come from spherulite and shish-like structure, respectively. At the shear rate $\dot{\gamma}$ = 28 s^{-1}, as mentioned above, isotropic scattering follows up the anisotropic scattering. This indicates that polymer chains oriented by the shear form the shish structure while polymer chains which are not influenced by the shear flow would form spherulites.

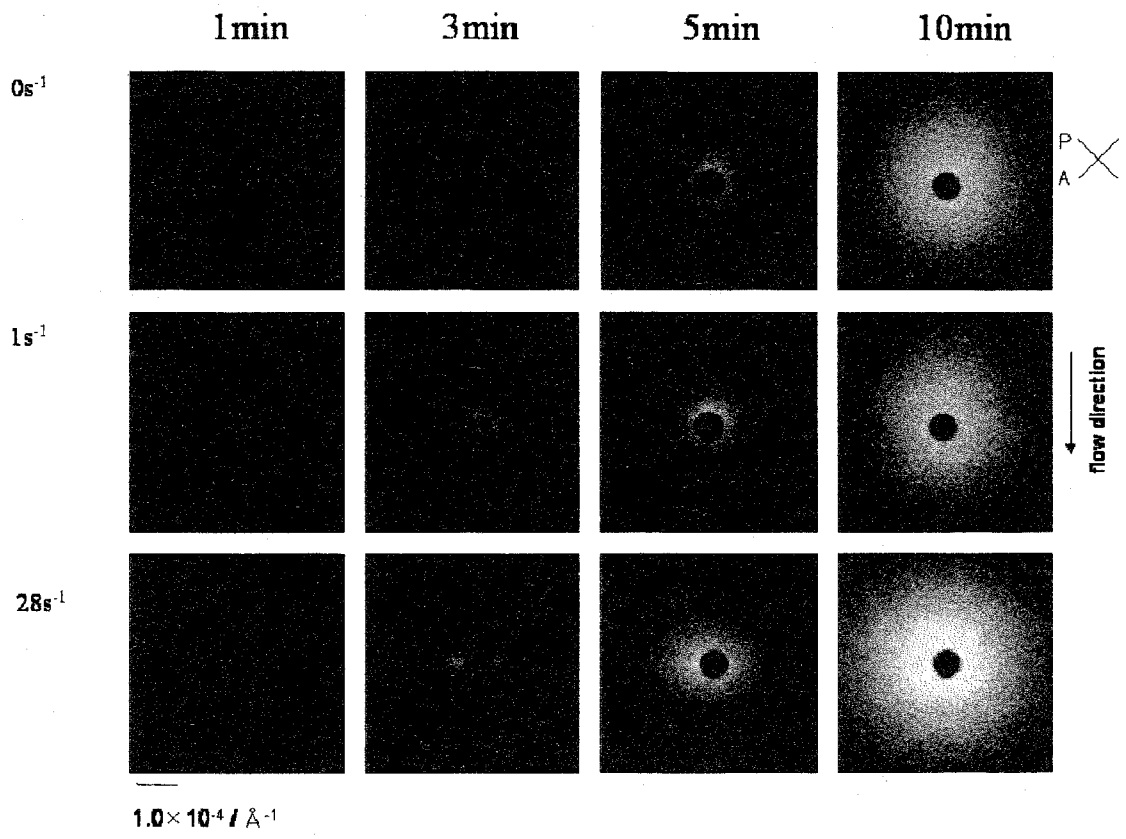

Fig. 2. Time evolution of 2D depolarized light scattering (DPLS) pattern from i-PP during the crystallization process at 132 °C. Upper row: under quiescent condition, middle row: after pulse shear with shear rate of $1s^{-1}$ and shear strain of 5600 %, lower row: after pulse shear with shear rate of 28 s^{-1} and shear strain of 5600 %.

Fig. 3 shows the time evolution of 2D scattering patterns under the shear flow as a function of shear strain ε at the shear rate $\dot{\gamma}$ = 28 s^{-1}. At the shear strain ε = 2800 %, the scattering pattern is almost isotropic. On the other hand, with increasing shear strain, we observe a streak-like scattering pattern in the early stage of crystallization. The onset time of scattering intensity becomes earlier as the shear strain increases even though the scattering pattern is isotropic. This result suggests that not only shear rate but also shear strain accelerates the crystallization rate in the low shear rate and makes the structure anisotropic at rather high strain.

3-3-1 Evaluation of critical shear rate for induction time

In Fig. 4 the time evolution of the integrated intensity normal to the flow direction is plotted as a function of annealing time. In the early stage of the crystallization the intensity does not increase with annealing time and then begins to increase at a certain annealing time. This time was defined as an induction period of the crystallization t_{ind}, which is a measure of the crystallization rate. Fig. 5 shows the induction time t_{ind} as a function of the shear rate $\dot{\gamma}$ for various shear strains ε. In the low shear rate the induction time of the crystallization t_{ind} is almost constant and the same as the quiescent value while it begins to decrease at a certain shear rate. This shear rate is defined as a critical shear rate $\dot{\gamma}_{ani,c}$ which depends on the shear strain ε. The larger the shear strain ε, the shorter the critical shear rate $\dot{\gamma}_{ani,c}$. As seen in Fig. 5, the linear relationship between the induction time t_{ind} and the logarithm of the shear rate $\dot{\gamma}$ holds, at least in the present shear rate rang as observed for PE (see Chapter 2). The relation is

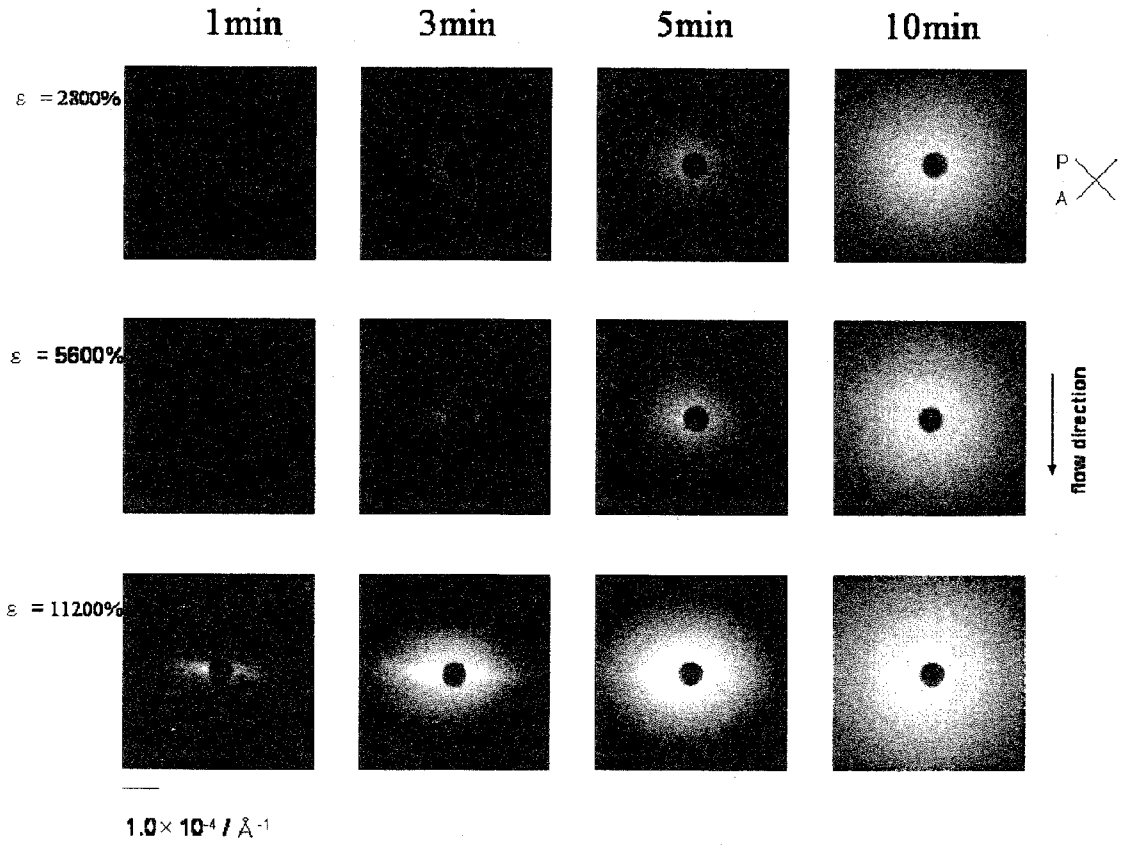

Fig. 3. Time evolution of 2D DPLS pattern from i-PP during the crystallization process at 132 °C after pulse shear with shear rate of 28 s^{-1}. Upper row: shear strain 2800 %, middle row: 5600 %, and lower row: 11200 %.

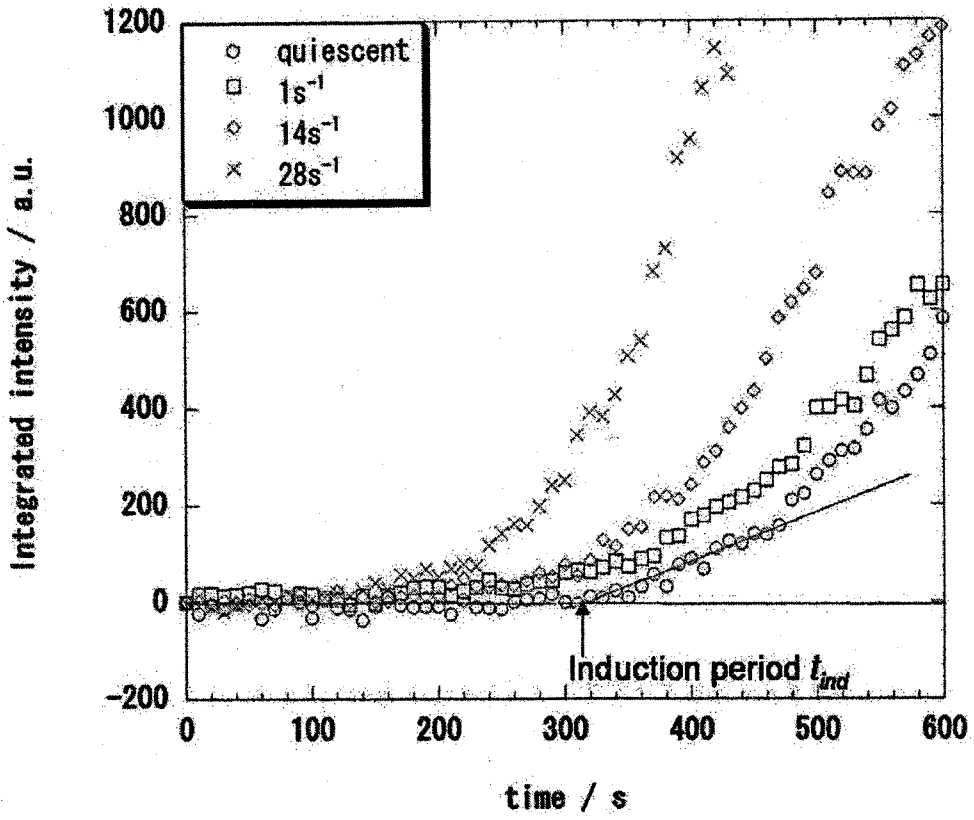

Fig. 4. Time evolution of integrated DPLS intensity of i-PP at 132 °C normal to the flow direction for various shear rates, showing the definition of induction time. The shear strain is 5600 % for all the measurements.

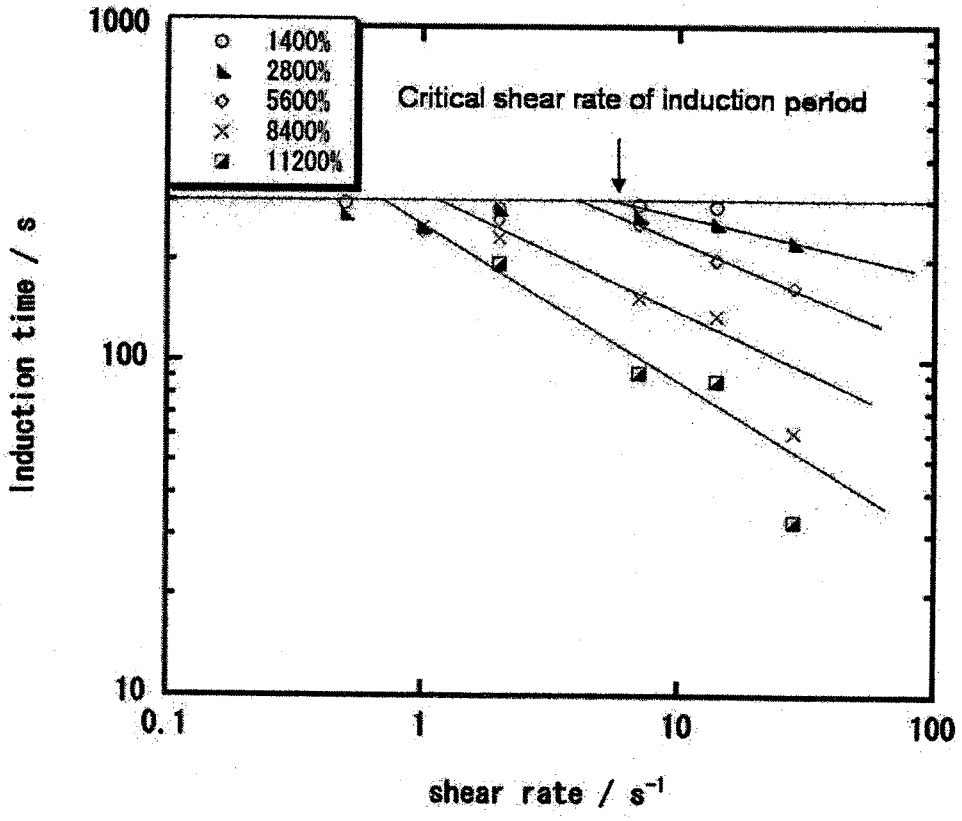

Fig. 5. Shear rate dependence of the induction period for various shear strains.

given by

$$\dot{\gamma}_{ind,c} = \dot{\gamma}\exp\left[\frac{t_{ind} - t_{ind,0}}{\tau_{ind}}\right] \tag{3.1}$$

where $\dot{\gamma}_{ind,c}$, $t_{ind,0}$ and τ_{ind} are the critical shear rate for the induction time, the induction time under quiescent condition and a constant with unit of time. The critical shear rate $\dot{\gamma}_{ani,c}$ is plotted as a function of inverse of the shear strain in Fig. 6, and extrapolated the critical shear rate $\dot{\gamma}_{ani,c}$ to the infinite shear strain or $1/\varepsilon = 0$, which correspond to the critical shear rate $\dot{\gamma}_{ani,c}$ for the apparent continuous shear flow. The critical value is about 0.69 s^{-1}. The meaning of the critical shear rate is considered as follows. Orientation of polymer chains may enhance the formation of crystal nuclei. However, if the oriented polymer chains are relaxed before the nucleation, the acceleration of crystallization rate is not observed. This is the situation below the critical shear rate $\dot{\gamma}_{ani,c}$. It is noted that anisotropic scattering pattern is not observed at the critical shear rate $\dot{\gamma}_{ani,c}$. This problem will be discussed later.

3-3-2 Evaluation of critical shear rate for anisotropy

A typical 2D scattering pattern is shown in Fig. 7(a) and the corresponding scattering intensities normal and parallel to the flow direction are plotted against Q in Fig. 7(b). We employed a ratio of integrated intensity normal to the flow direction to the parallel one in a Q range of 0.35 to 2.5 x 10^{-4} $Å^{-1}$ as a measure of degree of anisotropy R_{ani}. In Fig. 8, the degree of anisotropy R_{ani} is plotted against the logarithm of the shear rate for various shear strains. The degree of anisotropy R_{ani} is 1 when the scattering pattern is

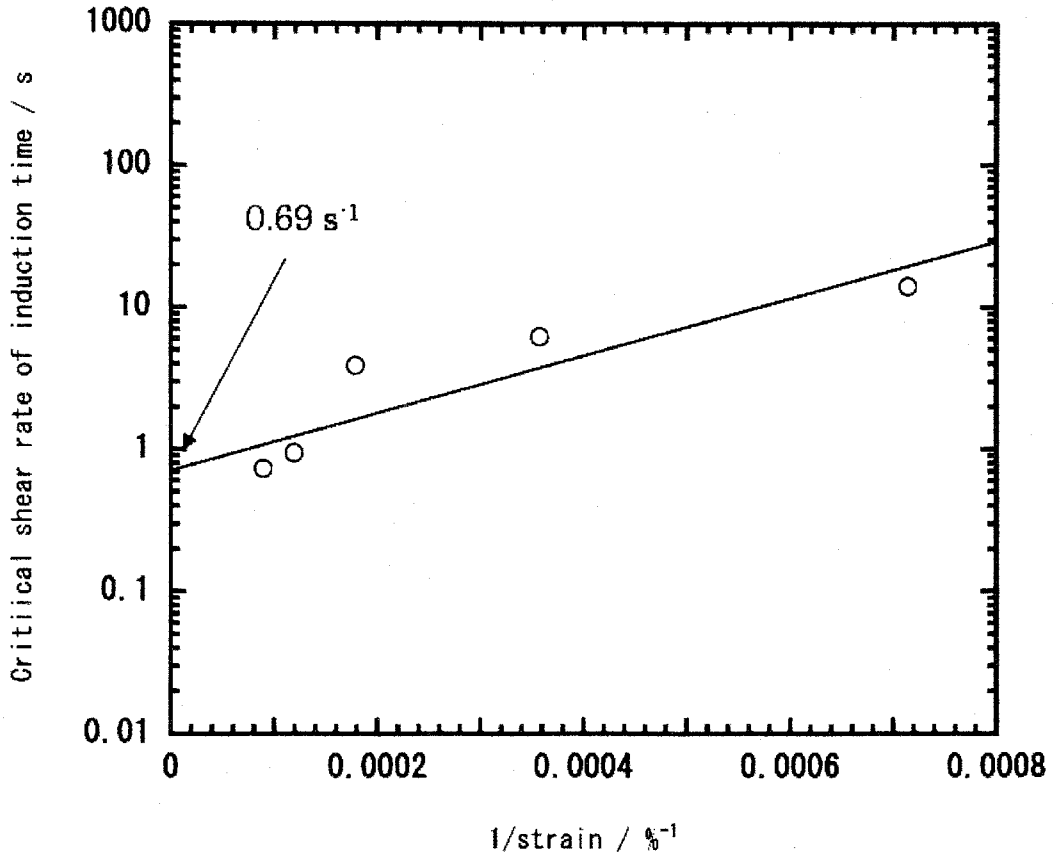

Fig. 6. Dependence of critical shear rate for induction time on the inverse of shear strain, and the critical shear rate under infinite flow is about 0.69 s^{-1}.

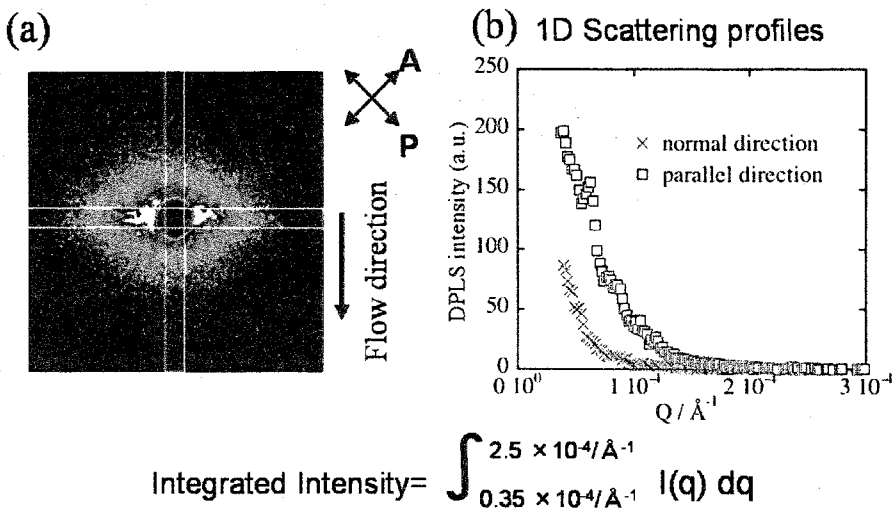

Anisotropy= Integrated Intensity (normal direction) /Integrated Intensity (parallel direction)

Fig. 7. (a): A typical anisotropic 2D scattering pattern. (b) 1D scattering intensity normal and parallel to the flow direction, and the definition of degree of anisotropy.

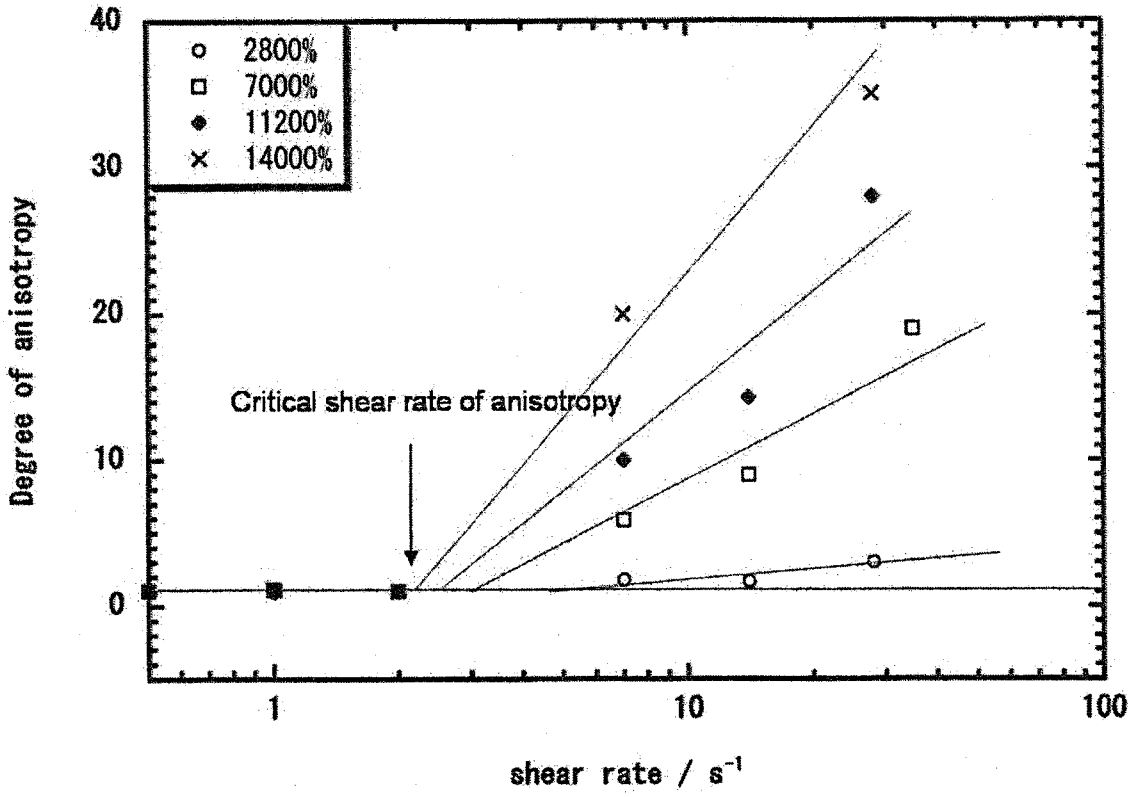

Fig. 8. Shear rate dependence of degree of anisotropy R_{ani} for various shear strains.

isotropic. The anisotropic ratio R_{ani} increased with the shear rate $\dot{\gamma}$ and the shear strain ε. We evaluated the critical shear rate for anisotropy $\dot{\gamma}_{ani,c}$ by extrapolating the degree of anisotropy R_{ani} to 1 for various shear strains ε. The relation between the degree of anisotropy R_{ani} and the logarithm of the shear rate $\dot{\gamma}$ is given by

$$\dot{\gamma}_{ani,c} = \dot{\gamma}\exp\left[-\frac{R_{ani} - R_{ani,0}}{r_{ani}}\right] \tag{3.2}$$

where $\dot{\gamma}_{ani,c}$, $R_{ani,0}$ and r_{ani} are the critical shear rate for the anisotropy, the degree of anisotropy under quiescent condition (= 1), and a dimensionless constant. Fig. 9 shows the critical shear rate as a function of the inverse of shear strain. Extrapolating the critical shear rate to the infinite shear strain or $1/\varepsilon = 0$, we evaluated the critical shear rate $\dot{\gamma}_{ani,c}$ for the infinite shear strain, which is about 2.0 s^{-1}. This value corresponds to the critical shear rate $\dot{\gamma}_{ani,c}$ under continuous shear flow.

The same analysis has been done on the shear strain dependence of the degree of anisotropy R_{ani}. The degree of anisotropy R_{ani} is plotted against the shear strain ε for various shear rates $\dot{\gamma}$ of 0.5 to 35 s^{-1} in Fig. 10. In the similar manner as in the evaluation of the critical shear rate $\dot{\gamma}_{ani,c}$, we estimated the critical shear stain $\varepsilon_{ani,c}$ for the anisotropy for each shear rate. The inverse of critical shear strain thus obtained is plotted as a function of shear rate $\dot{\gamma}$ in Fig. 11. Extrapolating to the infinite critical shear strain or $1/\varepsilon = 0$ we have estimated the critical shear rate $\dot{\gamma}_{ani,c}$ for the infinite critical shear strain, which is about 2.1 s^{-1}. This value almost agrees with the critical shear rate for the infinite shear strain evaluated from the relation between the critical shear rate and the inverse of shear strain.

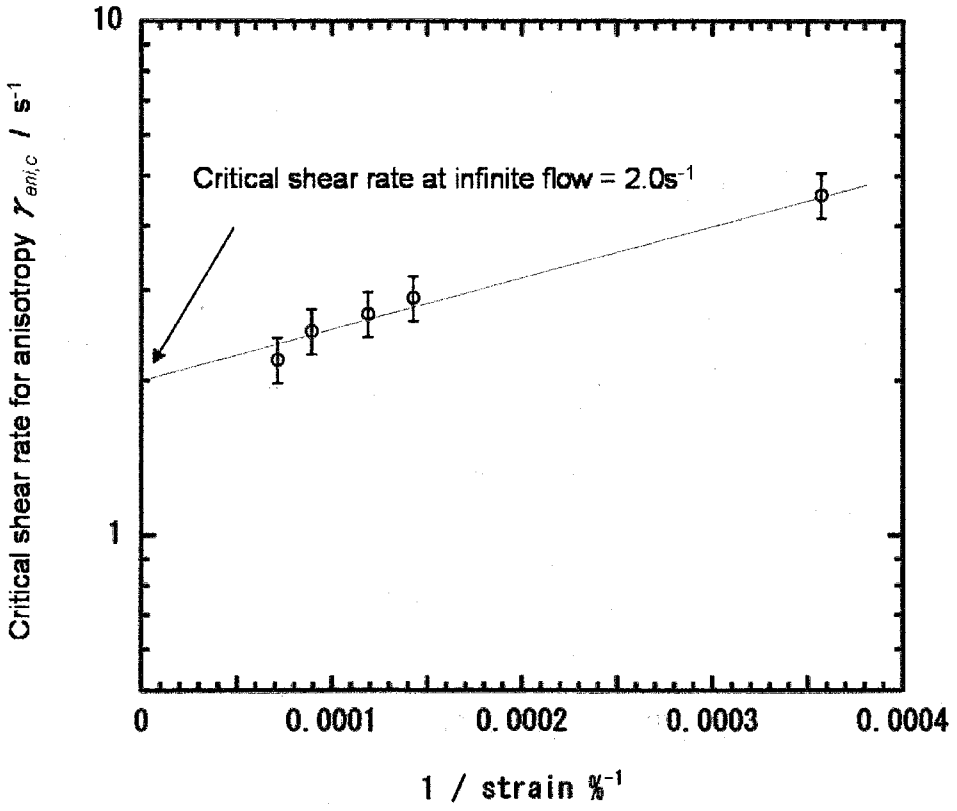

Fig. 9. Critical shear rate for anisotropy $\dot{\gamma}_{ani,c}$ against inverse of shear strain.

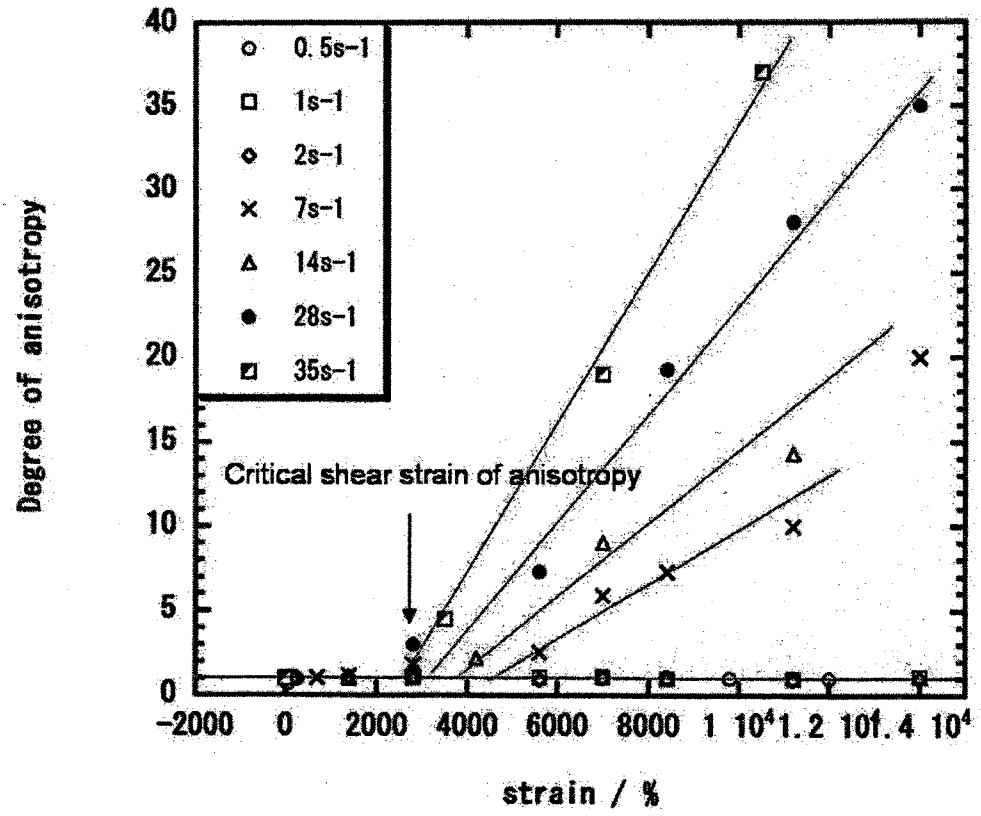

Fig. 10. Shear strain dependence of the degree of anisotropy R_{ani} for various shear rate $\dot{\gamma}$.

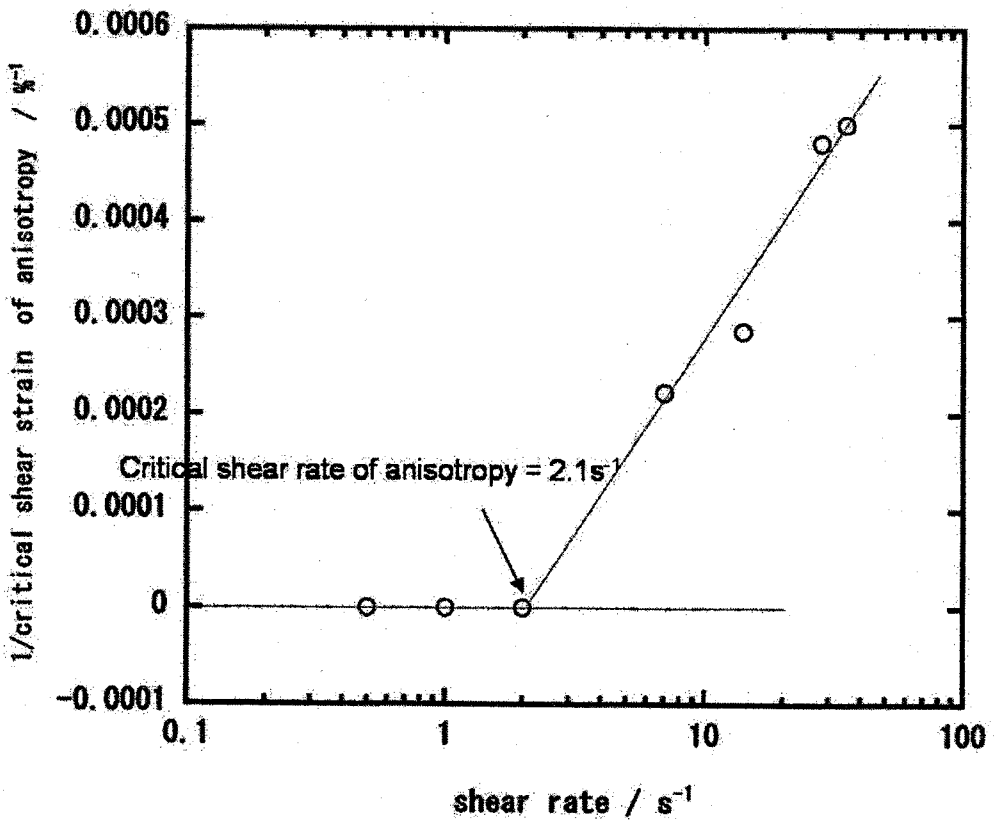

Fig. 11. Inverse of critical shear strain $1/\varepsilon_{ani,c}$ for anisotropy against shear rate $\dot{\gamma}$.

Similar to the results in Chapter 2, the values of the critical shear rates evaluated by the two methods agree with each other, showing the validity of the evaluation. This must correspond to the critical shear rate for anisotropy for the continuous shear flow.

As discussed in Chapter 2, under the continuous shear flow, the extension of polymer chain is almost dominated by the relation between the shear rate and the longest relaxation time τ. If the shear rate is larger than the relaxation rate (or inverse of the relaxation time) τ^{-1}, the polymer chains are somewhat extended and oriented under the flow. The polymer chains are in the supercooled state below the melting temperature, and hence tend to crystallize. The orientation must accelerate the crystallization rate (orientation-induced crystallization). Thus, the critical shear rate is related to the relaxation rate: $\dot{\gamma}_{ani,c} \backsim \tau^{-1}$, if we neglect a numerical factor in order of unity. This is one of tentative scenarios for the shish formation in the early stage of crystallization. In order to confirm this scenario it must be essential to examine effects of the molecular weight distribution and the rheological properties on the crystallization.

Finally we would like to mention about the difference of the critical shear rates for the acceleration of the crystallization rate (or the induction time) (= 0.69 s^{-1}) and the anisotropic structure formation (= 2.0 s^{-1}). The former is much smaller than the latter. This means that the formation of anisotropic structure, which must correspond to the shish-like structure, requires much higher orientation of polymer chains. In the shear rate range between the two critical shear rates crystal nucleation is accelerated by local orientation of polymer chains, but this orientation is too local to develop the oriented

crystal structure in micrometer, which must be shish-like structure.

3-4 Conclusion

We investigated the structure formation of i-PP in the early stage of the crystallization after a pulse shear using depolarized light scattering (DPLS), focusing on the effects of the shear rate and the shear strain. We observed streak-like scattering pattern normal to the flow direction in the early stage of crystallization in some shear conditions. This oriented structure would be the shish-like structure. We determined the critical shear rate for the induction time at the infinite shear strain, which was 0.69 s^{-1}. We also estimated the critical shear rate for the anisotropic structure formation at the infinite shear strain (= 2.0 s^{-1}) in two ways. This critical shear rate must be determined by the relation between the crystallization rate and the longest relaxation time of polymer chain. The critical shear rate for the induction time is smaller than that for the anisotropic structure. In the shear rate range between the two critical shear rates crystal nucleation is accelerated by local orientation of polymer chains, but the this orientation is too local to develop the oriented crystal structure in micrometer.

References

[1] Norton, D. R.; Keller, A. *Polymer* **1985**, *26*, 704.

[2] Phillips, P. J. *Reports on Progress in Physics* **1990**, *53*, 549.

[3] Jones, A. T.; Aizlewood, J. M.; Beckett, D. R. *Makromolekulare Chemie* **1964**, *75*, 134.

[4] Lovinger, A. J.; Chua, J. O.; Gryte, C. C. *Journal of Polymer Science Part B-Polymer Physics* **1977**, *15*, 641.

[5] Ferro, D. R.; Bruckner, S.; Meille, S. V.; Ragazzi, M. *Macromolecules* **1992**, *25*, 5231.

[6] Morrow, D. R. *Journal of Macromolecular Science-Physics* **1969**, *B 3*, 53.

[7] Lotz, B.; Graff, S.; Straupe, C.; Wittmann, J. C. *Polymer* **1991**, *32*, 2902.

[8] Kardos, J. L.; Christia.Aw; Baer, E. *Journal of Polymer Science Part a-2-Polymer Physics* **1966**, *4*, 777.

[9] Miller, R. L. *Polymer* **1960**, *1*, 135.

[10] Hendra, P. J.; Vile, J.; Willis, H. A.; Zichy, V.; Cudby, M. E. A. *Polymer* **1984**, *25*, 785.

[11] Somani, R. H.; Hsiao, B. S.; Nogales, A.; Fruitwala, H.; Srinivas, S.; Tsou, A. H. *Macromolecules* **2001**, *34*, 5902.

[12] Seki, M.; Thurman, D. W.; Oberhauser, J. P.; Kornfield, J. A. *Macromolecules* **2002**, *35*, 2583.

[13] Huo, H.; Jiang, S. C.; An, L. J.; Feng, J. C. *Macromolecules* **2004**, *37*, 2478.

[14] Jay, F.; Haudin, J. M.; Monasse, B. *Journal of Materials Science* **1999**, *34*, 2089.

[15] Somani, R. H.; Yang, L.; Sics, I.; Hsiao, B. S.; Pogodina, N. V.; Winter, H. H.; Agarwal, P.; Fruitwala, H.; Tsou, A. *Macromolecular Symposia* **2002**, *185*, 105.

[16] Elmoumni, A.; Winter, H. H.; Waddon, A. J.; Fruitwala, H. *Macromolecules* **2003**, *36*, 6453.

[17] Brandup, J.; Immergut, E. H.; Grulke, E. A., Editor, *POLYMER HANDBOOK fourth edition*, Wiley-Interscience **1999**, V23.

Chapter 4

Crystallization of isotactic polypropylene under shear flow

- Observations in a wide spatial range -

4-1 Introduction

As mentioned in Chapters 2 and 3, extensive studies have been performed to elucidate the formation mechanism of the shish-kebab structure for a long time [1,2]. Recently, using new experimental techniques such as SR X-ray scattering, laser light scattering and neutron scattering [3-6], new aspects of the shish-kebab was clarified and computer simulation works also gave many interesting features of the shish-kebab formation [7,8].

Nevertheless, there are still many unsolved problems in the shish-kebab formation. In Chapters 2 and 3, we investigated the effects of shear rate and shear strain on the shish structure formation in μm scale using depolarized light scattering, and found that there existed the critical shear rate and the critical shear strain for the formation of shish structure. This strongly suggests that the relaxation of polymer chains plays an important role in the shish structure formation. In other words, the formation of the shish structure is dominated by the relation between the relaxation rate and the crystallization rate.

In this chapter, we further studied the formation mechanism of shish-kebab structure during the crystallization process of isotactic polypropylene (i-PP) under shear flow using polarized optical microscope (POM), depolarized light scattering (DPLS), small-angle X-ray scattering (SAXS) and wide-angle X-ray scattering (WAXS) techniques to cover a wide

spatial scale from Å scale to μm, and hence we could investigate not only the formation of the shish in μm scale but also the forming of the kebab in nm scale.

4-2 Experimental

4-2-1 Sample

In the experiment we used isotactic polypropylene (i-PP) with the molecular weight M_w = 238,000 and the polydispersity M_w/M_n = 5.1, where M_w and M_n are the weight-average and number-average molecular weights, respectively. The i-PP was synthesized using metallocene catalysis. Tetrad tacticity determined by NMR measurements was *mmmm* = 0.974. DSC measurements were carried out to characterize the thermal properties of the sample using Perkin-Elmer DSC-7.

The sample thickness was 300 μm for the DPLS, SAXS and WAXS measurements.

4-2-2 Measurements

DSC measurements All the DSC scans were performed under nitrogen environment. The nominal melting temperature of the i-PP determined by DSC measurements was 149 °C at the heating rate of 20 °C/min.

POM measurements Polarized optical microscope (POM) measurements were carried out with OLYMPUS BX50 equipped with a CCD camera as a detector.

DPLS measurements Two-dimensional (2D) depolarized light scattering (DPLS) measurements were carried out using a home-made apparatus with He-Ne laser (80 mW, wavelength λ = 632.8 nm) as a light source and a 2D screen and a CCD camera as a detector system. The range of length of scattering vector Q in this experiment is 3.5 x 10^{-5} to 3.0 x 10^{-4} $Å^{-1}$, where Q is given by $Q = 4\pi \sin\theta/n\lambda$ (2θ and n being scattering angle and the refractive index, respectively).

SAXS and WAXS measurements Small-angle and wide-angle X-ray scattering (SAXS and WAXS) measurements were performed using apparatuses installed at the beam line BL45XU [9-11] and BL40B2 [12] in the SR facility, Spring-8, in Nishiharima, respectively. Wavelengths of the incident X-ray were 1.0 and 0.9 Å and the camera lengths were 2.2 and 0.12 m for SAXS and WAXS, respectively. A CCD camera (C4880: Hamamatsu Photonics K.K.) with an image intensifier was used as a detector system for both the SAXS and WAXS measurements. The Q range covered in the SAXS and WAXS measurements were 0.008 to 0.2 $Å^{-1}$ and 0.1 to 2.5 $Å^{-1}$, respectively.

A Linkam CSS-450 high temperature shear cell was used to control the temperature and the shear conditions. The sample was placed between the two quartz plates for the POM and DPLS measurements and between two stainless steel plates with Kapton windows 50 μm thick for the SAXS and WAXS measurements, respectively. The temperature protocol for the shear experiments is shown in Fig. 1: (a) the polymer sample was heated up to 210 °C from room temperature at a rate of 30 °C/min, (b) held at 210 °C for 5 min,

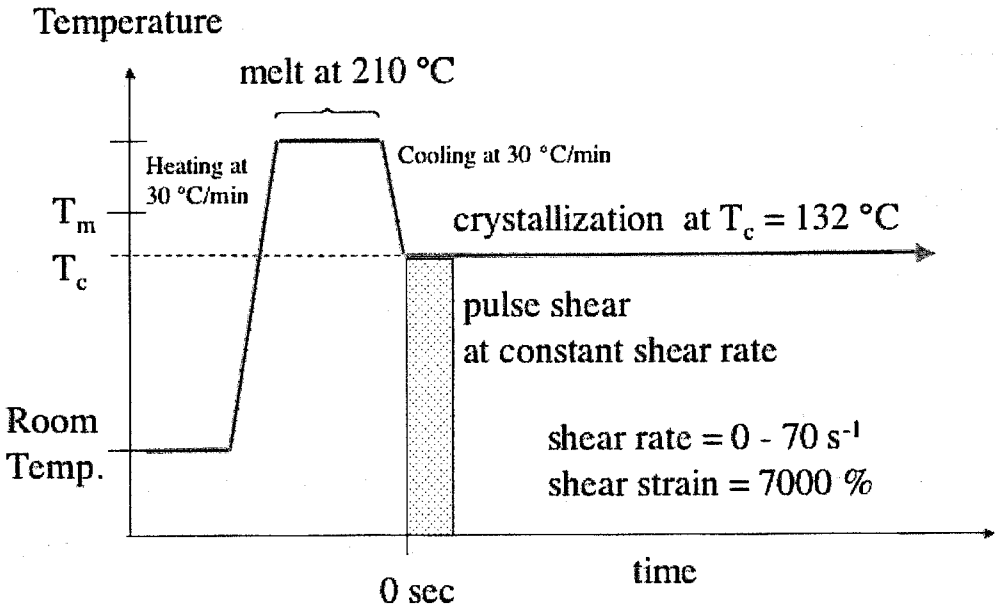

Fig. 1. Temperature protocol for the shear experiments on polypropylene.

(c) cooled down to the crystallization temperature T_c = 132 °C at a rate of 30 °C/min, and then (d) held at 132 °C for the measurements. The polymer melt was subjected to a pulse shear just after reaching the crystallization temperature T_c of 132 °C. The range of the shear rate was 0 - 70 s^{-1} and the shear strain was 7000 % at every shear rate.

4-3 Results and discussion

4-3-1 POM results

Polarized optical microscope (POM) measurements were carried out on the crystallization process of i-PP at 132 °C under quiescent and shear conditions. The sample was kept at 210 °C for 5 min and cooled down to a crystallization temperature T_c (= 132 °C) at a cooling rate of 30 °C/min. Just after reaching T_c we have applied a pulse shear with various shear rates and observed the crystallization process. The results are shown in Fig. 2 for the quiescent condition and the shear conditions with shear rates of 50 and 70 s^{-1}. The shear strains were 7000 % for all the measurements. Under the quiescent condition, we observed growth of usual isotropic spherulites. The first spherulite appeared at about 5 min after reaching the crystallization temperature T_c (= 132 °C). On the other hand, under the shear conditions, string-like structure or their bundles oriented along the flow direction appeared in the beginning of the crystallization. The onset time (or the induction time) of the string-like structure is much shorter than that of the spherulites under the quiescent condition and becomes shorter with increasing the shear rate. The number of the strings also increases with the shear rate. In the late stage of crystallization isotropic spherulites were

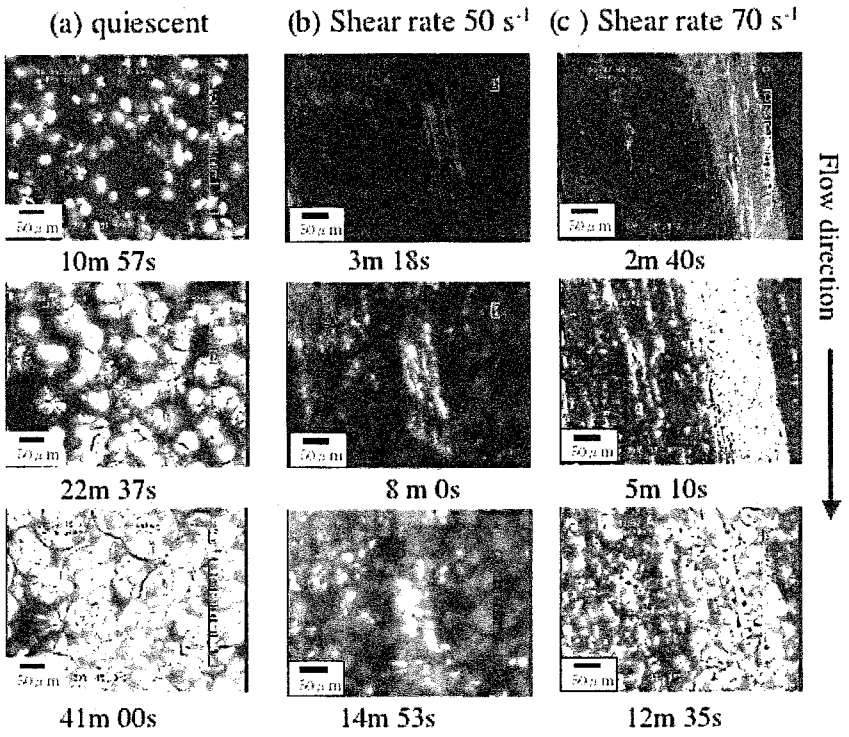

Fig. 2. Time evolution of polarized optical microscope images for shear rates of 50 and 70 s^{-1}.

also observed even under the shear condition. These may come from some parts in the sample which were not affected by the shear or from the low molecular weight polymer chains which were relaxed before the crystallization [13]. The string-like structure and their bundle must be the shish-kebab structure and/or their aggregates. These optical microscope measurements give us intuitive images of the crystallization process under the quiescent and flow conditions. However, for the quantitative studies scattering methods are more appropriate than microscope measurements. Then, we performed time resolved depolarized light scattering measurements.

4-3-2 DPLS results

Depolarized light scattering (DPLS) measurements were performed on the crystallization process of i-PP under the same thermal history and the same shear conditions as the POM measurements. In this measurement, we can cover the range of scattering vector from 3.5×10^{-5} to 3.0×10^{-4} $Å^{-1}$, corresponding to the spatial scale of ~18 to ~2.0μm. Hence, we will see the structure formation in μm scale, particularly the shish structure in the measurements. In Fig. 3, time evolutions of two-dimensional (2D) DPLS patterns are shown for various shear rates. The shear strains were 7000 % for all the measurements. Under the quiescent crystallization condition ($\dot{\gamma} = 0$ s^{-1}), we observed isotropic scattering patterns after an induction period before nucleation of about 5 min. This length of the induction period almost corresponds to the appearance of spherulites in the polarized optical microscope measurements. On the other hand, as the shear rate increases

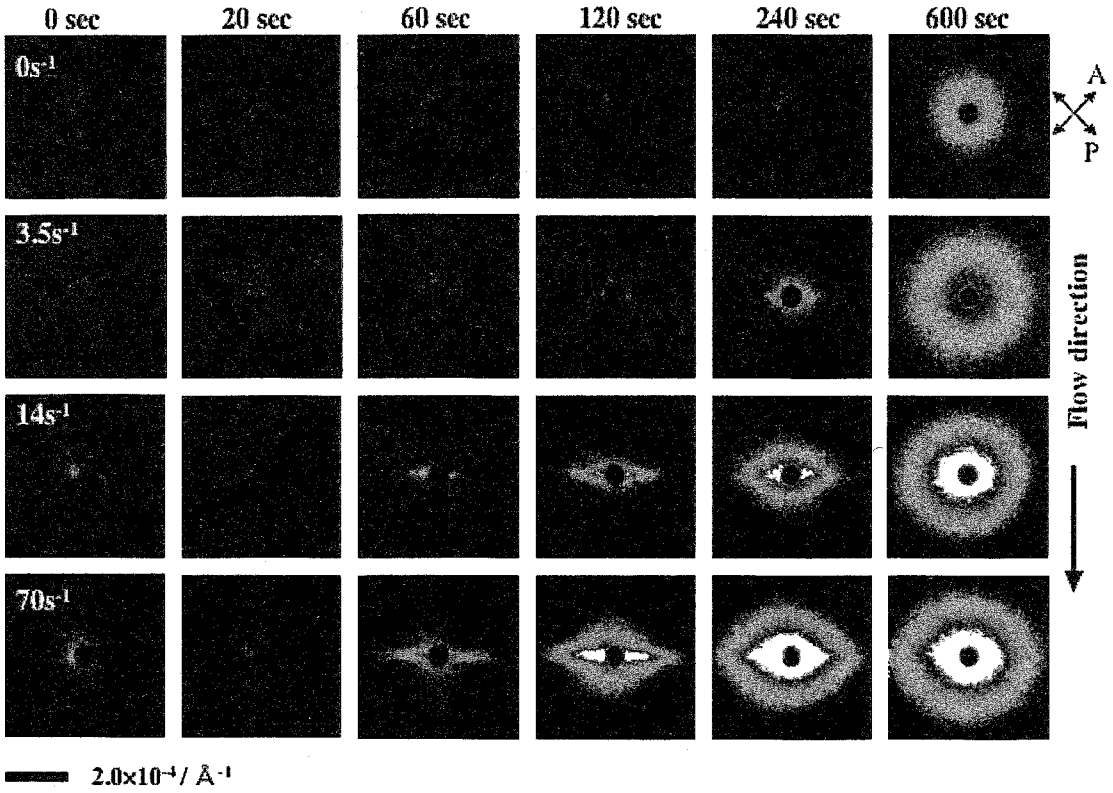

Fig. 3. Time evolution of 2D DPLS patterns for various shear rates.

we observe anisotropic streak-like scattering pattern along the direction normal to the shear. This indicates that there are long scattering objects aligned along the flow direction, which must be the shish structure or the precursor of shish structure. At the moment it is not clear if it is the shish structure or the precursor, and hence we call it the shish-like structure hereafter. The induction time and the anisotropy depend on the shear rate.

In order to analyze the DPLS data we employed two measures. One is the length of the induction period before the streak-like scattering appears in the direction normal to the flow, which corresponds to the onset time of the shish-like structure, and the other is the anisotropy in the 2D scattering pattern. First we discuss the length of the induction period. This is a sort of measure of the crystallization rate. Generally speaking, the crystallization rate is determined by both the nucleation rate and the growth rate [14]. The onset time is mainly related to the nucleation rate. In Fig. 4, the integrated DPLS intensity normal to the flow direction in a Q range of 0.35 to 2.5 x 10^{-4} $Å^{-1}$ (see also Fig. 6) is plotted as a function of annealing time at 132 °C for various shear rates. We observe the onset of the scattering intensity after a certain induction period, which decreases with increasing the shear rate. The length of the induction period was estimated as the onset time of the integrated intensity as shown in Fig. 4 for quiescent condition ($\dot{\gamma}$ = 0 s^{-1}), and was plotted against logarithm of the shear rate in Fig. 5. The induction period decreases with increasing the shear rate, in particular, in the low shear rate range below about 14 s^{-1} and gradually decreases above 14 s^{-1}. The critical shear rate for the induction period at the shear strain 7000 % is about 1.6 s^{-1}. Regarding the induction period, we

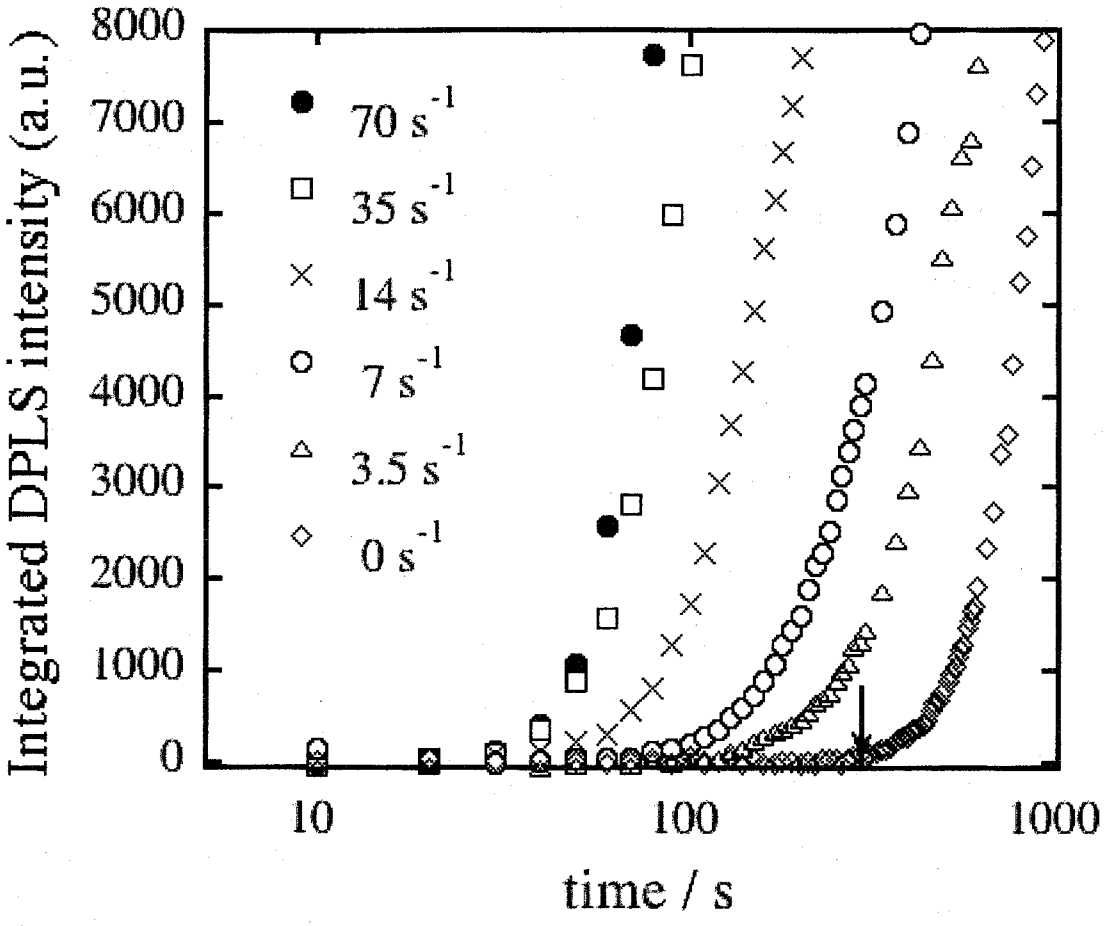

Fig. 4. Time evolution of the integrated DPLS intensity normal to the flow direction.

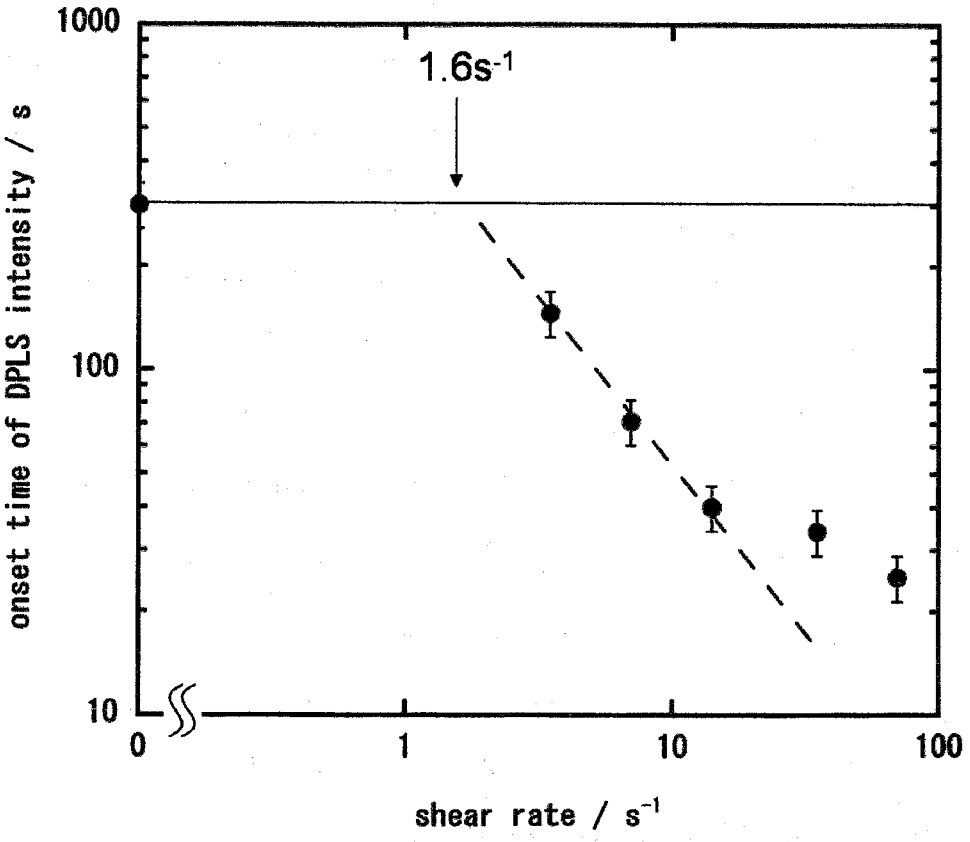

Fig. 5. Onset time of the integrated DPLS intensity normal to the flow direction.

have to emphasize the following problem. As mentioned in *Experimental* part, a pulse shear was applied to the sample just after reaching the crystallization temperature T_c (= 132 °C). During a few seconds after the pulse shear the detector screen of scattering light was bright, showing that the polymer chains are oriented due to the shear, and then the screen became dark. However, the scattering pattern appearing after a certain induction time was anisotropic, i. e., streak-like scattering was observed in a direction normal to the flow. Why could the completely relaxed polymer chains crystallize anisotropically in a long form aligned along the flow direction? There are two scenarios to explain the phenomenon that anisotropic scattering appeared after a certain induction period. One is that the orientation domain induced by the shear flow became too large to be detected in the Q range of our DPLS measurement and the anisotropic scattering pattern was hidden inside of the beam stopper. The other scenario is that the orientation of polymer chains relaxed within a few seconds to be isotropic, at least within the sensitivity of the light scattering measurements, but a small number of tiny oriented domains remained and the number of the tiny oriented domains was too small to be detected. If crystallization starts from the tiny oriented part, the growth direction of the crystal must be influenced by the orientation of the starting orientation, resulting in highly oriented crystals.

The second measure is a degree of anisotropy in the 2D scattering pattern. A typical 2D DPLS scattering pattern is shown in Fig. 6(a). As a measure of the anisotropy of the scattering pattern, we employed a ratio of integrated intensity in the normal direction to the parallel one in the Q range of 0.35 x

10^{-4} to 2.5 x 10^{-4} Å^{-1} (see Fig. 6(b)), and termed the degree of anisotropy R_{ani}. It is noted that the degree of anisotropy can be defined only after the induction period of the scattering intensity. After the induction period, it is almost constant for a while and began to decrease with annealing time. This decrease is due to the appearance of isotropic spherulites as seen in the polarized optical microscope pictures in Fig. 2. Then, we used the constant value of the degree of anisotropy R_{ani} in the following discussion.

The degree of anisotropy R_{ani} is plotted against logarithm of the shear rate in Fig. 7. It increases linearly with logarithm of the shear rate above a certain critical shear rate in the present shear range. This relation can be written in the following form.

$$\dot{\gamma}_{ani,c} = \dot{\gamma}\exp\left[-\frac{R_{ani} - R_{ani,0}}{r_{ani}}\right]. \tag{4.1}$$

where $\dot{\gamma}_{ani,c}$, $R_{ani,0}$, and r_{ani} are the critical shear rate for the anisotropy, the degree of anisotropy under quiescent condition (= 1), and a dimensionless constant. The critical shear rate $\dot{\gamma}_{ani,c}$ was evaluated to be 2.9 s^{-1} by extrapolating the degree of anisotropy to unity. The critical shear rate for the degree of anisotropy $\dot{\gamma}_{ani,c}$ is larger than that for the induction. Similar results were reported for other polymers [4]. The meaning of the critical shear rate is considered as follows. Orientation of polymer chains may enhance the formation of crystal nuclei. However, if the oriented polymer chains are relaxed before the nucleation, the acceleration of crystallization rate is not observed. Hence, it is considered that the crystal nucleation occurs before the relaxation of polymer chains above the critical shear rate.

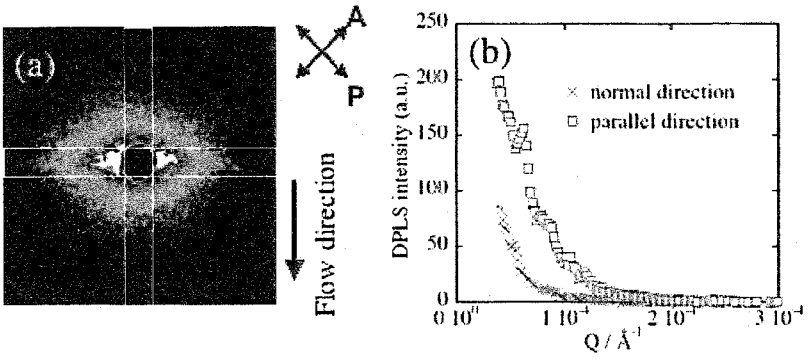

Fig. 6. (a) a typical 2D scattering pattern, (b) the corresponding 1D scattering curves normal and parallel to the flow direction. Degree of anisotropy is defined as a ratio of integrated intensity in the normal.

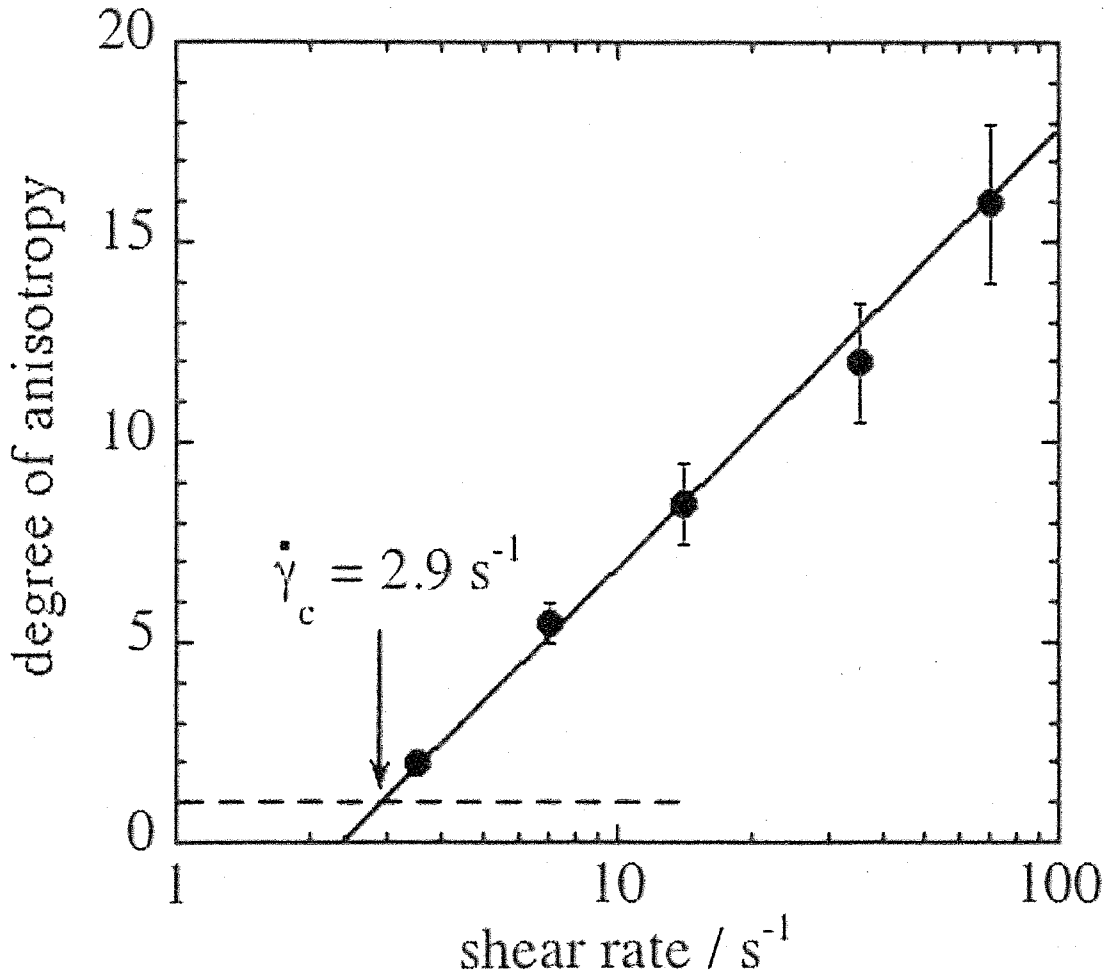

Fig. 7. The degree of anisotropy R_{ani} for DPLS measurements is plotted against logarithm of the shear rate.

In the above DPLS measurements we observed the formation process of the shish-like structure in a spatial scale of μ m. In order to see the formation process of the kebab structure we have to go down to hundreds Å scale, and hence we have performed time-resolved small-angle X-ray scattering measurements on the crystallization process of the same i-PP.

4-3-3 SAXS results

Time resolved small-angle X-ray scattering (SAXS) measurements were carried out under the same temperature and shear conditions as the DPLS. The same i-PP was heated up to 210 °C and held for 5 min, and then cooled down to the crystallization temperature T_c = 132 °C at a cooling rate of 30 °C/min. Just after reaching T_c a pulse shear was applied and the time resolved SAXS measurements were carried out at 132 °C. The shear rates were in a range of 0 to 70 s^{-1} and the shear strain was 7000 % for all the measurements. The observed time evolution of 2D SAXS patterns are shown in Fig. 8 for the shear rates of 7, 35 and 70 s^{-1}. Under the quiescent condition, only isotropic scattering patterns were observed and the onset time of the scattering intensity is about 11 min after reaching the crystallization temperature T_c (= 132 °C). On the other hand, under the shear condition, the onset time of the scattering intensity is earlier than that under the quiescent condition and the scattering pattern is anisotropic. For example, at the shear rate of 70 s^{-1}, weak streak-like scattering intensity appears along the flow direction at 72 sec in the early stage after applying the pulse shear, and the scattering pattern gradually becomes two-spot pattern. In addition, isotropic scattering ring also appears in the late stage

of the crystallization. The anisotropic SAXS scattering pattern is completely different from the DPLS one (see Fig. 3), in which streak-like scattering appears in a direction normal to the flow. The observed two-spot SAXS pattern parallel to the flow direction must correspond to the distance between the lamellae (kebab) periodically aligned along the shish-structure. In order to analyze these SAXS data quantitatively we also used the onset time and the degree anisotropy, which depend on the shear rate very much.

The time evolution of the integrated scattering intensity parallel to the flow direction in a Q range of 0.015 to 0.1 $Å^{-1}$ is shown in Fig. 9 for the shear rates of 0, 7, 14 and 70 s^{-1}. The onset time was defined as a rise-up time of the integrated scattering intensity in a direction parallel to the flow as shown by an arrow for the quiescent condition. The estimated onset time is plotted against logarithm of the shear rate in Fig. 10. In the low shear rate region, it seems to decrease drastically, showing large effects of the shear rate on the crystallization rate. Critical shear rate for the acceleration of the onset time at the shear strain 7000 % is about 2.8 s^{-1}. This value is almost the same as that in the DPLS measurement and we discuss in the next section.

We defined the degree of anisotropy for the SAXS data as a ratio of integrated intensity parallel to the flow direction to the normal one. The ratio cannot be calculated in the induction period, and fluctuates very much just after the induction period because of the weak intensity. The ratio becomes stable and almost constant in a period before the isotropic scattering appears. Hence, we employed the ratio in the stable region as the degree of anisotropy, which was plotted in Fig. 11 against logarithm of

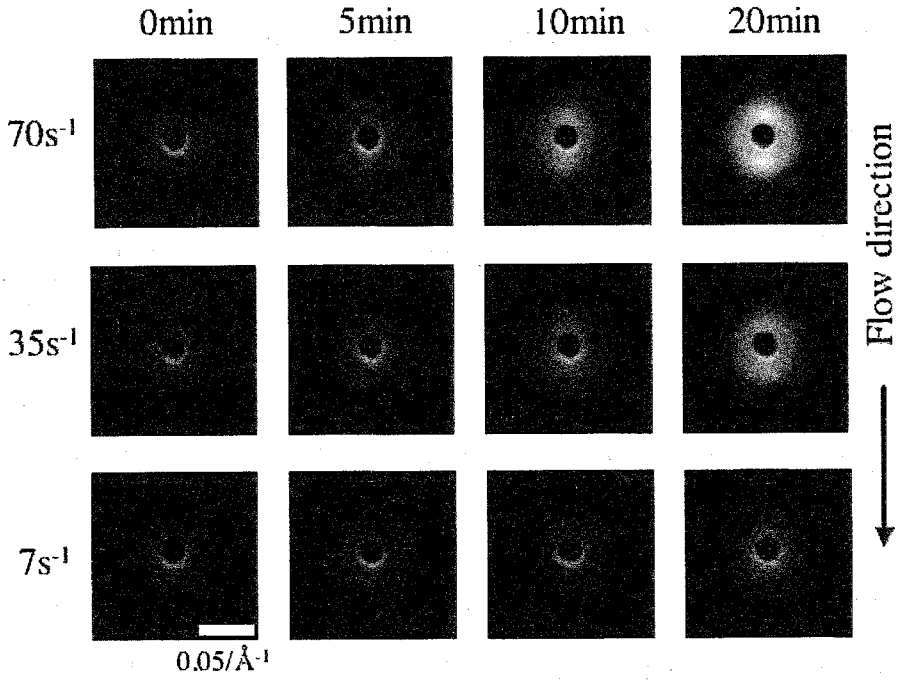

Fig. 8. Time evolution of 2D SAXS patterns for various shear rates.

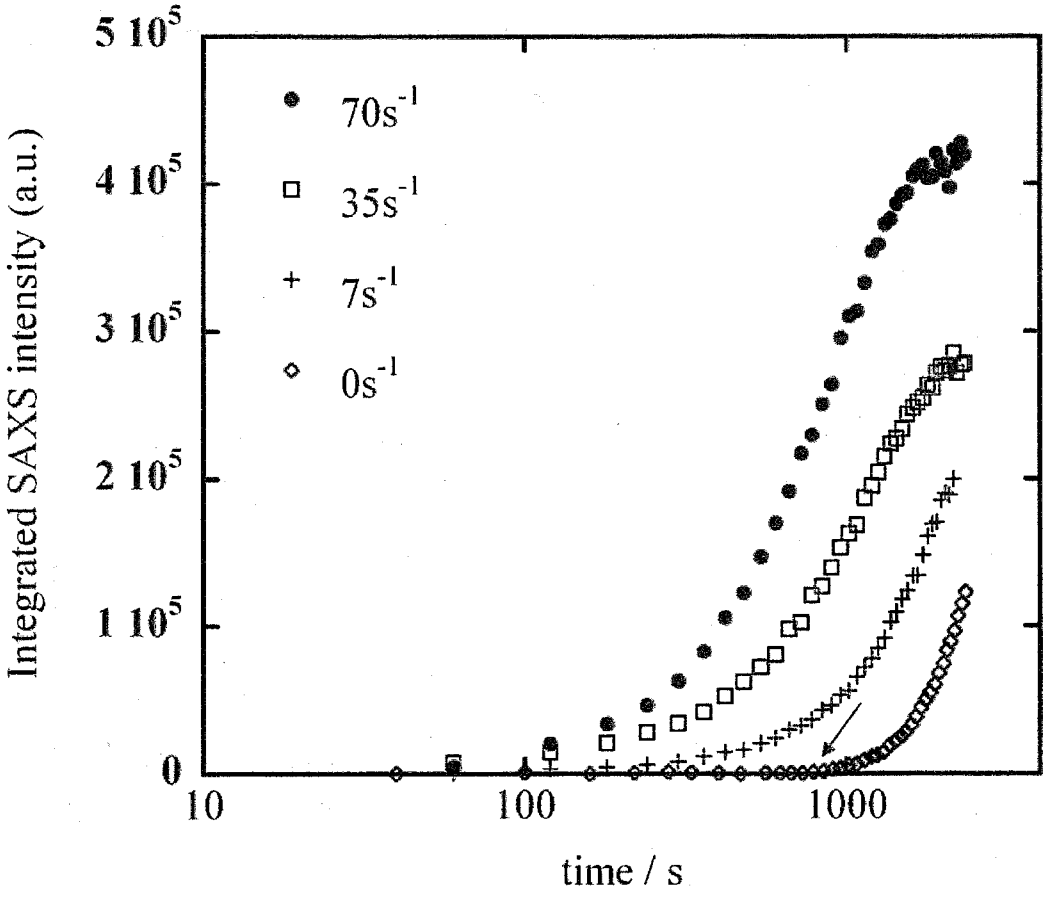

Fig. 9. Time evolution of the integrated SAXS intensity parallel to the flow direction.

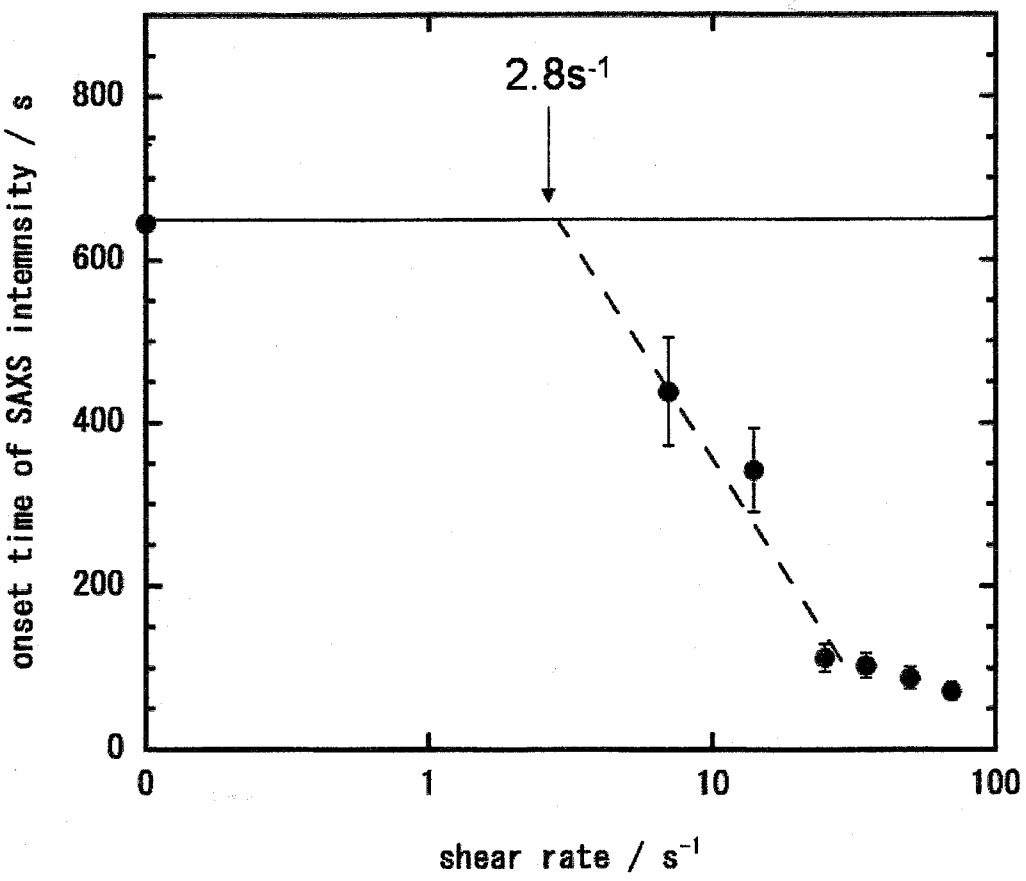

Fig. 10. Onset time of the integrated SAXS intensity parallel to the flow direction.

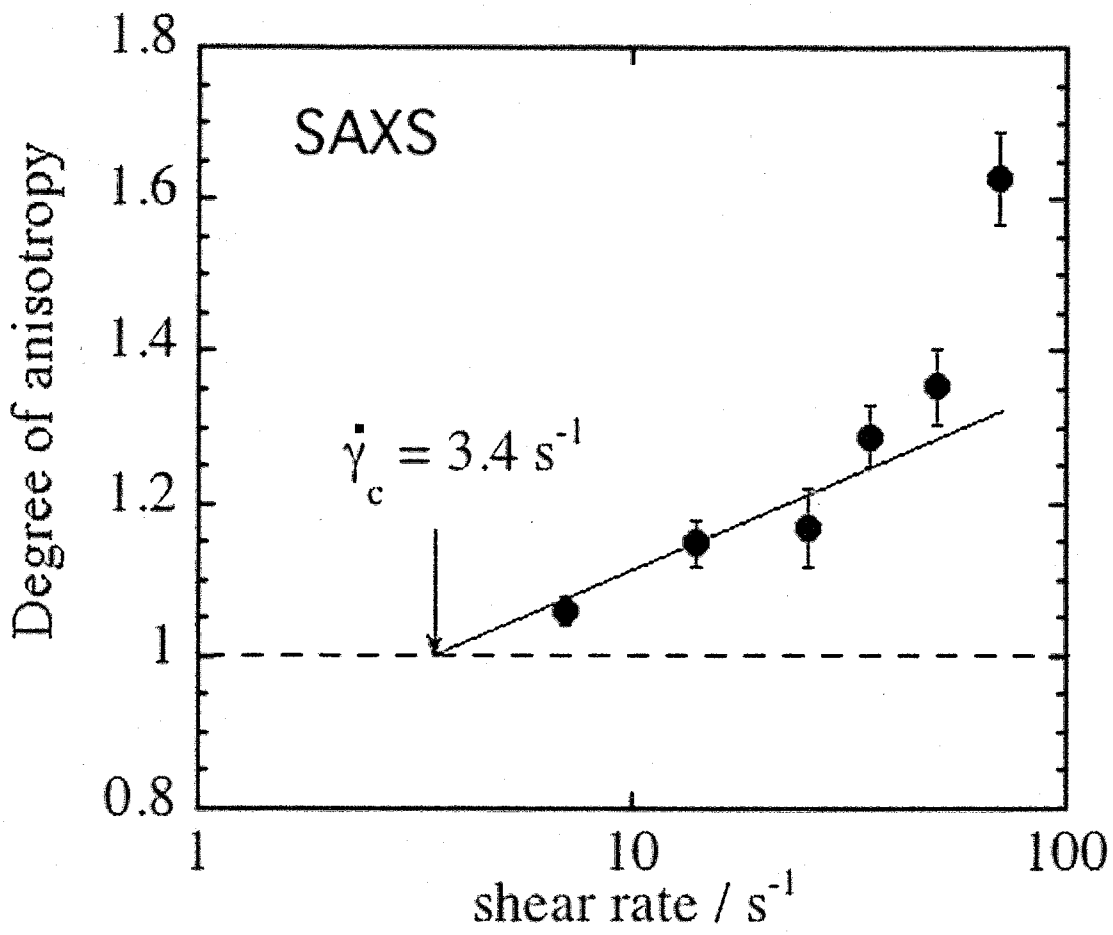

Fig. 11. The degree of anisotropy R_{ani} for SAXS measurements is plotted against logarithm of the shear rate.

the shear rate. In contrast to the onset time the degree of anisotropy is almost independent of the shear rate in the low shear rate region and increases with the shear rate above a certain critical shear rate. Assuming a linear relationship between the degree of anisotropy and the logarithm of the shear rate below 35 s^{-1}, we extrapolated the degree of anisotropy to unity to evaluate the critical shear rate to be 3.4 $\pm$0.6 s^{-1}. The error was estimated from the upper and lower slopes of the extrapolation. The critical shear rate for the anisotropy evaluated in the SAXS (or the kebab) (= 3.4 s^{-1}) is close to that in the DPLS (the shish) (= 2.9 s^{-1}). This must imply that the anisotropy of the kebab structure is dominated by the shish formation.

The Q dependence of the scattering intensities normal and parallel to the flow direction are shown in Fig. 12(a) and (b), respectively. The peak position Q_m of the scattering intensity parallel to the flow direction gives us the spacing between the kebab structure aligned along the shish structure. The spacing evaluated from $2\pi/Q_m$ is plotted as a function of the annealing time for the shear rate of 70 s^{-1} in Fig. 13 where the lamella spacing under the quiescent crystallization condition is also plotted. In the quiescent condition, the peak is first recognized at around 2500 s after induction period of about 700 s and the spacing is about 360 Å, which gradually decreases with annealing time to reach about 310 Å. On the other hand, under the shear condition of 70 s^{-1} the scattering peak is recognized at about 250 s after the pulse shear, which is much earlier than the quiescent condition. The initial spacing (= 475 Å) is longer than the quiescent condition (360 Å) and becomes smaller to level off at 320 - 310 Å, which is almost the same as the final value under the quiescent condition. The earlier appearance of the

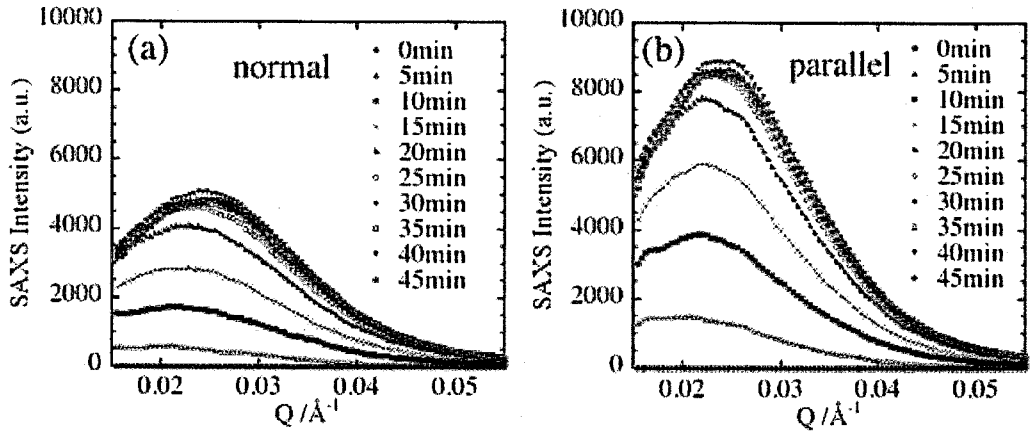

Fig. 12. The Q dependence of the scattering intensities normal (a) and parallel (b) to the flow direction.

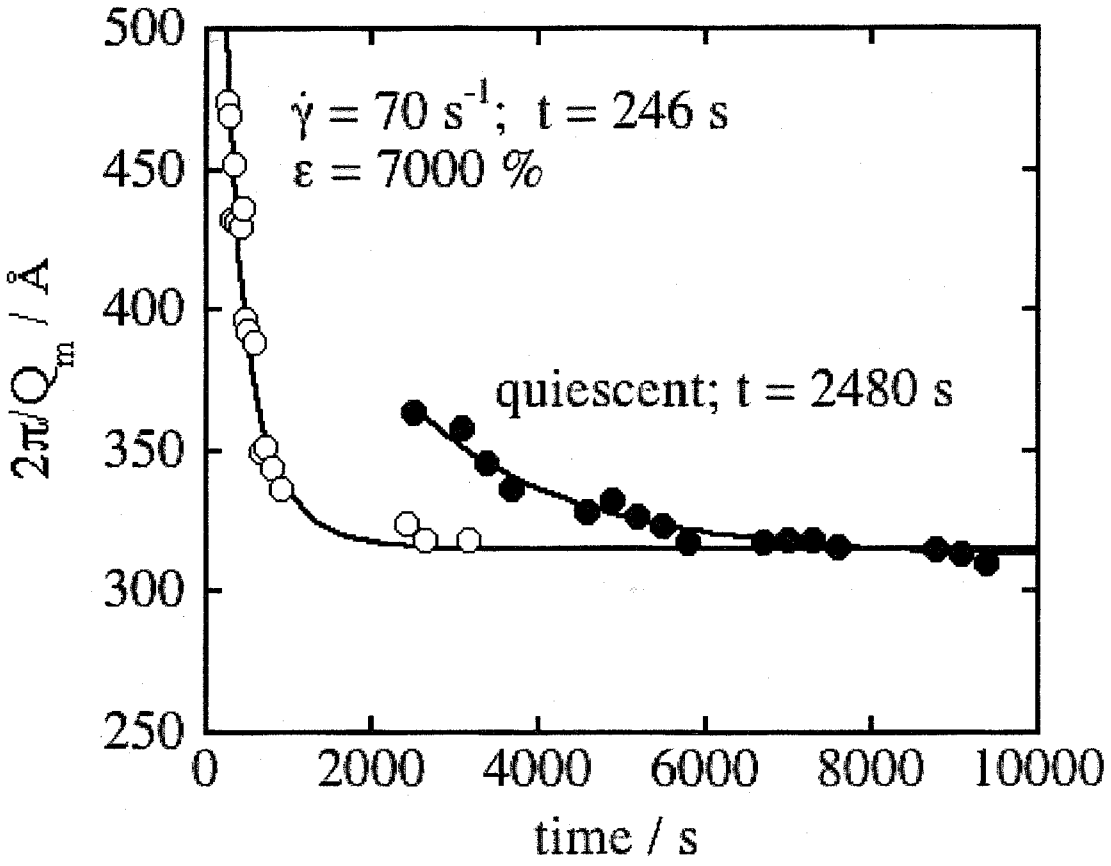

Fig. 13. The spacing evaluated as a function of the annealing time for the shear rate of 70 s^{-1} and quiescent state.

peak shows the acceleration of the crystallization rate under the shear. This must be caused by epitaxial secondary nucleation on the shish structure.

The large initial value of the lamella spacing under the shear must show that lamellae (the kebabs) grow site-randomly on the shish, but not regularly one by one on the shish. However, the same final spacing between the quiescent and shear conditions implies that it is not determined by the shear effects.

4-3-4 WAXS results

Time resolved wide-angle X-ray scattering (WAXS) measurements were performed on the crystallization process of i-PP under the same temperature and shear conditions as the DPLS and SAXS measurements. The crystallization temperature T_c was 132 °C and the shear strain was 7000 % for all the measurements. In the WAXS measurements we observed the time evolution of the local crystalline structure in both of the shish and the kebab, particularly in the kebab because the amount of kebab is much larger than the shish. Time evolution of 2D WAXS patterns are shown in Fig. 14 for the shear rates of 0, 7 and 70 s^{-1}. The scattering patterns are isotropic under the quiescent condition while it is anisotropic under the shear condition. In order to see the anisotropy clearly we plotted the scattering intensities in directions normal and parallel to the shear direction in Fig. 15(a) and (b), respectively, where the intensities are shifted vertically for clarification. The diffraction patterns show that the crystal has a α-form and the intensity must be from the kebab. The diffraction intensity from

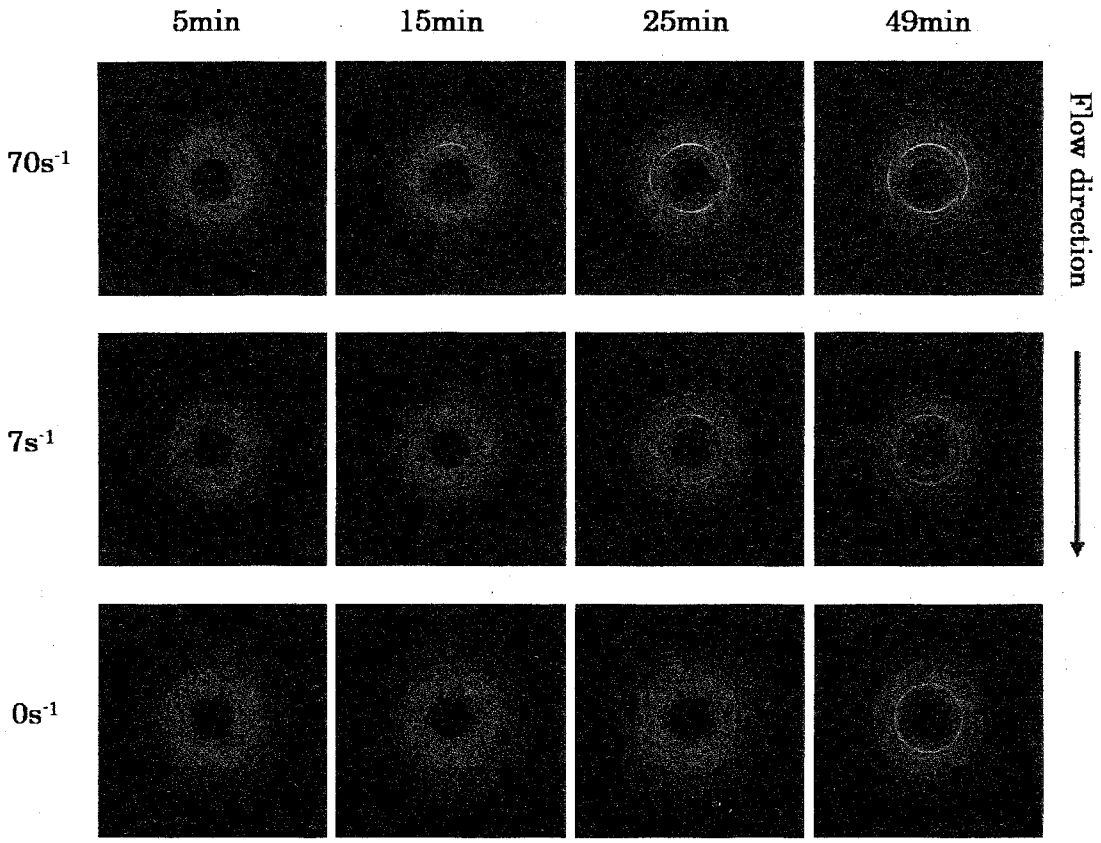

Fig. 14. Time evolution of 2D SAXS patterns for two shear rates.

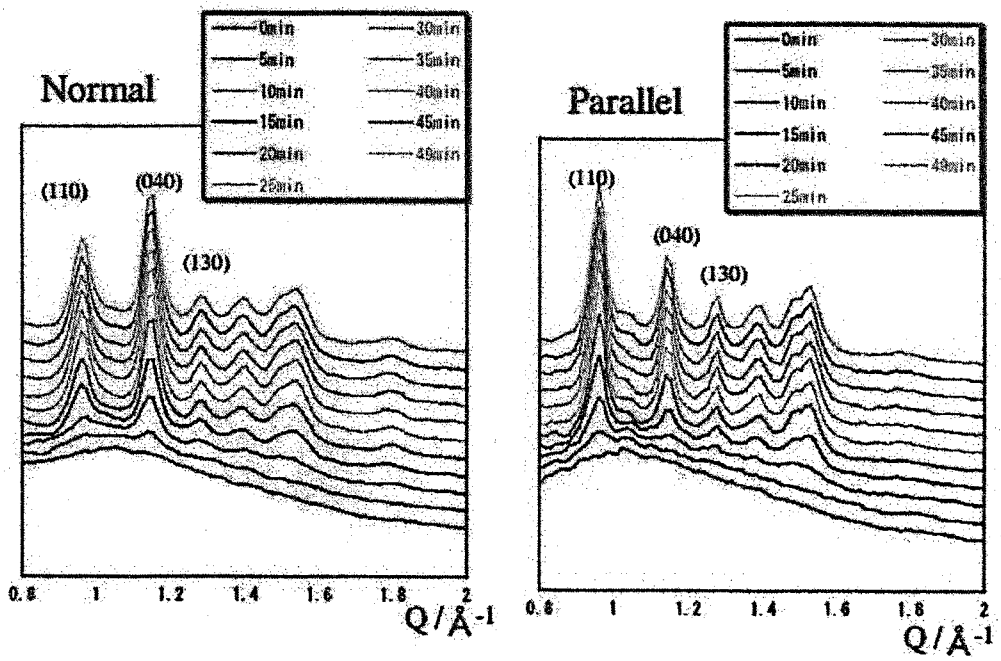

Fig. 15. The WAXS intensities in directions normal and parallel to the shear direction.

(040) plane is larger in the normal direction than in the parallel direction, suggesting that the b-axis of the lamella (the kebab) aligns normal to the shear direction, and is the growth direction. The (110) diffraction intensity is larger in the parallel direction than in the normal direction, and hence it is expected that the a-axis rotates around the b-axis during the kebab growth. As seen in Fig. 15(a) and (b), the (040) and (110) diffraction intensities appear earlier in the normal and parallel directions to the flow, respectively, and followed by the intensities in the parallel and normal directions, respectively. This suggests that the kebab grows in a particular direction (along the b-axis) in the early stage while gradually orients isotropically. This must be due to the growth of isotropic spherulites as observed in optical microscope. In fact, the onset time of the (040) diffraction intensity in the parallel direction is close to the onset of the isotropic spherulites under quiescent states (~900 s). Onset time was plotted as a function of shear rate (Fig. 16). The critical shear rate of onset time was 2.3 s^{-1}. This value almost agrees with the values of DPLS (= 1.6 s^{-1}) and SAXS (= 2.8 s^{-1}). These results indicate that the critical shear rates of onset time of DPLS, SAXS and WAXS are dominated by the same origin. The critical shear rate of onset time is a shear rate above which the generation of spherulites is accelerated. Thus it is reasonable that the critical shear rates of onset time determined by DPLS, SAXS and WAXS measurements are agree with each other.

The degree of anisotropy for the (040) diffraction intensity was defined as intensity ratio of the normal direction to the parallel one after subtracting the intensity at t = 0, and plotted in Fig. 17 as a function of logarithm of the

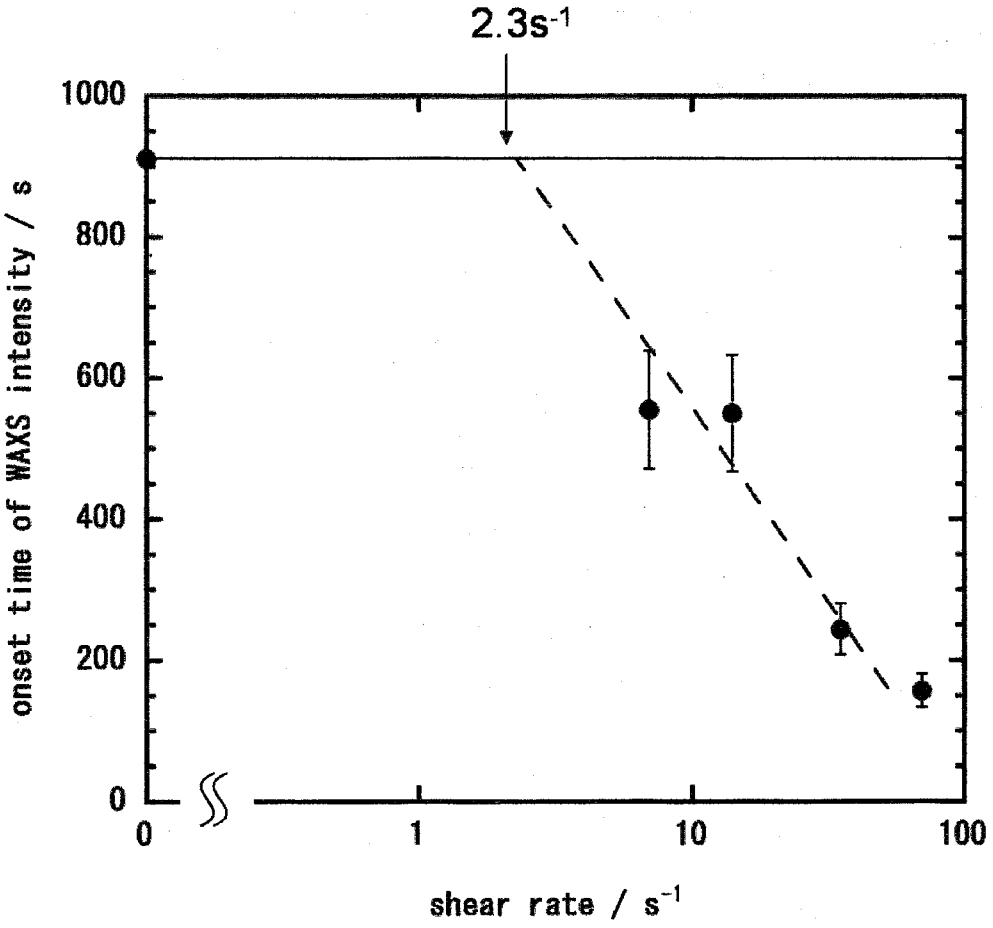

Fig. 16. Onset time of the integrated WAXS intensity normal to the flow direction in the range of (040) peak position.

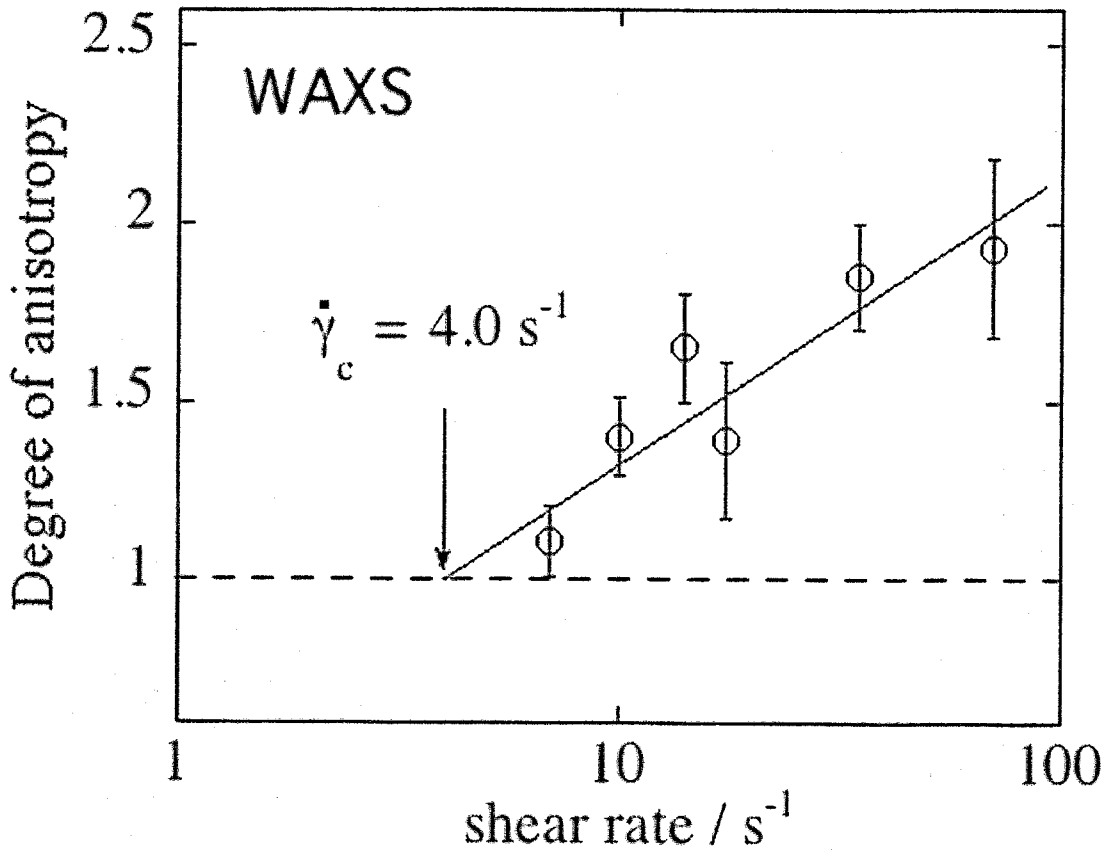

Fig. 17. The degree of anisotropy R_{ani} for WAXS measurements is plotted against logarithm of the shear rate.

shear rate. Although the data points rather scattered, there certainly exists a critical shear rate for the anisotropy or the kebab formation.

Extrapolating the data to the degree of anisotropy of unity, we have evaluated the critical shear rate to be 4.0 s^{-1}. This value is rather close to the critical values for the anisotropic structure formations in DPLS (= 2.9 s^{-1}) and in SAXS (= 3.4 s^{-1}), suggesting that the anisotropic structure is dominated by the same origin.

4-3-5 Comparison of DPLS, SAXS and WAXS data

The time evolutions of the intensities of DPLS, SAXS and WAXS are shown for the crystallization process of i-PP after applying a pulse shear with shear rate of 70 s^{-1} at 132 °C in Fig. 18, where the intensities were normalized to the initial intensity at t = 0 s. We compare scattering intensity as a function of annealing time among DPLS, SAXS, WAXS (Fig. 18). Fig. 18 shows that the onset time of DPLS is the earliest, that of SAXS is second and that of WAXS is the last. The oriented structure parallel to the flow direction in μm scale would be the shish or the precursor of shish, and the oriented structure in nm scale would be the kebab. These results indicate that the shish forms earlier than the kebab.

4-3-6 Generation of shish and kebab

On the basis of the results of Fig. 17 and Fig. 18, we present a schematic drawing of the shish kebab formation (Fig. 19). We suggested that the anisotropic structure was dominated by the same origin in the section **4-3-4.**

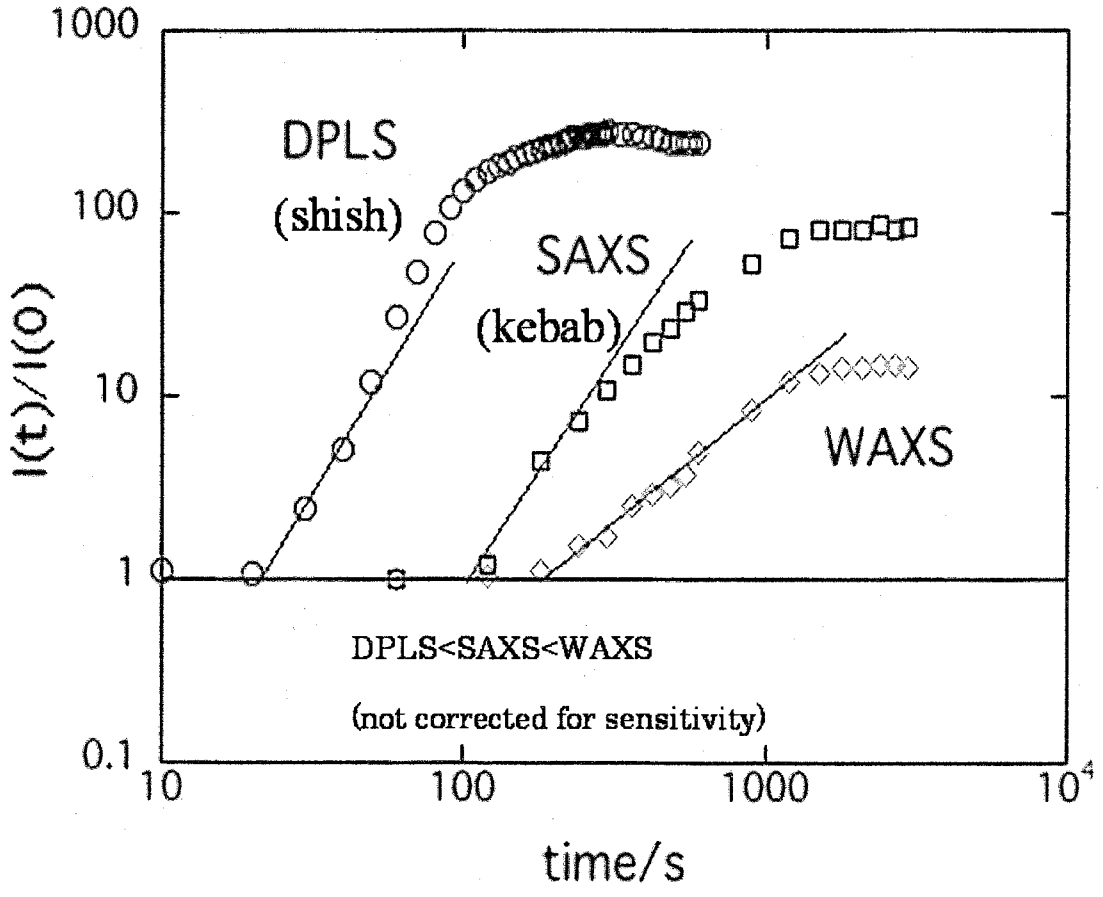

Fig. 18. Comparison of scattering intensity as a function of annealing time among DPLS, SAXS, WAXS.

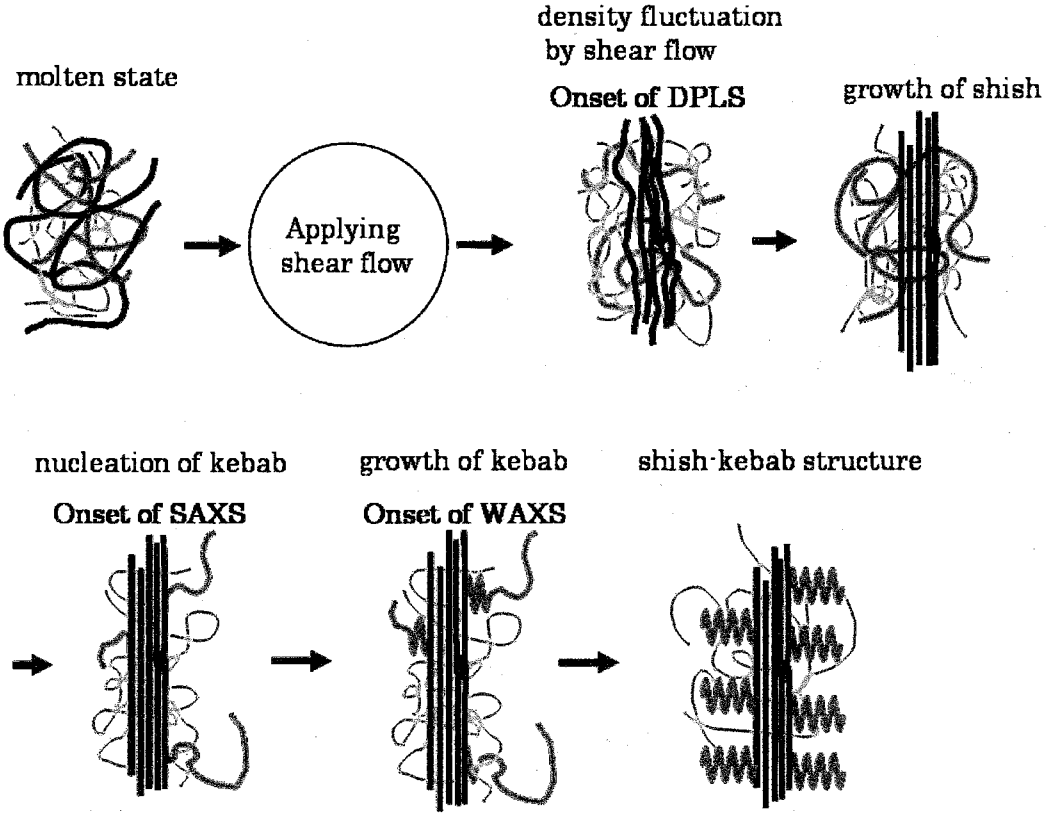

Fig. 19. The schematic drawing of shish kebab formation.

In the section **4-3-5**, we suggested the shish or the precursor of shish formed earlier than the kebab. The conclusions of the sections 4-3-4 and 4-3-5 indicate that generation of the kebab depends on existence of the shish or the precursor of shish. In the early stage of the formation process of the shish kebab structure, it orients to the flow direction. In next, nucleation of the kebab occurs on the shish and grows epitaxially.

4-4 Conclusion

In this chapter, we observed the formation of shish kebab structure under shear flow in a wide spatial scale. These observations indicate us an image of the shish kebab formation (Fig. 19). We suggest that the shish formation dominates the shish-kebab structure.

We also observed the critical shear rate to form the shish kebab structure, and we suggest that shear rate is an important factor to form the shish or the precursor of shish, and the critical shear rate must be dominated by the relation between the relaxation rate of polymer chain and the crystallization rate. For the formation of shish or precursor of shish, polymer chains must be oriented and the orientation must not be relaxed before the crystallization. Many researchers reported that high molecular weight component enhanced the formation of anisotropic structure under many kinds of flow. This must be due to the longer relaxation time of high molecular weight polymer chains.

In the next chapter, we investigate the effects of high molecular weight polymer chain on the shish kebab formation to elucidate the role of the molecular weight.

References

[1] Hoffman, J. D. *Polymer* **1979**, *20*, 1071.

[2] Lieberwirth, I.; Loos, J.; Petermann, J.; Keller, A. *Journal of Polymer Science Part B-Polymer Physics* **2000**, *38*, 1183.

[3] Elmoumni, A.; Winter, H. H.; Waddon, A. J.; Fruitwala, H. *Macromolecules* **2003**, *36*, 6453.

[4] Fukushima, H.; Ogino, Y.; Matsuba, G.; Nishida, K.; Kanaya, T. *Polymer* **2005**, *46*, 1878.

[5] Sharma, L.; Ogino, Y.; Kanaya, T. *Macromolecular Materials and Engineering* **2004**, *289*, 1059.

[6] Agarwal, P. K.; Somani, R. H.; Weng, W. Q.; Mehta, A.; Yang, L.; Ran, S. F.; Liu, L. Z.; Hsiao, B. S. *Macromolecules* **2003**, *36*, 5226.

[7] Dukovski, I.; Muthukumar, M. *Journal of Chemical Physics* **2003**, *118*, 6648.

[8] Liu, C.; Muthukumar, M. *Journal of Chemical Physics* **1998**, *109*, 2536.

[9] Fujisawa, T.; Inoue, K.; Oka, T.; Iwamoto, H.; Uruga, T.; Kumasaka, T.; Inoko, Y.; Yagi, N.; Yamamoto, M.; Ueki, T. *Journal of Applied Crystallography* **2000**, *33*, 797.

[10] Fujisawa, T.; Inoko, Y.; Yagi, N. *Journal of Synchrotron Radiation* **1999**, *6*, 1106.

[11] Fujisawa, T *SPring-8 Beamline Handbook* **2003**, 132.

[12] Shimizu, N.; Inoue, K. *SPring-8 Beamline Handbook* **2003**, 90.

[13] Keller A. and Kolnaar J.W.H.: Meijer, H.E.H. Editor, *Processing of polymers*, VCH, New York 1997, 189.

[14] Mandelkern L; *Crystallization of Polymers Kinetics and Mechanisms*, Cambridge, University Press, 2004, *2*, 1.

Chapter 5

Effects of high molecular weight component on crystallization of polyethylene under shear flow

5-1 Introduction

It was elucidated in Chapters 2, 3 and 4 that formation of shish-kebab structure is governed by the shish structure. Polymer chains must be extended and oriented to form the shish structure. If the oriented state is relaxed before crystallization, the shish structure may not be formed, meaning that the relation between the relaxation rate and the crystallization rate must play an important role in the shish formation. In this chapter, we have investigated effects of the high molecular weight (HMW) component on the shish-kebab formation under shear flow because relaxation time of HMW polymer chain is longer than that of low molecular weight (LMW) one.

The effect of the high molecular component has been investigated for long time. There are already some papers reporting the effects of the HMW component on the crystallization under flow [1-7]. Most of the results indicated that the presence of HMW component or long chains enhanced the crystallization in the rate and the orientation. In the early stage of research in this field, Ward et al. studied effects of HMW component on cold drawing, and showed that it affected the final morphology [1]. Recently, Kornfield et al. [7] have studied effects of the HMW component using model blends of HMW isotactic polypropyrene (M_w = 923,000) and LMW one (M_w = 186,000), both of which have rather narrow molecular weight distributions, and found that the role of the HMW component in shear-induced

crystallization is cooperative, enhanced by the entanglements among the long chains. Hsiao and coworkers [2] also demonstrated the role of the HMW component in blends of non-crystallizing low molecular weight polyethylenes (M_w = 50,000 and 100,000) and crystallizing HMW polyethylene (PE) (M_w = 250,000) using in situ rheo-SAXS and rheo-WAXD techniques. The results indicated that the high molecular weight component dominates the formation of crystallization of precursor structures in the blend under shear flow, and the viscosity of the matrix (low molecular weight component) plays an important role to influence the formation of crystallization precursor structure of the HMW component.

In this chapter we have also investigated the role of the HMW component in the crystallization of blends of HMW PE (M_w = 2,000,000) and LMW PE (M_w = 586,000) under shear flow using depolarized light scattering. In addition, to elucidate that the shish structure is mainly formed from the HMW component, we performed small-angle neutron scattering (SANS) and small-angle X-ray scattering (SAXS) measurements on an elongated blend of HMW hydrogenated PE (M_w = 2,000,000) and low molecular weight deuterated PE (M_w = 200,000).

5-2 Experimental

5-2-1 Samples

In the DPLS studies we used two polyethylenes (PE) with molecular weight M_w = 58,600 and 2,000,000 and the polydispersity M_w/M_n = 8.01 and 12, respectively, where M_w and M_n are the weight- and number-average molecular weight, respectively. The LMW PE was kindly supplied by

Showa Denko Ltd., and the HMW PE by Mitsui Chem. Co. Ltd. The nominal melting temperatures of the LMW and HMW PEs determined by DSC measurements were 134 and 135 °C at the heating rate of 20 °C/min. It should be noted that the molecular weight distributions of the PEs are broad, which may smear the effect of the high molecular weight component. However, the large molecular weight difference [M_w(HMW)/M_w(LMW) ~ 34] may overcome the difficulty.

Two polyethylenes were blended in a solution to ensure the intimate mixing at the molecular level. The mixture of HMW and LMW PEs with a given concentration of the HMW component (0.2 - 3 wt%) was dissolved in xylene with anitoxidant regent (2,6-tert-butyl-*p*-cresole) to form a homogeneous solution at 130 °C under nitrogen atmosphere. After keeping the solution at 130 °C for 1 h, it was quenched into ice water to precipitate as a gel, filtered from xyelene and washed with methanol several times. The gel was vacuum-dried at 70 °C for 2 days and then hot-pressed at 165 °C for 5 min and quenched rapidly to ice water to get a thin film ~0.3 mm thick. The LMW PE film was prepared under the same procedure as a control sample. In the DPLS measurements, the thin film was placed between two quartz plates and the thickness was controlled at 0.3 mm before applying the shear.

For the SANS and SAXS measurements, we used HMW hydrogenated PE with M_w = 2,000,000 and M_w/M_n = 12 and LMW deuterated PE with M_w = 200,000 and M_w/M_n = 5. The HMW PE is the same PE as in the DPLS measurements. Strips of the blend film of HMW hydrogenated PE (3 wt%) and LMW deuterataed PE (97 wt%), which was prepared in the same procedure as the DPLS samples, were elongated about 6 times at 133 °C just

below the nominal melting temperature (= 135 °C) and quenched to ice water. These elongated strips were aligned on the cell window. It is noted that the quenching of the blends was done as rapidly as possible to avoid the segregation [8-10]. However, in this work we did not check the segregation directly.

5-2-2 Measurements

DSC measurements DSC measurements were carried out to characterize the thermal properties of the sample using Perkin-Elmer DSC-7. All the DSC scans were performed under nitrogen environment.

DPLS measurements Two-dimensional (2D) depolarized light scattering (DPLS) measurements were carried out using a home-made apparatus with He-Ne laser (80 mW, wavelength λ = 632.8 nm) as a light source and a CCD camera with 2D screen as a detector system. The range of length of scattering vector Q in this experiment is 4 x 10^{-5} to 2.6 x 10^{-4} $Å^{-1}$, where Q is given by $Q = 4\pi\sin\theta/n\lambda$ (2θ and n being scattering angle and the refractive index, respectively).

A Linkam CSS-450 high temperature shear cell with quartz windows was used to control the temperature and the shear conditions. The sample thickness in the cell was 0.3 mm for all the DPLS measurements. The temperature protocol for the shear experiments is shown in Fig. 1: (a) heat the polymer sample from room temperature to 165 °C at a rate of 30 °C/min, (b) hold at 165 °C for 5 min, (c) cool down to the crystallization temperature T_c = 129 °C at a rate of 30 °C/min, and (d) hold the temperature at 129 °C

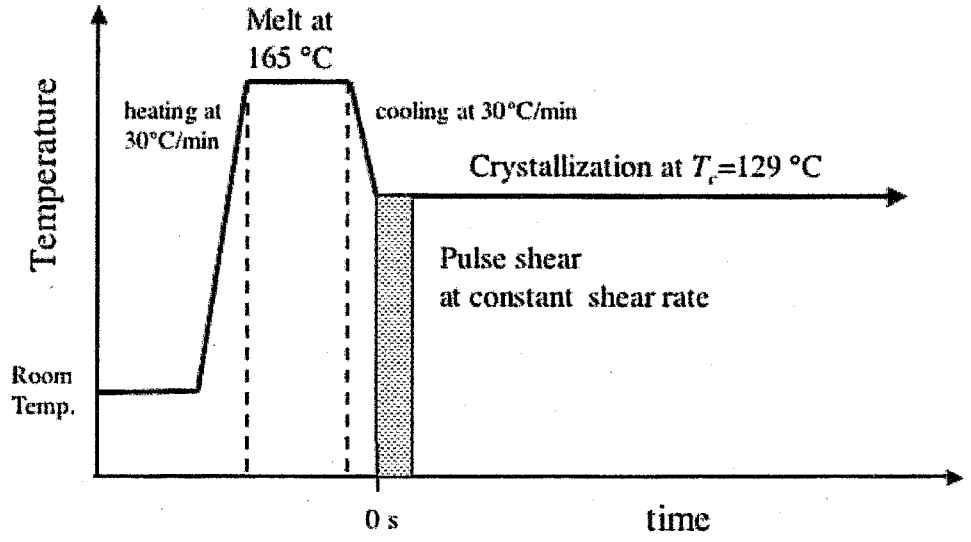

Fig. 1. Temperature protocol for the shear experiments on polyethylene.

for the DPLS measurements. The polymer melt was subjected to pulse shear just after reaching the crystallization temperature T_c of 129 °C.

SANS measurements Small-angle neutron scattering (SANS) measurements were performed with SANS-U spectrometer [11] at the JRR-3M reactor in Japan Atomic Energy Research Institute (JAERI), Tokai, Japan. Neutron wavelength λ in this measurement was 7 Å with the dispersion $\Delta\lambda/\lambda$ of 10 %. The scattered neutrons were detected by a two-dimensional position sensitive detector having 65 x 65 cm^2 (128 x 128 pixels) area. In the measurements, we covered a range of magnitude of scattering vector Q (= $4\pi\sin\theta/\lambda$; λ and 2θ being neutron wavelength and scattering angle, respectively) from 0.005 to 0.13 $Å^{-1}$.

SAXS measurements Small-angle X-ray scattering (SAXS) measurements were carried out with a small-angle scattering apparatus installed at the beam line BL45XU [12] in the Synchrotron Radiation Facility, SPring-8, in Nishiharima, Japan. The wavelength of the incident X-ray was 0.9 Å and scattered X-ray was detected by a two dimensional CCD camera with an image intensifier. The Q range covered in this measurement was 0.009 to 0.15 $Å^{-1}$.

5-3 Results and discussion

Fig. 2 shows an example of the time evolution of 2D DPLS pattern for the LMW PE during the crystallization process after pulse shear with the shear rates of 1, 8 and 16 s^{-1}. The shear strain was 3200 % for all the

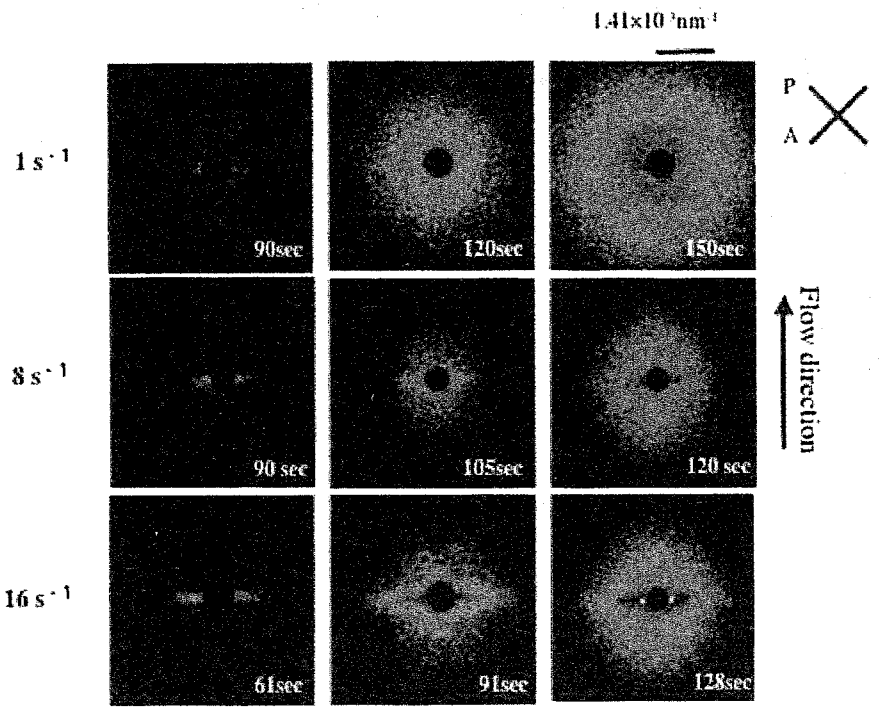

Fig. 2. Time evolution of 2D DPLS patters form the matrix PE (LMW PE) during the crystallization process at 129 °C after pulse shear with shear rates $\dot{\gamma}$ of 1, 8 and 16 s-1 from top to bottom. The shear strain ε was 3200 %.

measurements. After a certain induction period for the structure formation, we observed isotropic 2D DPLS pattern for the shear rate $\dot{\gamma}$ of 1 s^{-1}. The induction period becomes shorter with increasing the shear rate although the 2D pattern is isotropic, showing the acceleration of the crystallization rate with increasing the shear rate. As the shear rate further increases, the 2D scattering pattern becomes anisotropic above about $\dot{\gamma}$ = 6 s^{-1} in addition of the acceleration of the crystallization rate. For example, the 2D pattern for $\dot{\gamma}$ = 16 s^{-1} shows a streak-like scattering normal to the flow direction in the early stage as seen in the lowest row in Fig. 2. The streak-like scattering means that long scattering objects are aligned along the flow direction, which must be a shish structure or a precursor of the shish-structure.

As further annealing, the isotropic scattering emerges and covers the anisotropic scattering.

5-3-1 Evaluation of critical concentration of high molecular weight component for anisotropy

In order to evaluate the anisotropy of the 2D scattering pattern quantitatively we have defined a measure for the anisotropy. A typical 2D anisotropic scattering pattern is shown in Fig. 3(a) and the scattering intensities normal and parallel to the flow direction are plotted against Q in Fig. 3(b), respectively. The scattering intensities are very weak in the high Q range while they begin to increase at a certain onset Q values in the low Q range, depending on the scattering direction. We have defined a ratio of the onset Q value normal to the flow direction to the parallel one (= $Q_{\perp}/Q_{\parallel}$) as a

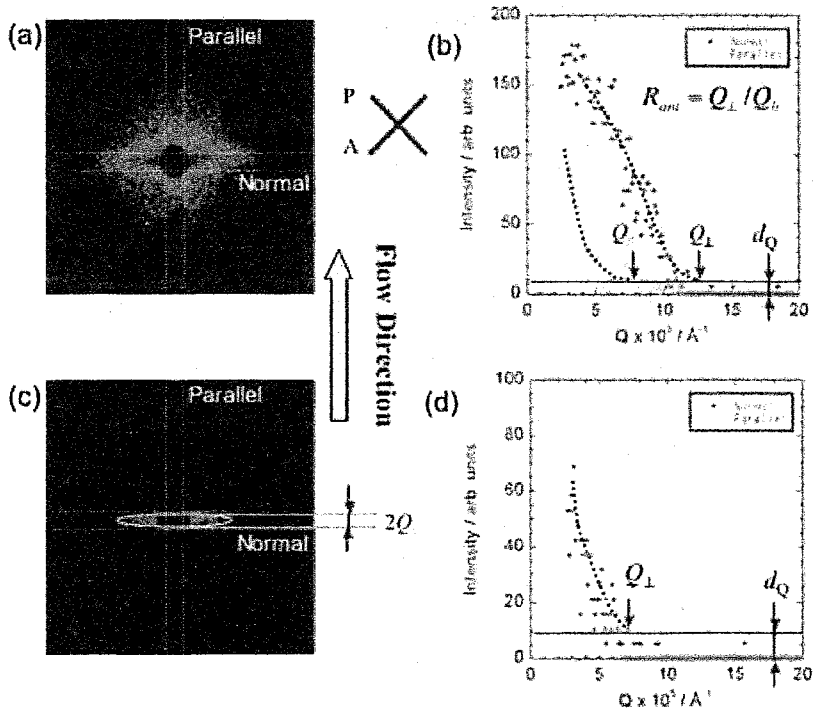

Fig. 3. (a), (c): Typical 2D DPLS patterns, and (b), (d): the definitions of the degree of anisotropy R_{ani} ($=Q_\perp / Q_{//}$) corresponding to (a) and (c), respectively.

measure of anisotropy, and termed the degree of anisotropy R_{ani} in this chapter. The degree of anisotropy R_{ani} is time-dependent: it has a maximum in the early stage and decreases with annealing time. We have employed the maximum value of R_{ani} for the discussion of the degree of anisotropy in this chapter.

The maximum value of the degree of anisotropy R_{ani} is plotted as a function of shear rate at various shear strains in Fig. 4 for the matrix PE. In the low shear rate region, the value of R_{ani} is unity, meaning that the scattering is isotropic, and begins to increase at a critical shear rate $\dot{\gamma}$, which depends on the shear strain. For example, the degree of anisotropy R_{ani} is unity below the shear rate of 6 s^{-1} and begins to increase at around 6 s^{-1} for the shear strain ε of 3200 %. On the basis of the results, we adopted such shear condition for the experiments of the PE blend that the matrix PE does not show anisotropic scattering pattern. If we observe anisotropic scattering pattern in the PE blend during the crystallization we can directly attribute to the effects of the HMW PE.

Fig. 5 shows the time evolution of 2D DPLS patterns of the matrix PE and the PE blend including 3 wt% HMW one during the crystallization process after the pulse shear at 129 °C. The shear rate $\dot{\gamma}$ and the shear stain ε are 4 s^{-1} and 1600 %, respectively. In the case of the matrix PE isotropic scattering pattern appears at around 80 s after applying the pulse shear and increases in intensity with annealing time. On the other hand, the 3 % blend shows a very sharp streak-like scattering normal to the flow direction, which appears at around 30 s after the pulse shear, corresponding to the shish-like structure. At about 80 s in the late stage, isotropic scattering

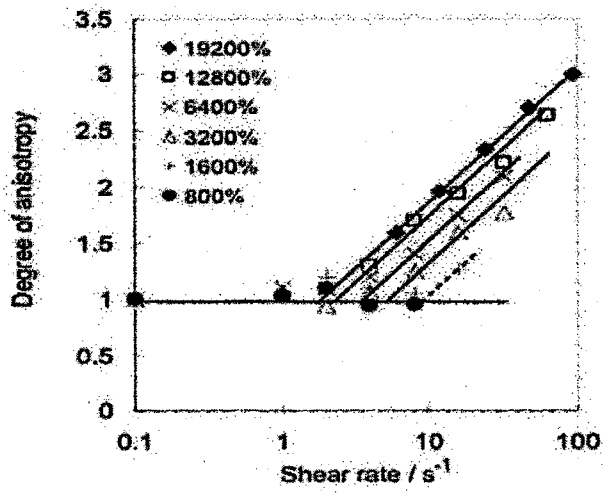

Fig. 4. Shear rate dependence of the degree of anisotropy R_{ani} for the matrix PE (LMW PE) at various shear strains ε from 800 to 19200 %.

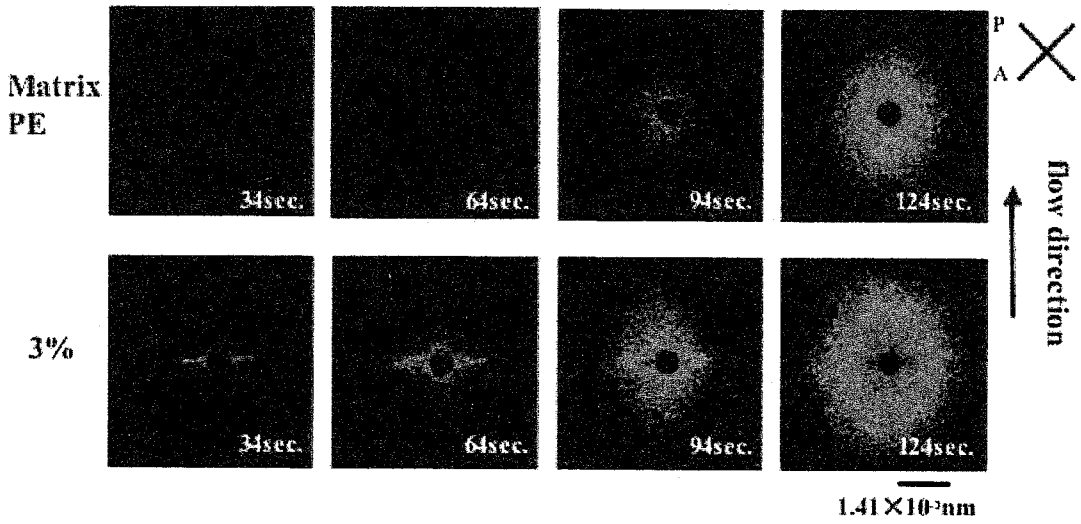

Fig. 5. Time evolution of 2D DPLS patters for the matrix PE (LMW PE) and the PE blend including 3 wt% HMW PE during the crystallization process at 129 °C after pulse shear. The shear rate $\dot{\gamma}$ and the strain ε were 4 s^{-1} and 1600 %, respectively.

appears to cover the anisotropic one. The onset time of the isotropic component in the 3 wt% blend is very close to that in the matrix PE, suggesting that the isotropic scattering in the blend is coming from the matrix PE. On the other hand, it is evident that the streak-like scattering is due to the HMW PE because the matrix PE does not show any anisotropic scattering under this shear condition. From these observations, we can directly conclude that the HMW component enhances the formation of the shish-like structure.

In the next step we have examined the effects of the concentration of the HMW PE C_{HMPE}. Fig. 6 shows the 2D scattering patterns of the PE blends at 68 and 98 s after the pulse shear as a function of the concentration C_{HMPE}. The shear rate and the shear strain were 4 s^{-1} and 3200 %, respectively. Anisotropic scattering patterns were not observed when the concentration C_{HMPE} of the HMW PE was less than 0.5 wt %. At around C_{HMPE} = 0.5 wt%, a very weak anisotropic scattering was observed at 68 s after the pulse shear as seen in Fig. 6 and the 2D scattering intensity increases in the anisotropy with the concentration C_{HMPE}, suggesting that there is a critical concentration C^*_{ani} for the anisotropic scattering at around C_{HMPE} = 0.5 wt%. This will be discussed quantitatively later. It should be noted that we showed 2D patterns at 68 s after the pulse shear in Fig. 6 because the anisotropy was the highest at around this time at any concentrations above C_{HMPE} = 0.5 wt%. After the onset of the anisotropic scattering, the isotropic scattering appears at around 80 s after the pulse shear and covers the anisotropic scattering. It is interesting to point out that the onset time of the isotropic scattering, which must come from the LMW PE, is almost

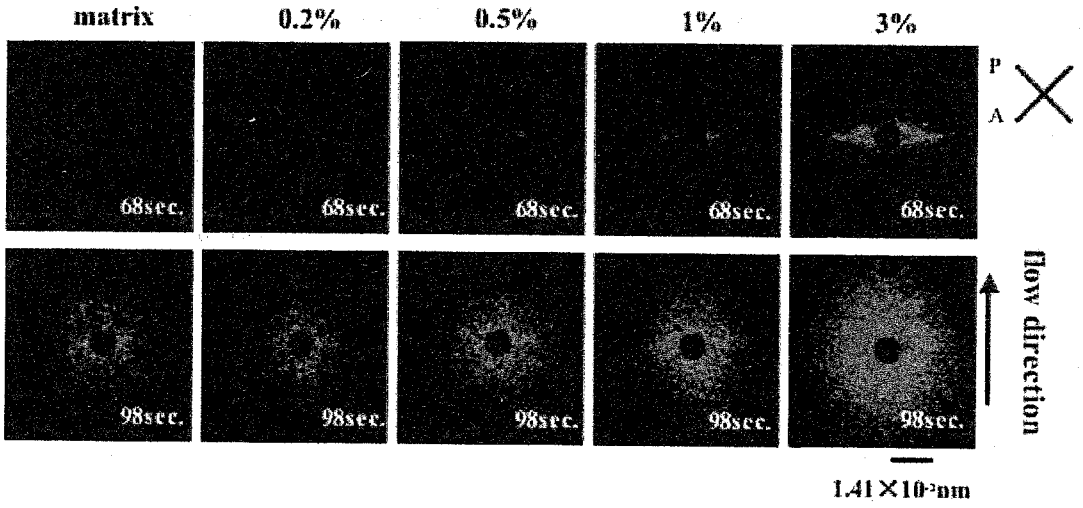

Fig. 6. 2D DPLS patters of the PE blends with various concentrations of the HMW PE from 0 to 3 wt % at 68 and 98 s after pulse shear. The shear rate $\dot{\gamma}$ and the strain were ε 4 s^{-1} and 1600 %, respectively.

independent of the concentration below C_{HMPE} = 0.5 wt%, suggesting that the HMW PE hardly affect the crystallization process of the LMW PE below the critical concentration around C_{HMPE} = 0.5 wt%. On the other hand, the isotropic scattering slightly increases in intensity and the onset time becomes shorter with increasing the concentration C_{HMPE} above C_{HMPE} = 0.5 wt%.

In Fig. 7, the degree of anisotropy R_{ani} at 68 s after the pulse shear is plotted against the concentration of the HMW PE C_{HMPE} for three shear conditions, under which the matrix PE does not show the anisotropic scattering pattern. It is obvious that the degree of anisotropy is almost unity below C_{HMPE} = 0.5 - 0.6 wt% while it abruptly increases above this concentration, showing that the critical concentration for the anisotropy C^*_{ani} is 0.5 - 0.6 wt%. It should be noted that the critical concentration is almost independent of the shear strain although the degree of anisotropy increases with the shear strain. This gives us a hint to consider the physical meaning of the critical concentration for the anisotropy C^*_{ani}.

We compare the critical concentration C^*_{ani} to the chain overlap concentration C^*_{Rg} of the HMW PE. The overlap concentration of polymer chains with radius of gyration R_g is given by

$$C^*_{Rg} = \frac{M_w}{\frac{4}{3}\pi\left\langle R_g^2\right\rangle^{3/2} N_A}, \tag{5.1}$$

where $\left\langle R_g^2\right\rangle$ is the mean square radius of gyration of the polymer chain, which is given by eq. (5.2) under the Gaussian chain approximation with molecular weight distribution $U = (M_w/M_n)^{-1}$ [13].

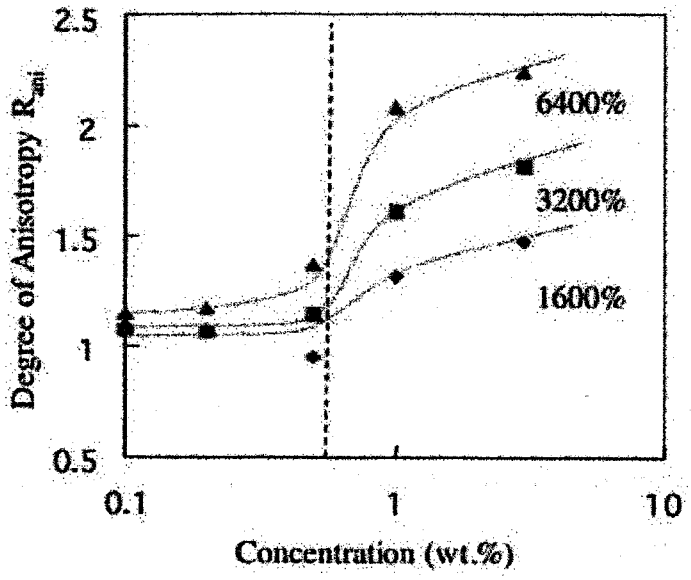

Fig. 7. Degree of anisotropy R_{ani} as a function of the concentration of HMW PE. Shear rate $\dot{\gamma}$ = 4 s^{-1}, shear strain ε = 1600, 3200 and 6400 %.

$$\left\langle R_g^2 \right\rangle = \frac{bL(2U+1)}{3(U+1)}, \tag{5.2}$$

where b and L are the persistence length and the contour length. Taking the literature data $[\left\langle R_g^2 \right\rangle / M_w]^{1/2}$ = 0.46 [10], we have calculated the overlap concentration C^*_{Rg} to be 0.178 g/cm^3 or 0.209 wt%, which is smaller than the critical concentration. The ratio of the critical concentration to the overlap concentration C^*_{ani} / C^*_{Rg} is 2.5 - 3. This strongly suggests that entanglements of the HMW PE are very important for the formation of the shish-like structure. This agrees with the finding of Kornfield et al. [7] that the role of the long chain in the shear-induced crystallization is cooperative rather than a single chain event. This result may be understood in the following picture. In order to produce the shish-like structure polymer chains must be extended due to the shear. Suppose that the HMW PE are isolated in the blend, they are somewhat extended by the shear flow, however it does not lead to the anisotropic structure formation as seen in Fig. 6. On the other hand, when the concentration of HMW PE is above the critical value for the entanglements, the chains must be extended due to the connectivity as polymer network is deformed. The critical concentration for the anisotropy C^*_{ani} must correspond to the critical concentration for the effective entanglements. This is schematically illustrated in Figs. 8(a) and 8(b). This picture reminds us the gel spinning technique [14-17] to produce ultra-high strength and ultra-high modulus fiber of PE although all of the situations are not the same. In this procedure, PE chains are extremely extended because the tension is transmitted though the cross-linking points in the gel network. On the other hand, in order to obtain the ultra-high

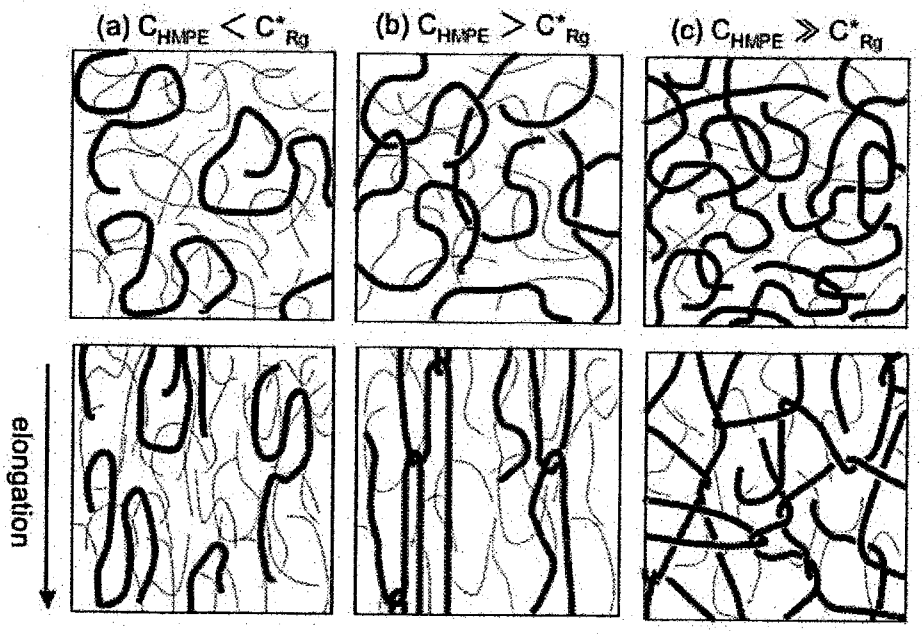

Fig. 8. Schematic illustrations of the role of HMW PE in formation of shish-like structure. Thin and thick curves represent HMW and LMW PEs, respectively. (a) $C_{HMPE} < C^*_{Rg}$: HMW PE chains are isolated and slightly extended by the shear, (b) $C_{HMPE} > C^*_{Rg}$: HMW PE chains are entangled and extended due to the connectivity as polymer network is deformed, (c) $C_{HMPE} >> C^*_{Rg}$: too many cross-linking points (or entanglements) prevent extension of HMW PE chains.

strength fiber the number of the cross-linking points should be as little as possible because too many cross-linking points prevent the extension of polymer chains. It is therefore expected in the crystallization of the PE blend under the shear that the formation of the shish-like structure is depressed at a rather high concentration of the HMW PE above C^*_{ani} because the polymer chains cannot be extended due the shear because of too many entanglements as illustrated in Fig. 8(c).

5-3-2 Comparison between small angle neutron scattering and small angle X-ray scattering 2D-patterns

The DPLS measurements indicated that the formation of shish-like structure is enhanced by addition of the HMW component. It is therefore expected that the shish-like structure is mainly formed from the HMW PE. However, it has not been directly confirmed in the experiments. Furthermore, in small-angle X-ray scattering (SAXS) measurements [18,19] the shish-like structure was not always observed even though the shear condition was stronger than in the present experiment. In cases of observing no shish-like structure, many interpretations are possible, e. g., the shish-like structure is once formed but it disappears immediately after the formation; the number of the shish is too little to be detected within the sensitivity of SAXS; the length of the shish is too long to be detected within the SAXS resolution. In order to shed light on these problems, we have performed SANS and SAXS measurements on an elongated blend of HMW hydrogenated PE (3 wt%) with M_w = 2,000,000 and LMW deuterated PE with M_w = 200,000. This experiment is on the basis of the following idea. From

the results of the DPLS measurements, we expect that the shish-like structure is mainly formed from the HMW hydrogenated PE. It is well known in SANS that the scattering contrast between hydrogenated and deterated PEs is very large [20], so that we can observe the shish-like structure if it is formed from the HMW hydrogenated PE due to the high scattering contrast. On the other hand, in the SAXS case the scattering contrast arises from the electron density difference, which corresponds to the mass density difference in one component systems. Therefore, we expect very large difference between the SANS and SAXS scattering profiles. However, if the HMW hydorogenated PE chains are homogeneously distributed in the shish and the kebab structure, the SANS scattering contrast in the small-angle region arises only from the density difference similar to the SAXS. In this case, we expect that the scattering patterns are almost the same in both the SANS and SAXS. Hence, we can see whether or not the shish is mainly formed from the HMW PE by comparing the SANS data to the SAXS data.

The observed 2D SANS pattern is shown in Fig. 9(a). Very strong streak-like scattering intensity is observed along the direction normal to the elongation in the low Q range, suggesting that the shish structure is formed during the elongation process. Two-spot scattering pattern is also observed in the direction parallel to the elongation. This must correspond to the spacing between the neighboring kebabs (lamellar crystalline structure) periodically attached along the shish. The scattering contrast seems very large in the streak-like scattering compared to the two-spot scattering. In order to see it quantitatively, the sector averaged scattering intensities in

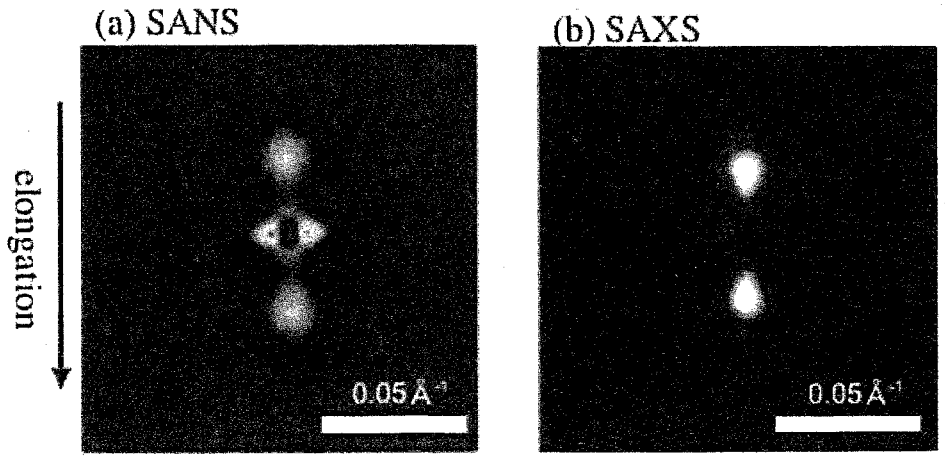

Fig. 9. 2D SANS (a) and 2D SAXS (b) patterns from an elongated blend of LMW deuterated PE and HMW hydrogenated PE (3 wt%).

the azimuthal angle ranges between –5° and +5° and between 85° and 95° are plotted against Q in Fig. 10(a), where the azimuthal angle of 0° corresponds to the elongational direction. In the direction normal to the elongation the scattering intensity has no peaks and is very strong in the low Q range below about 0.02 $Å^{-1}$. On the other hand, the intensity parallel to the elongation shows a peak at around Q = 0.025 $Å^{-1}$, corresponding to the spacing between the neighboring kebabs. What we have to emphasize here is that the intensity from the shish below about 0.01 $Å^{-1}$ is much stronger than that from the kebab, showing the high scattering contrast of the shish. This implies that the shish structure is mainly formed from the HMW hydrogenated PE and the kebab is formed from the LMW deuterated PE.

Small-angle X-ray scattering (SAXS) measurements were also performed on the same sample in the SR facility, SPring-8 in Nishiharima, and the observed 2D scattering pattern is shown in Fig. 9(b). In contrast to the SANS result, the streak-like scattering due to the shish structure was not observed although the two-spot pattern due to the spacing between the kebabs was clearly observed in the direction parallel to the elongation. The sector averaged SAXS intensities are also shown in Fig. 10(b) in the azimuthal angle ranges between –5° and +5° and between 85° and 95°. The scattering intensity parallel to the elongation shows a peak corresponding to the kebab spacing similar to the SANS result. On the other hand, the intensity normal to the elongation is very weak, particularly in the low Q range below about 0.02 $Å^{-1}$ in contrast to the SANS data, corresponding to the fact that the shish structure is not observed in the SAXS measurement although the shish structure is certainly present in the elongated blend as

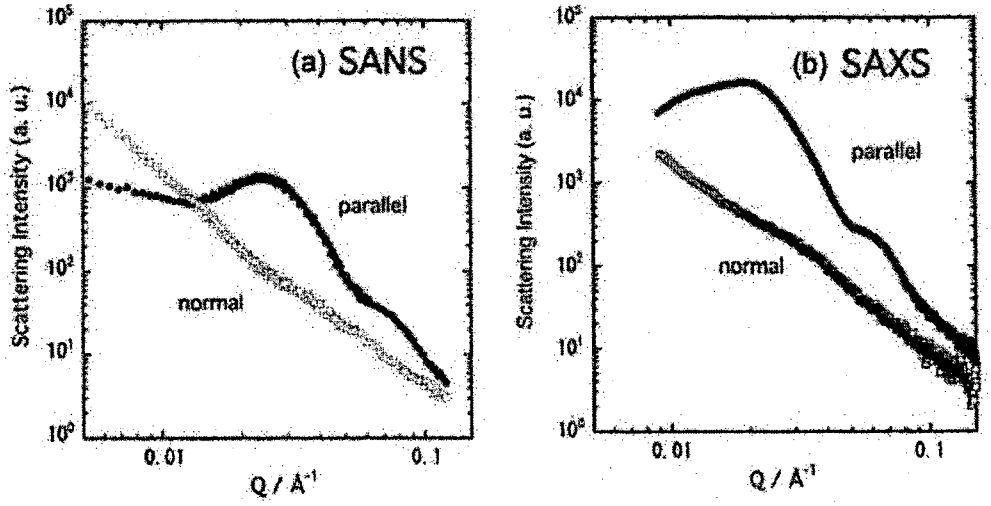

Fig. 10. Sector averaged SANS (a) and SAXS (b) intensities from an elongated blend of LMW deuterated PE and HMW hydrogenated PE (3 wt%) in directions normal and parallel to the elongation.

seen in the SANS result (Fig. 9(a)). In combination of the SANS and SAXS results, we can directly conclude that the shish is mainly formed from the HMW component and the number of shish is too little to be detected within the present SAXS sensitivity.

5-4 Conclusion

We have studied the crystallization process of blends of the HMW polyethylene (PE) and LMW PE under shear flow using DPLS with the pulse shear technique as a function of the concentration of HMW PE in the range of 0 to 3 wt %, focusing on effects of the HMW PE on the shish-like structure formation. It was found that the shish-like structure formation is enhanced by the HMW component above a critical concentration C^*_{ani} of the HMW PE. This critical concentration is 2.5 - 3 times larger than the chain overlap concentration C^*_{Rg}, suggesting that the entanglements of HMW PE chains play an essential role for the formation of shish-like structure. On the basis of the results, it was suggested that a gel spinning-like mechanism for the shish-like structure formation. The DPLS results also suggest that the shish-like structure is made from the HMW component. In order to confirm it we performed the small-angle neutron scattering (SANS) and X-ray scattering (SAXS) measurements on the elongated blend of the HMW hydrogenated PE (3 wt%) and LMW deuterated PE. In the SANS streak-like scattering due to the shish structure was clearly observed in the direction normal to the elongation although it was absent in the SAXS. This is due to the high neutron scattering contrast between the hydrogenated and deuterated PE, confirming that the shish structure is

mainly formed from the HMW PE and the number of the shish is too little to be detected within the present SAXS sensitivity.

References

[1] Capaccio, G.; Ward, I. M. *Polymer* **1974**, *15*, 233.

[2] Yang, L.; Somani, R. H.; Sics, I.; Hsiao, B. S.; Kolb, R.; Fruitwala, H.; Ong, C. *Macromolecules* **2004**, *37*, 4845.

[3] Sherwood, C. H.; Price, F. P.; Stein, R. S. J.Polym. Sci., Polym. Symp. **1978**, *63*, 77.

[4] Lagasse, R. R.; Maxwell, B. *Polymer Engineering and Science* **1976**, *16*, 189.

[5] Vleeshouwers, S.; Meijer, H. E. H. *Rheologica Acta* **1996**, *35*, 391.

[6] Keller, A.; Odell, J. A. *Colloid and Polymer Science* **1985**, *263*, 181.

[7] Seki, M.; Thurman, D. W.; Oberhauser, J. P.; Kornfield, J. A. *Macromolecules* **2002**, *35*, 2583.

[8] Schelten, J.; Wignall, G. D.; Ballard, D. G. H. *Polymer* **1974**, *15*, 682.

[9] Schelten, J.; Wignall, G. D.; Ballard, D. G. H.; Schmatz, W. *Colloid and Polymer Science* **1974**, *252*, 749.

[10] Schelten, J.; Ballard, D. G. H.; Wignall, G. D.; Longman, G.; Schmatz, W. *Polymer* **1976**, *17*, 751.

[11] Ito, Y.; Imai, M.; Takahashi, S. *Physica B* **1995**, *213*, 889.

[12] Fujisawa, T.; Inoue, K.; Oka, T.; Iwamoto, H.; Uruga, T.; Kumasaka, T.; Inoko, Y.; Yagi, N.; Yamamoto, M.; Ueki, T. *Journal of Applied Crystallography* **2000**, *33*, 797.

[13] Oberthuer, R. c. Makromol. Chem. **1978**, *179*, 2693.

[14] Smith, P.; Lemstra, P. J.; Kalb, B.; Pennings, A. J. *Polymer Bulletin* **1979**, *1*, 733.

[15] Smith, P.; Lemstra, P. J. *Journal of Materials Science* **1980**, *15*, 505.

[16] Lemstra, P. J.; Vanaerle, N.; Bastiaansen, C. W. M. *Polymer Journal* **1987**, *19*, 85.

[17] Bastiaansen, C. W. M. *Journal of Polymer Science Part B-Polymer Physics* **1990**, *28*, 1475.

[18] Somani, R. H.; Hsiao, B. S.; Nogales, A.; Srinivas, S.; Tsou, A. H.; Sics, I.; Balta-Calleja, F. J.; Ezquerra, T. A. *Macromolecules* **2000**, *33*, 9385.

[19] Liangbin, L.; Jeu, W. H d. *Macromolecules* **2003**, 36, 4862.

[20] Higgins, J. S.; Benoit, H. C. *Polymer and Neutron Scattering.* Oxford Clarendon Press **1994**

Chapter 6

Crystallization of polyhydroxybutyrate under shear flow

-Effect of shear rate-

6-1 Introduction

Environmental pollution is a big and serious problem all over the world, which includes air pollution, acid rain, environmental hormone, industrial waste and so on. Recently, many countries in the world tackle the environmental issues from various points of view. Form the polymer science point of view, one of the most serious problems is that synthetic polymers are not degradable in the natural environment, and hence in many countries they try to change current synthetic plastic (or polymer) products to the so-called green products degradable in the natural environment. In other words, synthetic polymer products currently used do not return to the soil. When we dispose such products in the natural environmental, it is desired that they return to the soil. It is argent to produce plastic products degradable in the natural environment. One of the solutions to this problem is to use naturally produced polymers degradable in the natural environmental. However, such polymers do not have good mechanical, thermal and optical properties compared to currently used synthetic polymers. To improve the properties, polymer scientists are extensively investigating biodegradable polymers as new polymer materials. However, bioplastics or biopolymers still have many problems to be improved about their properties.

In this chapter, we studied crystallization of a well-established bioplastic,

polyhydroxybutyrate (PHB) under shear flow, which is a bacterially synthesized biodegradable semi-crystalline polymer belonging to the family of polyhydroxyalkanoates [1-4]. The fundamental issue regarding PHB involves underpinning of the spherulites during secondary crystallization, which causes severe cracking, and renders the material brittle - a process referred to as embrittlement [5-7]. To overcome weaknesses in polymers, polymer blending has been applied [8-10] and researchers have used this method to blend PHB with a synthetic polymer, hoping the second component will nullify this cracking process [11-13]. Another alternative is to alter the spherulite morphology by varying the structural orientation of PHB. By achieving a PHB shish-kebab structure we believe that this embrittlement problem can be solved and a whole range of properties can be improved.

We investigated the basic effects of shear rate for shish-kebab structure formation of polyethylene and isotactic polypropylene in Chapters 2-4, and found that shear rate was one of the most important factors to control the shish-kebab structure. As a first step in the study of PHB crystallization, we investigated the effects of shear rate on the shish-kebab formation process using in-situ optical microscope (OM), depolarized light scattering (DPLS) and small-angle X-ray scattering (SAXS) techniques. We would like to establish whether PHB can attain a shish-kebab morphology and gain further insight into the shish-kebab formation mechanism.

6-2 Experimental

6-2-1 Sample

Polyhydroxybutyrate with M_w = 360,000 was purchased from Aldrich Chemicals, Japan and pressed at 180 °C to obtain sheets about 0.3 mm thick.

6-2-2 Measurements

Optical microscope measurements Optical microscope (OM) measurements were performed with Olympus BX50 with video attachment. The shear cell Linkam CSS-450 with quartz windows was connected to the OM.

Depolarized light scattering measurements Depolarized light scattering (DPLS) measurements were carried out using a home-made apparatus with a detector system consisting of a screen and CCD camera (model CS8300, Tokyo Electronic Industry Co., Ltd), and a He-Ne laser light source (wavelength λ = 632.8 nm) covering a range of scattering vector Q of 3.5 x 10^{-5} to 3.0 x 10^{-4} $Å^{-1}$ to determine the shish formation in PHB. The shear cell Linkam CSS-450 was also connected to the DPLS apparatus.

Small-angle X-ray scattering measurements Small-angle X-ray scattering (SAXS) measurements were performed using a small-angle scattering machine at a beam line BL40B2 in the Synchrotron Radiation Facility SPring-8, Nishiharima, involving the shear cell apparatus Linkam CSS-450 with Kapton film windows 25 μm thick. The wavelength of incident X-ray was 1 Å and the camera length was 2 m, covering a Q range of 0.015 to 0.47 $Å^{-1}$.

The sample thickness in the cell was 0.3 mm for all the OM, DPLS and

SAXS measurements. The temperature protocol for the shear experiments is shown in Fig. 1: (a) heat the polymer sample from room temperature to 190 °C at a rate of 30 °C/min, (b) hold at 190 °C for 3 min, (c) cool down to the crystallization temperature T_c = 130 °C at a rate of 30 °C/min, and (d) hold the temperature at 130 °C for the measurements. The polymer melt was subjected to pulse shear just after reaching the crystallization temperature T_c of 130 °C.

6-3 Results and discussion

6-3-1 Optical microscope measurements

Fig. 2 shows the in-situ optical microscope images of PHB during the crystallization process under quiescent and shear conditions (shear rate = 35 s^{-1}). It is natural that under quiescent condition we observed normal spherulites as shown in Fig. 2(a). At the low shear rates such as 10 and 35 s^{-1}, only spherulites are achieved, similar to the condition where no shear is applied. This is demonstrated in Fig. 2(b). However, as the shear rate is increased up to 50 s^{-1} this leads to distinctive row nucleated structures which become a unified single structure with annealing time. This time evolution of the row nucleated structure is shown in Fig. 3. A row of nuclei initially forms in the shear path, with no visible interconnecting structure. These individual nuclei emerge in an irregular pattern, i.e., non equi-distant alignment, this is contrary to other researchers findings [14] where the nuclei appear in an ordered and regular fashion. The nuclei then grow until they meet, which terms the rosary-like structure (Fig. 3(b)), and they merge into a distinct orientated structure aligned along the flow direction, which

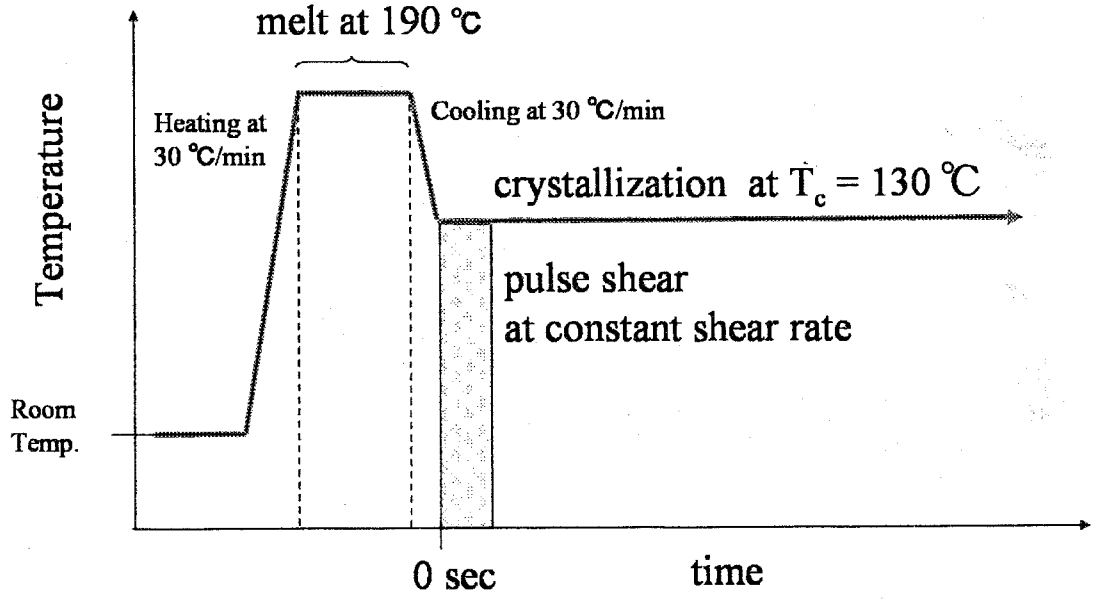

Fig. 1. Temperature protocol for the shear experiments on PHB.

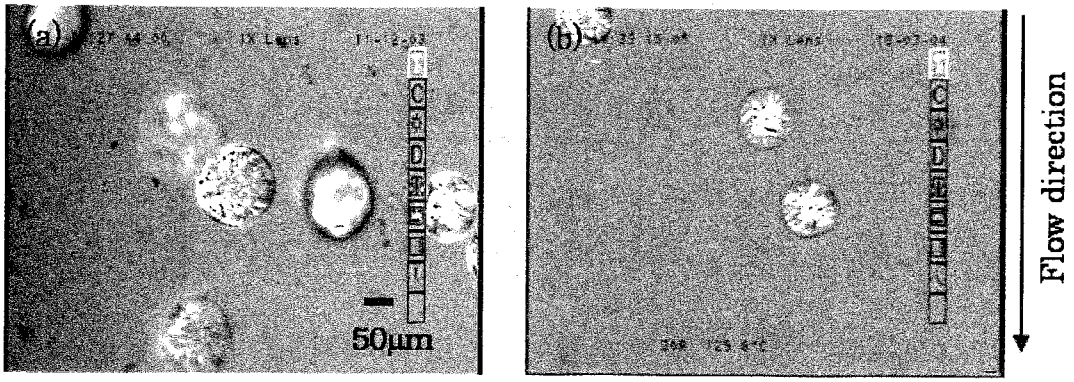

Fig. 2. The optical microscope images of PHB at low shear rate (a) with no shear, and (b) at 35 s^{-1}.

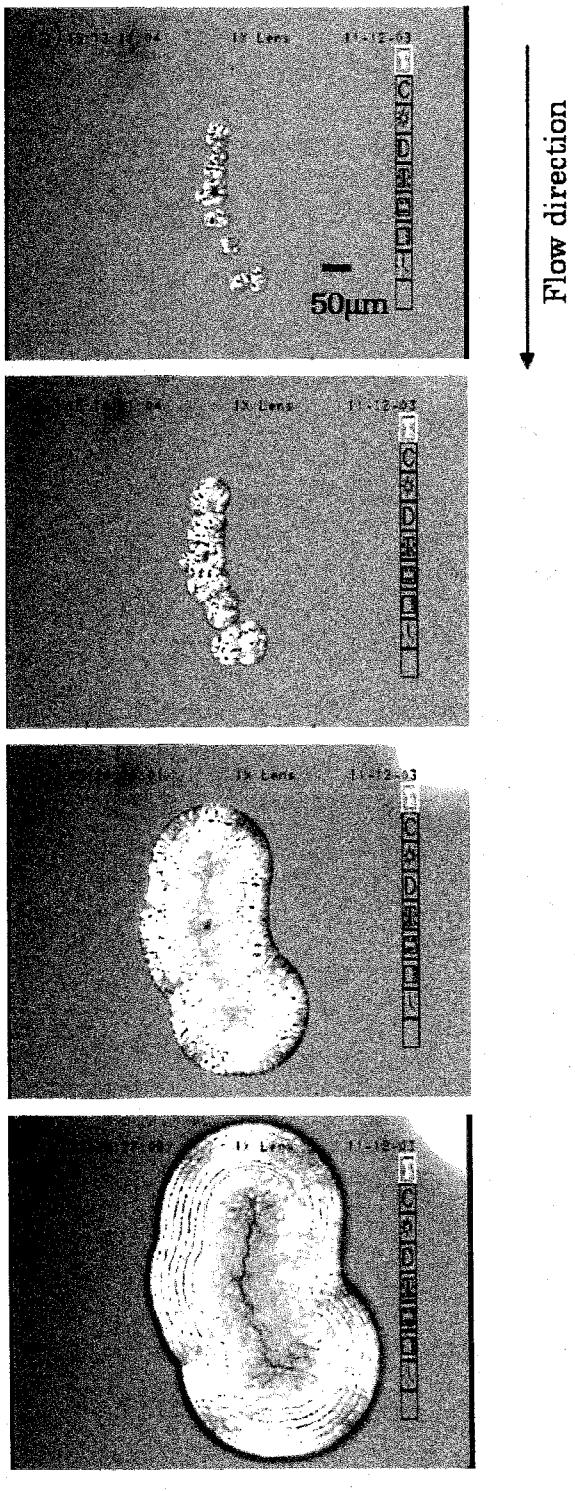

Fig. 3. The optical microscope images of PHB at $50s^{-1}$. (a) 96sec, (b) 159sec, (c) 255sec, (d) 834sec after applying shear flow.

terms the cylinder-like structure (Fig. 3(d)).

It is clear that there are differences in the morphology and the crystal growth between low and high shear rate conditions although we do not observed a clear shish-kebab structure. At the high shear rate, we could observe connected spherulites oriented along the flow direction (the rosary-like structure). However we could not observe any visible interconnected structure between the nuclei of spherulites. If there is not interconnected structure (or shish-like structure) between the nuclei how can the spherulites align along the flow direction?

In the OM observations, the magnification and the sensitivity are limited, so that there is a possibility that we could not observe interconnected structures even if they were there. In order to tackle this problem we performed the DPLS measurements.

6-3-2 Depolarized light scattering measurements

Under the same shear conditions, we have performed depolarized light scattering (DPLS) measurements on crystallization process of PHB. The DPLS results were also found to be extremely dependent on the shear conditions applied. At a low shear rate of 35 s^{-1} isotropic scattering patterns appeared as shown in Fig. 4(a) and (b). These isotropic patterns may be scattering from normal spherulite structure observed in the optical microscope measurements (see Fig. 2(b)). As well known that light scattering pattern of spherulite usually shows the so-called clover pattern, but the observed pattern is not. In this measurement we used a sample 300 μm thick to focus on the structure formation process in the early stage of

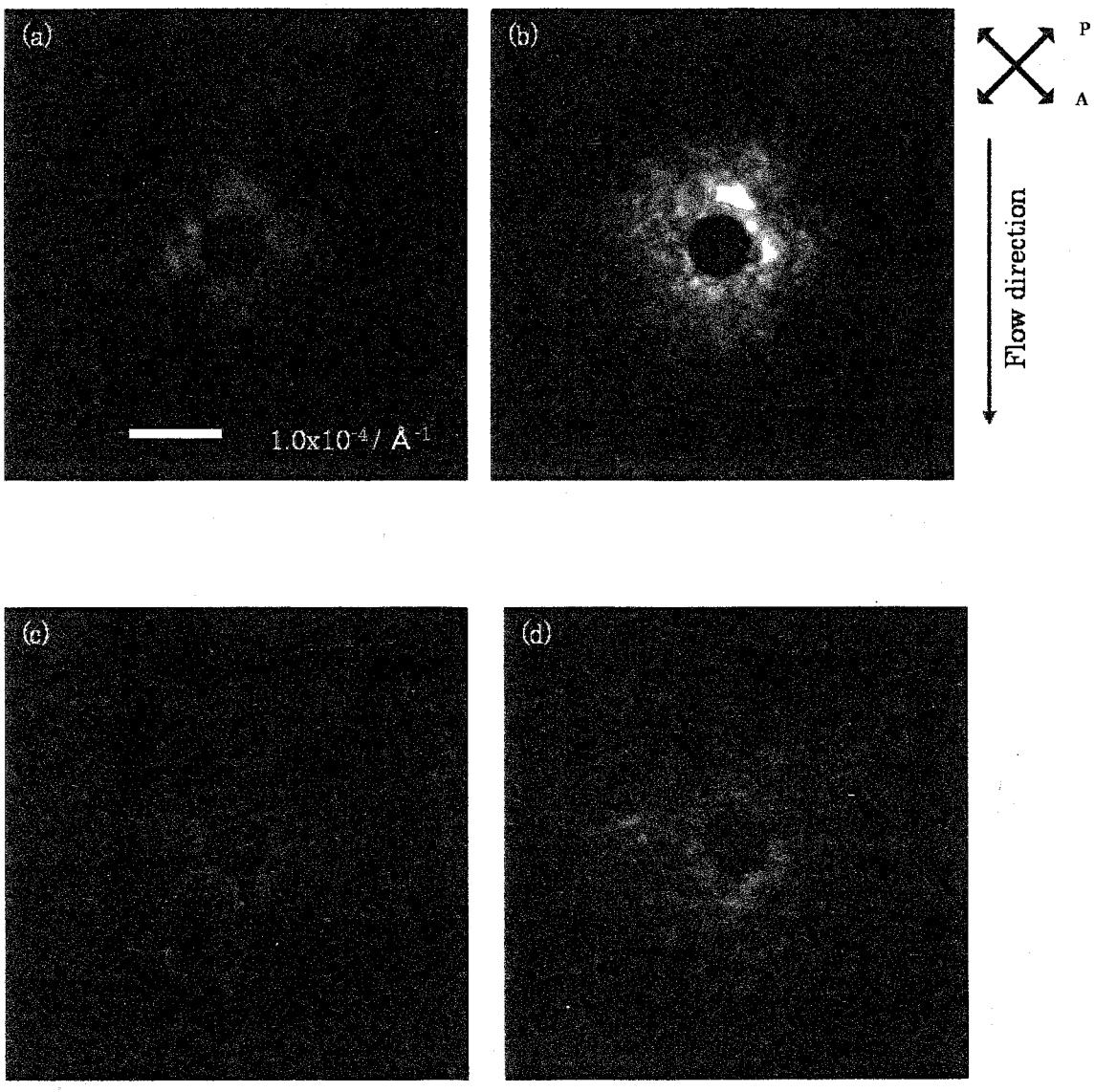

Fig. 4. The DPLS images of PHB at $35s^{-1}$ (a)240sec, (b) 480sec, at $100s^{-1}$ (c) 180sec, (d) 300sec.

crystallization, and the 300 μm is too thick to observe the structure in the late stage due to multiple scattering. This must be a reason why we could not observe the clover pattern. Fig. 4(c) and (d) show the scattering pattern at a shear rate of 100 s^{-1}. Fig 4(c) shows slightly anisotropic scattering pattern in a direction normal to the flow direction at about 180 s after applying a pulse shear. This result indicates that an ordered structure aligned along the flow direction generates although the degree of orientation is not high and the number of the anisotropic objects is not large. This anisotropic scattering pattern changes to an isotropic one as the crystallization proceeds (Fig. 4(d)). Judging from the Q range in the present DPLS measurements the anisotropic objects are too small to assign the rosary-like structure and/or the cylinder-like structure observed in the OM (see Fig. 3), implying that some other anisotropic objects aligned along the flow direction are formed in the initial stage of the crystallization of PHB under shear flow. This must be a threadlike structure (or a shish-like structure), which could not observed in the OM. Therefore, when we discuss the formation mechanism of the rosary-like structure and/or the cylinder-like structure, we have to take into accounts that the threadlike structure or the shish-like structure, the orientation of which is not high, is formed in the initial stage of crystallization under flow.

6-3-3 Small-angle X-ray scattering measurements

In order to observe the structure formation in nm scale during the crystallization of PHB under shear flow we also performed SAXS measurements under the same shear condition as the OM and DPLS

measurements.

Fig. 5 shows the time evolution of the 2D SAXS patterns at the shear rates of 0 and 50 s^{-1}. At the shear rate 0 s^{-1}, the scattering patterns are isotropic and show a ring corresponding to the lamella spacing (the so-called long period) at round 400 s after applying a pulse shear. At the shear rate 50 s^{-1}, very weak anisotropy was observed in the direction parallel to the flow in the early time of crystallization. In order to confirm the anisotropic orientation of the lamellae, we have calculated 1D scattering profiles parallel and perpendicular to the flow direction and shown in Fig. 6. It is clear that the intensity of the parallel direction is stronger than that of normal one, showing that the lamella structure preferably aligned along the flow direction *in average* although the degree of orientation is not high.

It is interesting to point out that the anisotropy appeared in the early stage at the shear rate 50 s^{-1} decreases with annealing time, and again increases in the late stage. It could be discussed in connection with the OM observation in Fig. 3. In the early stage of crystallization, oriented nuclei induced by shear flow may generate and the lamellae grow epitaxially on the nuclei, giving the anisotropic SAXS pattern. However, as seen in Fig. 3(b) when isotropic spherulites form in the shear (rosary-like structure) the SAXS pattern may be isotropic. After the spherulites merge and the morphology changes to cylinder-like (cylinder-like structure), lamellae grow on the cylinder-like structure aligned long the normal direction to the flow. Thus, the anisotropy again increases in the late stage of crystallization.

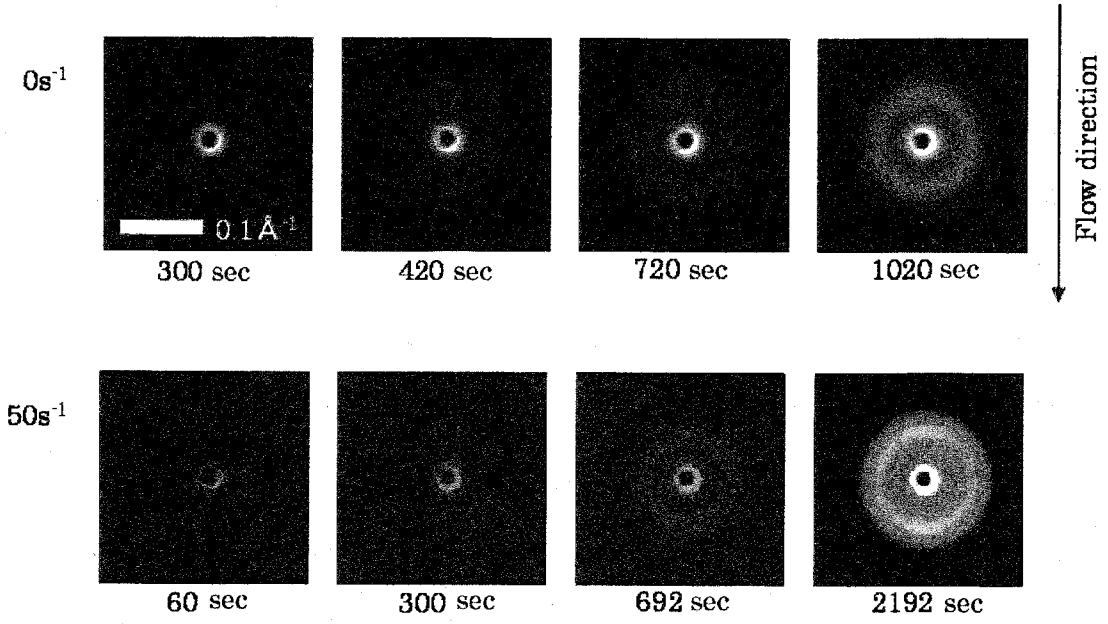

Fig. 5. Time evolution of SAXS images of PHB at shear rates of 0 s^{-1} and 50 s^{-1}.

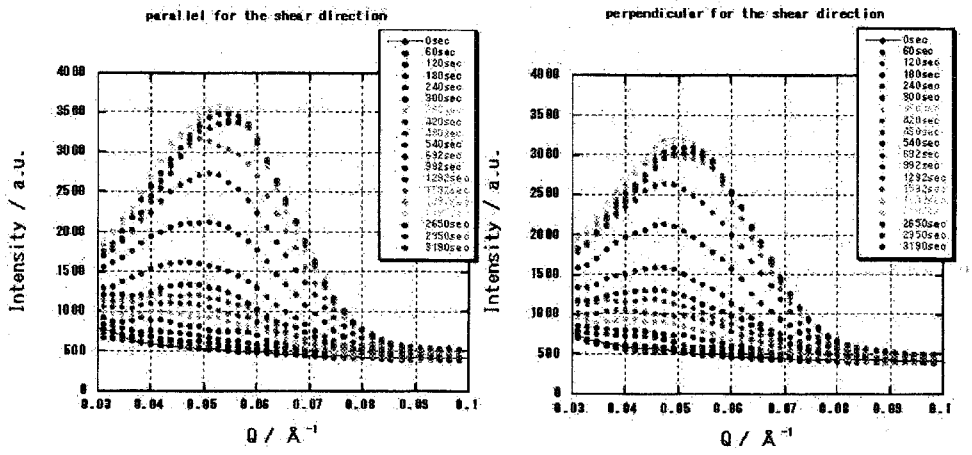

Fig. 6. The time evolution of 1D profile for parallel and normal to the flow direction at the shear rate 50 s^{-1}.

6-3-4 Formation mechanism of rosary-like and/or cylinder-like structure

In this section we consider the formation mechanism of the rosary-like structure and the cylinder-like structure on the basis of the above mentioned OM, DPLS and SAXS results. First we assume that the threadlike structure or the shish-like structure is formed in the very early stage of crystallization under shear flow because we observe the streak-like scattering in the DPLS measurements although the orientation is very broad. However, we did not observe this shish-like structure in the OM. This must be due to the limitation of sensitivity, implying that the number of shish-like structure is very small. Another point that we have to take into accounts is that the formation rate of spherulites is accelerated by the shear, suggesting that the nucleation rate is accelerated by the shear. These hidden nuclei must be aligned along the shear direction because the observed spherulites are aligned along the flow direction. These observations tell us the following scenario on the rosary-like structure formation, which was schematically illustrated in Fig. 7.

At a high shear rate above about 50 s^{-1}, the shish-like structure is formed in the very early stage of crystallization of PHB under shear flow (Fig. 7(a)) although the number of the shish-like structures is very small. The shish-like structure tends to relax to a coil structure. If the nucleation rate is faster than the relaxation rate, the oriented nature of the shish-like structure enhances the nucleation rate. We can expect a competition between the nucleation and the relaxation. In such situation that crystal nucleation occurs in some parts of the shish-like structure and the relaxation occurs in some other parts, we can expect a series of nuclei aligned along the

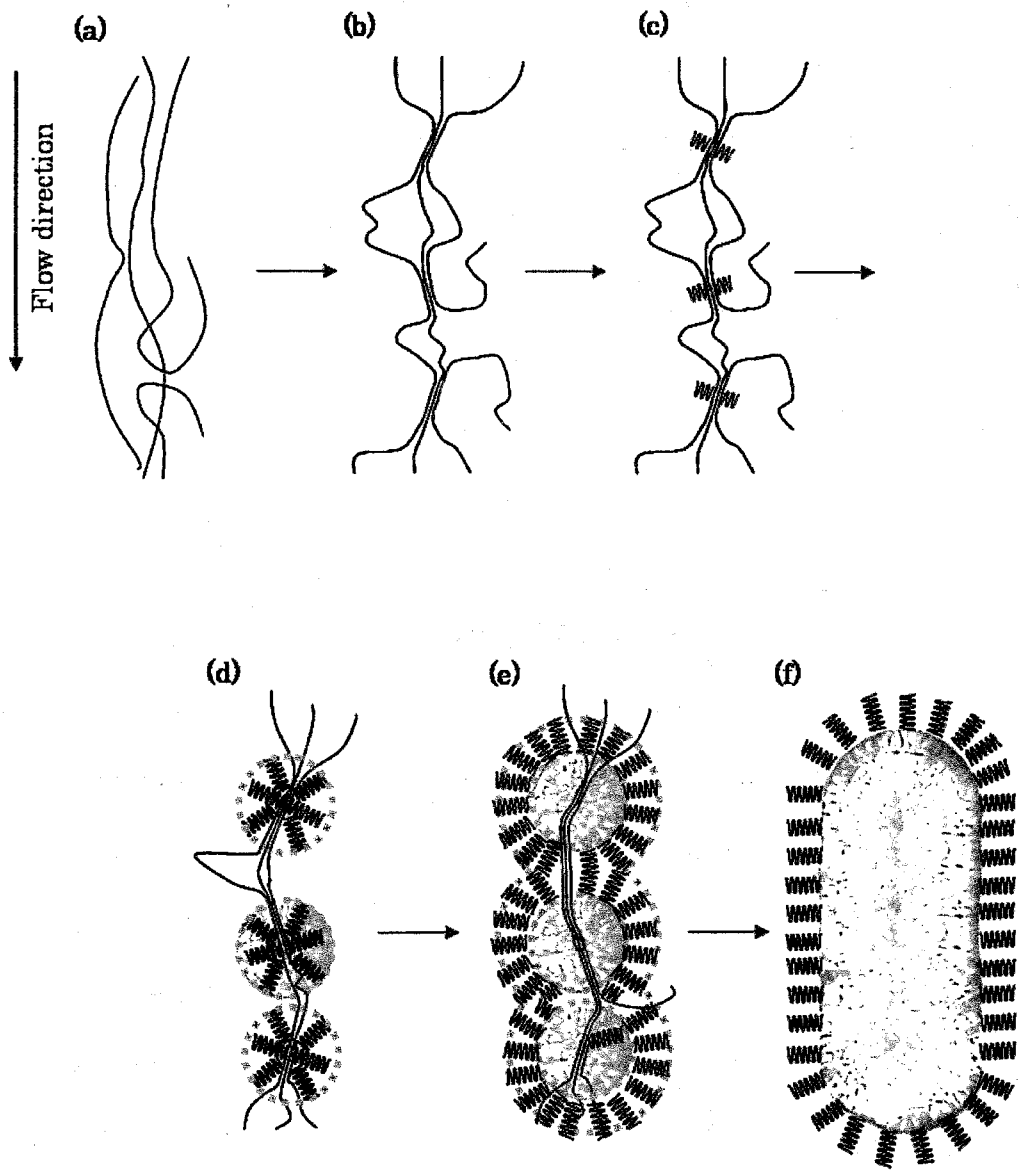

Fig. 7. Schematic illustration of the formation process of rosary-like structure after applying shear flow.

shish-like structure. This is illustrated in Fig. 7(b)-(c). These nuclei grow to spherulites to be a rosary-like structure (Fig. 7(d)), meet each other and are united to be one cylinder-like structure extended to the flow direction (Fig. 7(e)-(f)). The structure inside the rosary-like structure and/or the cylinder-like structure may be similar to that in normal spherulite because the observed SAXS patterns are very similar between the cylinder-like structure at the shear rate 50 s^{-1} and the spherulite under quiescent condition. However, the cylinder-like structure is slightly anisotropic *in average* (see Fig. 3), and hence it is not surprising that the observed SAXS pattern is anisotropic.

6-4 Conclusion

From in-situ optical microscope (OM), depolarized light scattering (DPLS), and small-angle X-ray scattering (SAXS) studies on the crystallization process of polyhydroxybutyrate (PHB) under shear flow, oriented structures (the rosary-like structure and/or the cylinder-like structure) are identified in the shear rate range above about 50 s^{-1}. From the scattering patterns of DPLS and SAXS and the OM images, we suggest that the threadlike structure or the shish-like structure appears in the early stage of crystallization, but it is unable to form a stable shish, and as a result the kebabs cannot continue to develop.

The formation mechanism of the rosary-like structure and the cylinder-like structure was discussed in terms of competition between the relaxation rate of polymer chains and the crystallization rate. On the basis of the discussion we anticipate that high molecular weight component is

effective to form the oriented structure, especially the shish-kebab structure because the relaxation rate of high molecular component is very slow. In the next chapter, we investigate the effect of high molecular weight component on crystallization process of PHB under shear flow.

References

[1] Muller, M.; Seebach, D. *Angewandte Chemie International Edition in English* **1993**, *32*, 477.

[2] Doi, Y. "*Microbial Polyesters*", 1st edition, VCH, New York **1990**.

[3] Sharma, R.; Ray, A. R. *Journal of Macromolecular Science-Reviews in Macromolecular Chemistry and Physics* **1995**, *C35*, 327.

[4] Sharma, L. Ph.D. thesis, Birmingham University, UK **1998**.

[5] Dekoning, G. J. M.; Lemstra, P. J. *Polymer* **1992**, *33*, 3292.

[6] Dekoning, G. J. M.; Lemstra, P. J. *Polymer* **1993**, *34*, 4089.

[7] Biddlestone, F.; Harris, A.; Hay, J. N.; Hammond, T. *Polymer International* **1996**, *39*, 221.

[8] Sharma, L.; Kimura, T.; Matsuda, H. *Polymers for Advanced Technologies* **2002**, *13*, 450.

[9] Sharma, L.; Matsuoka, T.; Kimura, T.; Matsuda, H. *Polymers for Advanced Technologies* **2002**, *13*, 481.

[10] Sharma, L.; Kimura, T. *Polymers for Advanced Technologies* **2003**, *14*, 392.

[11] Hay, J. N.; Sharma, L. *Polymer* **2000**, *41*, 5749.

[12] Sharma, L.; Nishida, K.; Kanaya, T. *Polymers & Polymer Composites* **2004**, *12*, 699.

[13] Sharma, L.; Nishida, K.; Kanaya, T. *Journal of Materials Science* **2004**, *39*, 7373.

[14] A. J. Pennings, A. M. Kiel, *Colloid Z. Polym.* 1965, **205**, 160.

Chapter 7

Crystallization of polyhydroxybutyrate under shear flow

- Effect of high molecular weight component-

7-1 Introduction

It was implied in Chapter 6 that shish-like structure was formed only in the initial stage of crystallization process of polyhydroxybutyrate (PHB) under shear flow at high shears around 50 s^{-1} [1], using in-situ optical microscopy (OM), depolarized light scattering (DPLS) and small-angle X-ray scattering (SAXS).

Many researches have focused on the role of the high molecular weight component in enhancing crystallization kinetics and melt orientation as well as the relationship between the molecular weight and the shear condition on the shish kebab morphology [2-4], and demonstrated that high shear rates for brief periods were the most effective. Haudin [5,6] observed that the effects of the shears is determined by the molecular weight. Significantly and indeed as a fundamental to current shear flow studies, the molecular weight distribution and its resultant rheo-morphological outcome were investigated by Eder et al. [7], Misra et al. [8], Sherwood et al. [9], Lagasseand Maxwell [10] and Wolkowicz [11]. They established that polymer chains relax to a random state rapidly at low molecular weight component compared to high molecular weight one, which remain highly orientated for longer. A critical orientation molecular weight [12,13] is postulated, which has marked sensitivity at low shear rates and generally remains constant at high shear rates. This

orientation mechanism and its dependency on molecular weight appear to be fundamental to the shish-kebab formation [2-14]. We have also examined the effects of high molecular weight component in the crystallization processes under shear flow for PE in Chapter 5, and found that the high molecular weight component really accelerates the shish formation and the shish is formed from the molecular weight component.

Achieving a stable shish-kebab structure using the high molecular weight component it is anticipated to solve PHB's embrittlement problem, where spherulitic impingement renders the material brittle. This information is essential to the PHB processing conditions. Understanding PHB's rheological characteristics enables promising properties and applications, unlike those of conventional PHB, and still possesses its unique biodegradable properties.

In this chapter, we explore the relationship among shear flow, molecular weight, and the resultant morphology using high molecular weight blended with medium molecular weight PHB.

7-2 Experimental

7-2-1 Samples

The medium molecular weight PHB (MMW PHB) with weight average molecular weight M_w = 360,000 was purchased from Aldrich Chemicals, Japan. The high molecular weight PHB (HMW PHB) was kindly supplied by Iwata and Doi. The high molecular weight PHB with weight average molecular weight M_w = 5x10^6 was biosynthesized from glucose using recombinant E. coli XL-1 blue (PSY 1105) bacterium harbouring R.

eutropha H16 PHB biosynthesis phbCAB genes [15]. The resultant material was re-precipitated in hexane from chloroform solution and dried under vacuum for a period of one week [16].

The blends were prepared with the high molecular weight component at 0.5, 1, 2, and 3 wt% composition of the blend weights, and hot chloroform was added with continual heating and stirring to aid dissolution. These solutions were then left for a week, guaranteeing complete dryness, and then pressed at 180 °C and used in this state for experiment.

7-2-2 Measurements

Optical microscope measurements Optical microscope (OM) measurements were performed with Olympus BX50 with video attachment. The shear cell Linkam CSS-450 was connected to the OM. The morphology was observed at shear rate 50 s^{-1} for duration time 2 s, keeping a constant strain of 10,000 %.

Depolarized light scattering measurements The same shear cell Linkam CSS-450 as the OM observation was connected to a depolarized light scattering (DPLS) apparatus with a He-Ne laser light source (wavelength λ = 632.8 nm), covering a range of scattering vector Q of 5 x 10^{-5} to 3.1 x 10^{-4} $Å^{-1}$. DPLS measurements were performed at shear rates 100, 50, and 10 s^{-1} with corresponding duration times of 1, 2, and 10 s, respectively, keeping a constant strain of 10,000 %.

Quartz plates 1 mm thick were used for windows in the Linkam CSS-450 high temperature shear cell. The sample thickness in the cell

was 0.3 mm for all the OM and DPLS measurements. The temperature protocol for the shear experiments is shown in Fig. 1: (a) heat the polymer sample from room temperature to 190 °C at a rate of 30 °C/min, (b) hold at 190 °C for 3 min, (c) cool down to the crystallization temperature T_c= 130 °C at a rate of 30 °C/min, and (d) hold the temperature at 130 °C for the OM and DPLS measurements. The polymer melt was subjected to pulse shear just after reaching the crystallization temperature T_c of 130 °C.

7-3 Results and discussion

7-3-1 Optical scope measurements

We have performed the OM observation on the crystallization of PHB and PHB blend of HMW PHB and MWM PHV on maintaining the same shear rate condition. Fig. 2 shows the observed optical scope images for the blends with HMW PHB concentration of 0.5, 1, 2, 3 wt%. For the 0.5 and 1 wt% blends we observed the oriented structure at around 1 min after applying the pulse shear while such structure was not observed in PHB without HMW component. Therefore, it is no doubt that this oriented structure is formed due to the shear. In the early stage of crystallization of the 2 wt% blend we observed many oriented structure similar to the case of 0.5 and 1 wt% blends, however they were soon covered by many spherulite-like structure. As a result we observed many row structures looking like rosary, similar to the late stage of crystallization process of the 0.5 and 1 wt% blends. This result suggests that high molecular weight component accelerates the formation of the

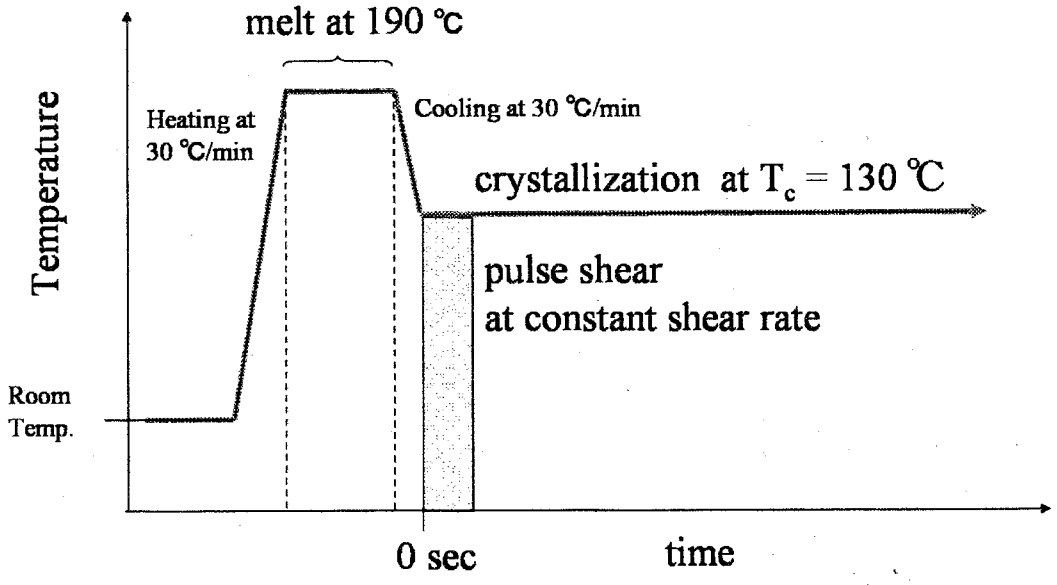

Fig. 1. Temperature protocol for the shear experiments on PHB.

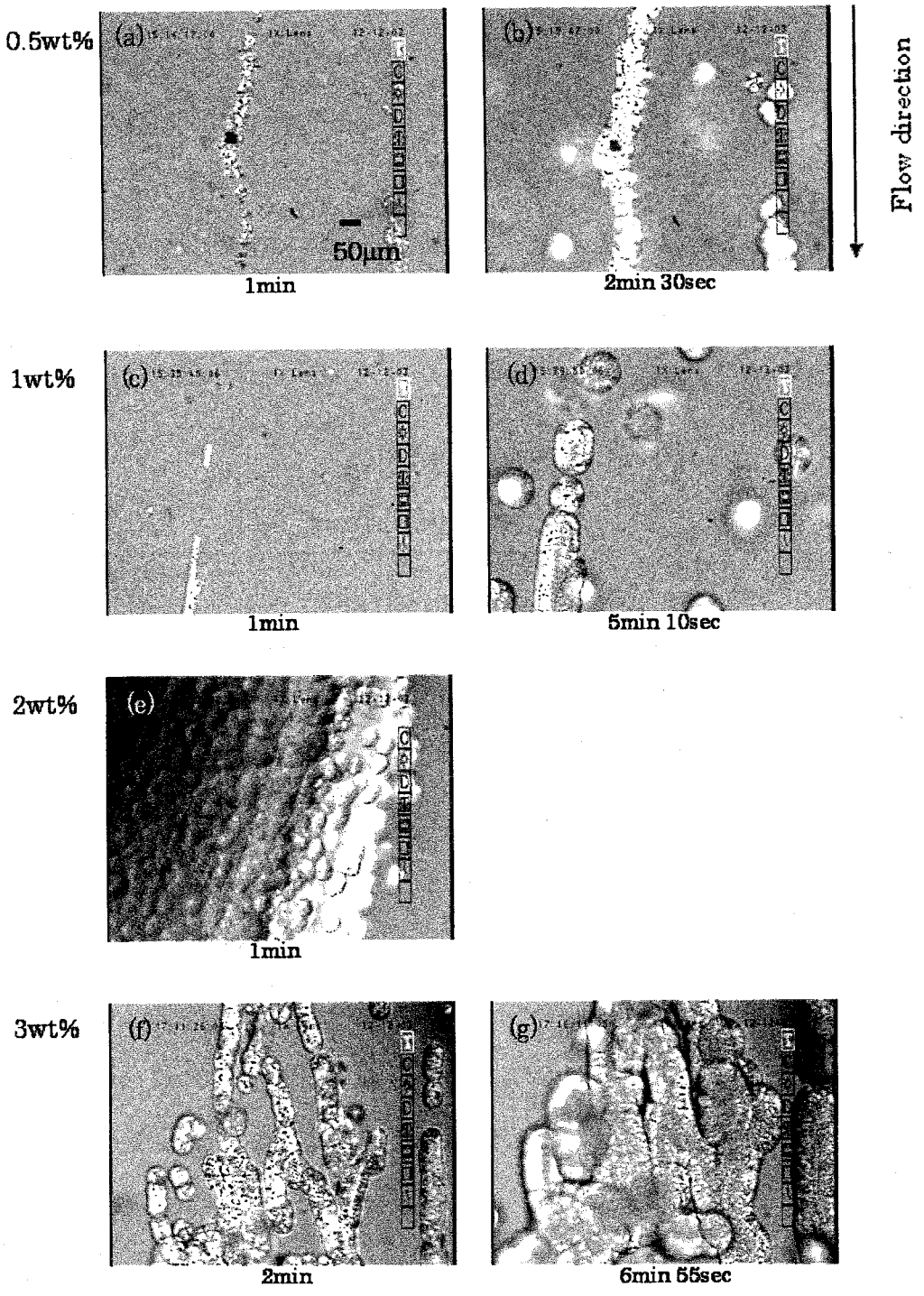

Fig. 2. Optical microscope images for various concentrations of HMW PHB.

oriented structure. It is noted that this oriented structure is not the shish. The shish must be much thinner than the oriented structure observed here. This problem will be discussed on the basis of the results of the depolarized light scattering in the next section.

In contrast to the 0.5, 1 and 2 wt% blends, the optical microscope image of the 3 wt% blend is different. The rosary-like oriented structure is shorter and their orientation distribution seems very broad. In addition, the number of the oriented structures is less than those in the 0.5, 1 and 2 wt% blends, suggesting the effects of the high molecular weight component on the formation of the oriented structure becomes weaker above the concentration of 2 wt%. Before going to the discussion on this problem we show the results of the DPLS measurements.

7-3-2 Depolarized light scattering measurements

As shown above the high molecular weight component accelerates the formation of oriented structure above about the 2 wt%. However, we did not confirm directly the shish structure formation due to the high molecular weight component. To confirm this we performed the DPLS measurements. Fig. 3 shows the observed 2D DPLS patterns for PHB and PHB blends with high molecular weight of 2 and 3 wt%. The shear rate was 50 s^{-1} and the duration time was 2 s. In the case of PHB, we did not observe streak-like scattering at any time during the crystallization after the pulse shear, showing that the isotropic structure formation. On the other hand, for the blends of 2 and 3 wt% we clearly observed streak-like scattering in a direction normal to the flow direction at around

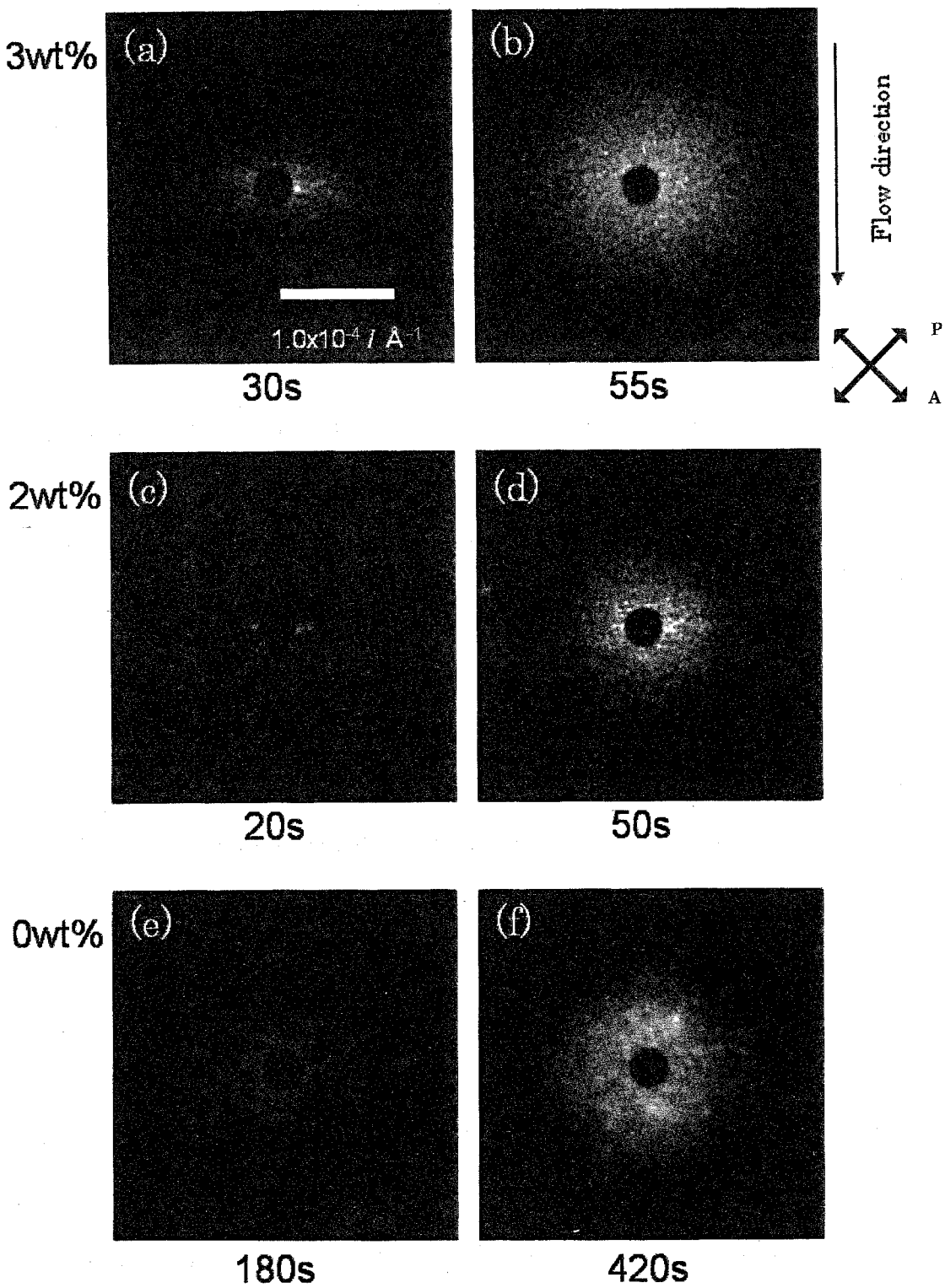

Fig. 3. 2D depolarized light scattering images for various concentrations of HMW PHB.

20 and 30 s in the early stage of the crystallization. This suggests that the shish-like structure is formed in the early stage. However, at around 1 min the scattering patterns become isotropic. This must be the formation of the isotropic spherulite-like structure after the shish formation. This observation agrees with the microscope observation at about 1 min after applying the pulse shear where isotropic spherulite-like structure is formed (see Fig. 2). Although in the OM observation we could not observed the shish-like structure formation even in the very early stage of crystallization, e. g., 20 or 30 s after the pulse shear. This must be due to the very small number of the shish-like structure. However, the shish-like structure is certainly formed as observed in the DPLS measurements, and this must be the origin of the oriented row structure in the OM observation.

It is very interesting to compare the results between the 2 and 3 wt% blends. The streak-like scattering which corresponds to the shish-like structure is sharper and stronger in the 2 wt% blend than the 3 wt% one. This means that better oriented shish-like structures are produced in the 2 wt% blend, which also agrees with the OM observation: the rosary-like oriented structure is shorter and their orientation distribution is broader and the number is less in the 2 wt% blends. Both the OM and DPLS observations suggests that the HMW component accelerates formation of the shish-like structure and the oriented structure in the concentration range of HMW PHB below about 2 wt%. However, at the 3 wt%, both the number and the anisotropy of the shish-like structure and the oriented structure decrease, implying there is an optimal concentration of the

HMW PHB for the shish-like structure formation. In what follows we will discuss this problem.

7-3-3 Effects of high molecular weight component

In Chapter 5 we have shown for polyethylene that the HMW PE accelerated the shish formation, and the shish is made of HMW component. However, in the case of PHB blends of HMW and MMW components we observed the number and the orientation of the shish-like structure decrease as the concentration of HMW PHB increases above about 2 wt%.

We discussed the effects of entanglements of polymer chains on the shish-like structure formation (see Fig. 8 in Chapter 5), and predicted the HMW component decelerated the formation of shish-like structure. This must be the case. The outline of the discussion is as follows.

In order to produce shish-like structure polymer chains must be extended due to shear. If the HMW polymer chains are isolated in the blend, they are somewhat extended by the shear flow, however it does not lead to the anisotropic structure formation. On the other hand, when the concentration of HMW component is above a threshold for entanglements, the chains must be extended due to the connectivity as polymer network is deformed. The threshold for the anisotropy must correspond to the concentration above which entanglements work effectively. This idea reminds us the gel-spinning technique to produce ultra-high strength and ultra-high modulus fiber of PE although all of the situations are not the same. In this procedure, polymer chains are extremely extended because

the tension is transmitted though the cross-linking points in the gel network. On the other hand, in order to obtain the ultra-high strength fiber the number of the cross-linking points should be as little as possible because too many cross-linking points prevent the extension of polymer chains. It is therefore expected in crystallization of HMA and LMW polymer blend under shear flow that the formation of the shish-like structure is suppressed at a rather high concentration because the polymer chains cannot be extended due the shear because of too many entanglements. This suggests that there is a critical concentration above which entanglements hinder the extension of polymer chain due to the shear between 2 and 3 wt% in the HMW and MMW PHB blends

In the experiments on the HMW and LMW PE blend, the molecular weight of the HMW component is M_w = 2,000,000. On the other hand that in the PHB blend is M_w = 6,000,000. Unfortunately, it is impossible to calculate the overlap concentration of HMW component of PHB using equations (1) and (2) because the persistence length of PHB is not known at the moment, which must be longer than that of PE. It is qualitatively expected that the critical concentration is smaller in the PHB blend than in the PE blend. Therefore, we observed the deceleration in the shish-like structure formation in the HMW and MMW PHB blend above about 2 wt%.

7-4 Conclusion

We have studied the crystallization process of blends of the HMW PHB and MMW PHB under shear flow using OM and DPLS with the pulse

shear technique as a function of the concentration of HMW PE in the range of 0 to 3 wt%, focusing on effects of the HMW PHB on the shish-like structure formation. It was found that the shish-like structure formation is enhanced by the HMW component below about 2 wt% while it is decelerated above about 2 wt%.

The results suggest that there is an optimal concentration of HMW component for the shish-like structure formation. This was discussed in terms of entanglements. Below the optimal concentration extension of the HMW chains is enhanced as the concentration increases while it is decelerated with increasing the concentration above the critical value because too many entanglements obstruct the extension.

References

[1] Sharma, L.; Ogino, Y.; Kanaya, T. *Macromolecular Materials and Engineering* **2004**, *289*, 1059.

[2] Nogales, A.; Hsiao, B. S.; Somani, R. H.; Srinivas, S.; Tsou, A. H.; Balta-Calleja, F. J.; Ezquerra, T. A. *Polymer* **2001**, *42*, 5247.

[3] Vleeshouwers, S.; Meijer, H. E. H. *Rheologica Acta* **1996**, *35*, 391.

[4] Moitzi, J.; Skalicky, P. *Polymer* **1993**, *34*, 3168.

[5] Tribout, C.; Monasse, B.; Haudin, J. M. *Colloid and Polymer Science* **1996**, *274*, 197.

[6] Jay, F.; Haudin, J. M.; Monasse, B. *Journal of Materials Science* **1999**, *34*, 2089.

[7] Eder, G.; Janeschitzkriegl, H.; Liedauer, S.; Schausberger, A.; Stadlbauer, W.; Schindlauer, G. *Journal of Rheology* **1989**, *33*, 805.

[8] Misra, S.; Lu, F. M.; Spruiell, J. E.; Richeson, G. C. *Journal of Applied Polymer Science* **1995**, *56*, 1761.

[9] Sherwood, C.; Price, F.; Stein, R. *Journal of Polymer Science* **1978**, *63*, 77.

[10] Lagasse R., Maxwell B., *Polymer Engineering and Science.* **1978**, *18*, 215.

[11] Wolkowicz, M. *Journal of Applied Polymer Science* **1978**, *63*, 365.

[12] Hosier, I. L.; Bassett, D. C.; Moneva, I. T. *Polymer* **1995**, *36*, 4197.

[13] Mano, J. F.; Sousa, R. A.; Reis, R. L.; Cunha, A. M.; Bevis, M. J. *Polymer* **2001**, *42*, 6187.

[14] Somani, R. H.; Yang, L.; Hsiao, B. S.; Agarwal, P. K.;

Fruitwala, H. A.; Tsou, A. H. *Macromolecules* **2002**, *35*, 9096.

[15] Kusaka, S.; Abe, H.; Lee, S. Y.; Doi, Y. *Applied Microbiology and Biotechnology* **1997**, *47*, 140.

[16] Iwata, T.; Aoyagi, Y.; Fujita, M.; Yamane, H.; Doi, Y.; Suzuki, Y.; Takeuchi, A.; Uesugi, K. *Macromolecular Rapid Communications* **2004**, *25*, 1100.

Summary

The present thesis includes studies on the formation mechanism of shish-kebab structure. The contents of the respective chapters are summarized below.

In Chapter 1, earlier and current researches on flow induced crystallization were introduced. In addition, we described basic theories of scattering to give a basis for readers to understand the contents of the thesis. We also introduced scattering apparatus, sample preparation and flow apparatus in this thesis.

In Chapter 2, we investigated the crystallization process of polyethylene (PE) after pulse shear using depolarized light scattering (DPLS) to elucidate the shear rate and shear strain effects on formation of shish-kebab structure. We analyzed the DPLS data to evaluate the critical shear rates for acceleration of the crystallization rate and the anisotropy at given shear strains. It was found that the former is much smaller than the later. Extrapolating to the infinite shear strain, we evaluated the critical shear rate for the anisotropic structure formation for apparent continuous shear flow. The value was 1.5 s^{-1}. This critical shear rate was discussed in relation to the competition between the chain relaxation and the orientation-induced crystallization rate.

In Chapter 3, we used isotactic polypropylene (i-PP) as a sample, and investigated the crystallization process after a pulse shear using DPLS to see the shear rate and shear strain effects on formation of shish-kebab structure. We estimated the critical shear rate for acceleration of crystallization and

the critical shear rate for the shish-like structure formation. The former is much smaller than the latter, similar to the results of PE. In the same ways as in Chapter 2, we evaluated the critical shear rate for the anisotropic structure formation or the shish-like structure formation for the apparent continuous shear flow, which was about 2.0 s^{-1}. The results on i-PP again suggest that the competition between the chain relaxation and the orientation-induced crystallization rate dominated the formation of the shish-like structure.

In Chapter 4, we used isotactic polypropylene as a sample and observed the crystallization process after a pulse shear using optical microscope (OM), depolarized light scattering (DPLS), small-angle X-ray scattering (SAXS) and wide-angle X-ray scattering (WAXS) to cover a wide spatial range from μm to Å. We evaluated the critical shear rates for the anisotropic structure formation in various spatial scales: the critical shear rates for the shish-like structure formation by DPLS, for the kebab structure formation by SAXS, and for crystal growth by WAXS. We found that all the critical shear rates are almost identical. This result indicates that the anisotropic structure is dominated by the same origin. Comparing the onset times of DPLS, SAXS and WAXS, onset time of DPLS is the earliest, that of SAXS is the second and that of WAXS is the last. These results suggest that the shish-like structure formed first and the kebab structure formed epitaxially on the shish. In such formation process, we expect that the critical shear rate of the kebab formation is dominated by the shish, agreeing with the present observations. Therefore, it is the most important point to elucidate the formation mechanism of the shish structure to understand the shish-kebab

formation.

In Chapter 5, we investigated the role of high molecular weight component in the shish structure formation using depolarized light scattering (DPLS), small-angle X-ray scattering (SAXS) and small-angle neutron scattering (SANS). For this purpose we prepared blends of low molecular PE and high molecular weight (HMW) PE and performed DPLS measurements on the crystallization process of the blends as a function of concentration of HMW component. We found that the anisotropic structure formation corresponding to the shish formation was accelerated above a critical concentration of HMW component. The critical concentration was 0.5 - 0.6 wt%, and this value is about three times larger than the overlap concentration of polymer chains. This result suggests that entanglements of the HMW PE are very important for the formation of the shish-like structure. In order to confirm that the shish is formed from the high molecular weight component, SANS and SAXS measurements were performed on an elongated blend of HMW hydrogenated PE (3 wt%) with M_w = 2,000,000 and LMW deuterated PE with M_w = 200,000. The scattering pattern of SANS shows strong steak-like scattering along the direction normal to the elongation and weak two spots pattern along the parallel to elongation. On the other hand, the scattering pattern of SAXS shows that only two spots pattern along the parallel to elongation. These results indicate that shish-like structure was made of HMW component.

In Chapter 6, we used polyhydroxybutyrate (PHB) as a sample because PHB is one of the candidates of bioplastic for practical use but still has many problems to be improved about its properties. Optical microscope (OM),

depolarized light scattering (DPLS) and small-angle X-ray (SAXS) measurements were performed on the crystallization process of PHB under shear flow focusing on the effect of shear rate. We observed anisotropic structure above the shear rate $50s^{-1}$. At the shear rate $50s^{-1}$, the anisotropic structure is not the shish-kebab structure but rosary-like structure of lined spherulites. We suggest a following scenario for the rosary-like structure formation. Threadlike structure or the shish-like structure appears in the early stage of crystallization and some parts of the shish-like structure crystallize, but it is unable to form a long stable shish because the chain relaxation rate is faster than the crystallization rate, and as a result the spherulites develop from the small crystallites on the shahs-like structure. Thus, the morphology of anisotropic structure form rosary-like structure. This result implies that high molecular weight component would be effective to have a stable shish because the relaxation rate of high molecular component is very slow.

In Chapter 7, we studied the effects of high molecular weight component on crystallization of polyhydroxybutyrate (PHB) under shear flow. We observed the crystallization process of PHB blends including small amount of high molecular weight (HMW) component under the shear flow using OM and DPLS as a function of the concentration of HMW PHB in a range of 0 to 3 wt%. It was found that the shish-like structure formation was enhanced by the HMW component below about 2 wt% while it was decelerated above about 2 wt%, showing an optimal concentration for chain extension at around 2 wt%. Below the optimal concentration extension of the HMW chains is enhanced as the concentration increases while it is decelerated

with increasing the concentration above the optimal value. This may be due to too many entanglements obstruct the chain extension.

List of publications

"Crystallization of polyethylene under shear flow as studied by time resolved depolarized light scattering. Effects of shear rate and shear strain"
Fukushima, H.; **Ogino, Y.**; Matsuba, G.; Nishida, K.; Kanaya, T.
Polymer **2005**, *46*, 1878-1885.
(Chapter 2)

"Crystallization of isotactic polypropylene under shear flow: Effects of shear rate and shear strain"
Ogino, Y.; Matsuba, G.; Nishida, K.; Kanaya, T.
Macromolecules, to be submitted.
(Chapter 3)

"Crystallization of isotactic polypropylene under shear flow: Observations in a wide spatial range"
Ogino, Y.; Fukushima, H.; Matsuba, G.; Nishida, K.; Kanaya, T.
Macromolecules, to be submitted.
(Chapter 4)

"Polymer crystallization under shear flow"
Kanaya, T.; **Ogino, Y.**; Fukushima, H.; Matsuba, G.; Nishida, K.
Proceedings of the 5th Osaka University Macromolecular Symposium, edited by Adachi, K.; Sato, T., **2005**, 49-56.
(Chapter 4 and 5)

"Effects of high molecular weight component on crystallization of polyethylene under shear flow"

Ogino, Y.; Fukushima, H.; Matsuba, G.; Takahashi, N.; Nishida, K.; Kanaya, T.

Polymer, in print.

(Chapter 5)

"Shish kebab morphology induced in polyhydroxybutyrate under shear flow"

Sharma, L.; **Ogino, Y.**; Kanaya, T.

Macromolecular Materials and Engineering **2004** *289*, 1059-1067.

(Chapter 6)

"Fiber formation in medium and ultra-high-molecular-weight polyhydroxybutyrate blends under shear flow"

Sharma, L.; **Ogino, Y.**; Kanaya, T.; Iwata, T.; Doi, Y.

Macromolecular Materials and Engineering **2004** *289*, 1068-1073.

(Chapter 7)

Other publications

"A new shear technique: Semi continuous shear flow (SCSF) in medium and ultra high molecular weight polyhydroxybutyrate blends"
Sharma, L.; **Ogino, Y.**; Kanaya, T.; Iwata, T.; Doi, Y.
Journal of Material Science, submitted.

"Precursor of primary nucleation in isotactic polystyrene induced by shear flow"
Kanaya, T.; Takayama, Y.; **Ogino, Y.**; Matsuba, G.; Nishida, K.
Progress in understanding of polymer crystallization, Lecture Notes in Physics, Springer, Berlin, in print.

"Crystallization of polyethylene and polypropylene under shear flow"
Kanaya, T.; **Ogino, Y.**; Fukushima, H.; Matsuba, G.; Nishida, K.
Abstracts of Papers of the American Chemical Society **2004**, *228*, U440-U440.

"Structural analysis of drawing polyethylene blends with ultra-high molecular weight component"
Matsuba, G.; **Ogino, Y.**; Fukushima, H.; Kanaya, T.; Nishida, K.
Abstracts of Papers of the American Chemical Society **2004**, *228*, U446-U446.

"Shish-Kebab Structure by SANS"

Kanaya, T.; **Ogino, Y.**; Matsuba, G.; Nishida, K.

RESEARCH HIGHLIGHTS, Activity Report on Neutron Scattering Research **2005** *12*, 42-43.

Acknowledgements

The present thesis is based on the study carried out under the guidance of Professor Toshiji Kanaya, at the Institute for Chemical Research (ICR), Kyoto University, from 2001-2006.

The author wishes to express her sincere gratitude to Professor Toshiji Kanaya for his continuous guidance, encouragement and valuable advices all throughout this thesis.

The author also wishes to express her sincere gratitude to Professor Emeritus Keisuke Kaji for his kind guidance, encouragement and valuable advices all throughout this thesis.

The author also wishes to express her thanks to Associate Professor Koji Nishida for his valuable suggestions, kind support and encouragement.

Professor Shinzaburo Ito and Professor Hiroshi Watanabe are especially acknowledged for their critical review of the thesis.

The author greatly acknowledges to Assistant Professor Go Matsuba for his valuable suggestion and kind support.

The author also greatly acknowledges to Professor Mitsuhiro Shibayama, Associate Professor Yoshiaki Takahashi and Dr. Satoshi Okabe for their valuable comments and kind support in neutron scattering experiments with SANS-U at JRR-3M reactor.

The author also greatly acknowledges to Dr. Tetsuro Fujisawa, Dr. Tetsutaro Iizuka, Dr. Katsuaki Inoue and Dr. Sono Sasaki for their valuable comments and kind support in X-ray scattering experiments with BL45XU and BL40B2 at SPring-8.

The author also greatly acknowledges to Mr. Ichiro Fujio, Mitsui Chemicals, Inc. for his valuable comments and kind support in X-ray scattering experiments.

The author wishes to express thanks to all of the postdoctoral fellows, students and secretaries of Emeritus Professor Kaji's laboratory in the past and Professor Kanaya's laboratory in the past and the current. They are Dr. Lakshimi Sharma, Dr. Takahiko Kawai, Dr. Tsukasa Miyazaki, Dr. Nobuaki Takahashi, Mr. Takashi Kito, Mr. Tomohiro Okuyama, Mr. Takashi Konishi, Mr. Hajime Fukushima, Mr. Hiroaki Yamano, Mr. Shinya Matsubara, Mr. Hiroki Ogawa, Mr. Taijiro Takeda, Mr. Rintaro Inoue, Mr. Shinya Sakamoto, Mr. Tsuyoshi Tsubouchi, Mr. Yoshiyuki Takayama, Mr. Wataru Akai, Mr. Toru Iseki, Mr. Tetsuo Hirabayashi, Mr. Naoya Takahashi, Mr. Junpei Yamamoto, Ms. Seung In Hong, Ms. Nelly Rahman, Ms. Yuri Nakamura, Ms. Nami Nakai and Ms. Hanako Ishida.

Thanks are also due to the member of Professor Hashimoto's laboratory in the past. They are Professor Emeritus Takeji Hashimoto, Associate Professor Hirokazu Hasegawa, Assistant Professor Mikihito Takenaka, Technical Instructor Kenji Saijo, Mr. Masayuki Adachi, Ms. Kayo Kawamura and Ms. Takako Kowada.

All of the students who have studied together with the author at Kyoto University are acknowledged for their heartfelt encouragement. All of the office workers in ICR and Department of Polymer Chemistry who supported the author and the cafeteria stuffs in Uji campus who encouraged the author are also acknowledged for their kindness.

Finally, the author expresses her heartfelt gratitude to her parents

Yasushige Ogino and Yoko Ogino, grandfathers and grandmothers late Akirato Ogino, late Masa Ogino, late Eiichi Honda, Yurika Honda and her relations for their heartfelt care and their continuous encouragement.

February 2006

Yoshiko Ogino